How stigmatic epidermis mediates the invading cell growth : the case of pollen tube and oomycete hypha

Lucie Riglet

Numéro National de Thèse : 2018LYSEN058

THESE de DOCTORAT de L'Université de Lyon
opérée par
l'Ecole Normale Supérieure de Lyon

Ecole Doctorale N° 340
Biologie Moléculaire Intégrative et Cellulaire

Spécialité de doctorat : Sciences de la Vie
Discipline : Biologie des Plantes

Soutenue publiquement le 26/10/2018, par :
Lucie RIGLET

How stigmatic epidermis mediates the invading cell growth: the case of pollen tube and oomycete hypha

---

Devant le jury composé de :

M. Herman HÖFTE, DR, Institut Jean-Pierre Bourgin, Versailles, Rapporteur
Mme Bénédicte CHARRIER, DR, Station Biologique de Roscoff, Rapporteure
Mme Naomi NAKAYAMA, Group Leader, University of Edinburgh, Edinburgh, Examinatrice
Mme Nathalie POUSSEREAU, MCF, Université Claude Bernard Lyon I, Examinatrice
M. Thierry GAUDE, DR, Ecole Normale Supérieure de Lyon, Directeur de thèse
Mme Isabelle FOBIS-LOISY, CR, Ecole Normale Supérieure, Lyon, Co-encadrante de thèse

Numéro National de Thèse : 2018LYSEN058

THESE de DOCTORAT de L'Université de Lyon
opérée par
l'Ecole Normale Supérieure de Lyon

Ecole Doctorale N° 340
Biologie Moléculaire Intégrative et Cellulaire

Spécialité de doctorat : Sciences de la Vie
Discipline : Biologie des Plantes

Soutenue publiquement le 26/10/2018, par :
Lucie RIGLET

Réaction de l'épiderme stigmatique à la croissance de cellules invasives: le cas du tube pollinique et de l'hyphe des oomycètes

---

Devant le jury composé de :

M. Herman HÖFTE, DR, Institut Jean-Pierre Bourgin, Versailles, Rapporteur
Mme Bénédicte CHARRIER, DR, Station Biologique de Roscoff, Rapporteure
Mme Naomi NAKAYAMA, Group Leader, University of Edinburgh, Edinburgh, Examinatrice
Mme Nathalie POUSSEREAU, MCF, Université Claude Bernard Lyon I, Examinatrice
M. Thierry GAUDE, DR, Ecole Normale Supérieure de Lyon, Directeur de thèse
Mme Isabelle FOBIS-LOISY, CR, Ecole Normale Supérieure, Lyon, Co-encadrante de thèse

Abstract

The epidermis is the first cellular barrier in direct contact with the environment in both animal and plant organisms. In plants, the result of the cell-to-cell communication that occurs between the pollen grain and the epidermal cells of the stigma, also called papillae, is crucial for successful reproduction. When accepted, the pollen grain germinates and emits a pollen tube that transports the male gametes towards the ovules. Effective fertilization in angiosperms depends on the proper trajectory that pollen tubes take while progressing within the pistil tissues to reach the ovules.

Pollen tubes grow within the cell wall of the papilla cells, applying pressure to the wall. Such forces are known to alter the cortical microtubule (CMT) network and cell behaviour. The first part of my PhD thesis aimed at investigating the role of the microtubule cytoskeleton of stigmatic cells in pollen tube growth. By combining cell imaging and genetic approaches, we found that CMT network of papilla cells is modified with ageing, CMT bundles being anisotropic at anthesis and becoming isotropic at later stages of stigma development. This change in CMT organisation was accompanied by a modification of the pollen tube growth direction, which passes from predominantly straight to coiled. In the Arabidopsis *katanin1-5* (*ktn1-5*) mutant, papillae have a highly isotropic CMT array, associated with a marked tendency of wild-type (WT) pollen tube to turn around the papillae. We could partially phenocopy this coiled growth of pollen tubes by treating WT papillae with the microtubule-depolymerizing drug oryzalin. As CMT pattern is linked to cellulose microfibrils organisation, and hence possibly to cell-wall stiffness, we assessed the stiffness of *ktn1-5* and aged papillae using Atomic Force Microscopy. We found that both papillae have a softer cell wall compared with WT cells, suggesting that the pollen tube growth phenotype might be dependent on cell wall alteration. We tested a series of cell wall mutants, including mutants described to exhibit CMT disorganisation and decreased cell wall rigidity and, astonishingly, none of them used as female induced turns of WT pollen tubes. Altogether, our results suggest that both organisation of CMT and cell wall properties dependent on KATANIN have a major role in guiding early pollen tube growth in stigma papillae.

Similarly to pollen tube growth within the stigmatic papilla, hypha of filamentous pathogens penetrates the epidermal tissue of the host. During pathogen attacks, epidermal cells promptly react to the invading organisms to adjust the most relevant response. Early response of the first cell layers including epidermal cells is decisive for the result of plant-pathogen interactions. The second part of my PhD work aimed at comparing the cellular response of stigmatic cells challenged by two types of invaders, the pollen tube during pollination and hyphae of two oomycete filamentous pathogens,

Phytophtora parasitica and *Hyaloperonospora arabidopsidis*, during the infection process. While *H. arabidopsidis* was unable to penetrate the stigma surface, pollen tubes and *P. parasitica* hyphae invaded the papilla cell wall, triggering specific cellular features, respectively. For instance, they did not deform the plasma membrane of papilla cells in the same manner. By real-time cell imaging, we found that both invaders mobilized actin and late endosome compartments at the contact site with the papilla, but only *P. parasitica* hyphae lead to *trans*-Golgi Network polarization at the infection site. Thus, we demonstrate that a stigmatic cell challenged by a pollen tube or an oomycete hypha adapts its response to the invader's identity.

Résumé

Chez les plantes à fleurs, la communication entre les grains de pollen et les cellules épidermiques du stigmate, aussi appelées papilles, est cruciale pour le succès de la reproduction. Lorsqu'il est accepté, le grain de pollen germe et émet un tube pollinique qui transporte les gamètes mâles jusqu'aux ovules. La rencontre et la fusion entre les gamètes mâles et femelles reposent par conséquent sur la bonne trajectoire des tubes polliniques lors de leur progression dans les différents tissus du partenaire femelle pour atteindre les ovules.

Les tubes polliniques croissent dans la paroi cellulaire des papilles stigmatiques et génèrent une pression sur ces dernières. De telles forces sont connues pour modifier le réseau de microtubules corticaux (MTC) ainsi que le comportement de la cellule. La première partie de mon travail de thèse a consisté à étudier le rôle des MTC du stigmate dans le contrôle de la croissance du tube pollinique. En combinant imagerie cellulaire et approches génétiques, nous avons mis en évidence que le réseau de MTC de la papille évolue au cours de son développement, passant d'un réseau anisotrope à l'anthèse, pour devenir isotrope à des stades plus âgés. Ce changement d'organisation s'accompagne d'une modification de la direction de croissance des tubes polliniques, passant de droite à spiralée. Chez le mutant *katanin1-5* (*ktn1-5*) d'Arabidopsis, les papilles ont un réseau de MTC très isotrope, associé à une forte tendance des tubes polliniques sauvages à faire des spires autour des papilles. Ce phénotype « spiralé » a pu être partiellement reproduit par traitement des papilles avec un agent dépolymérisant les MTC, l'oryzaline. Compte tenu que le réseau de MTC est fortement lié à l'organisation des fibres de cellulose, et donc potentiellement à la rigidité de la paroi, nous avons mesuré la rigidité des papilles âgées, ainsi que celles du mutant *ktn1-5* grâce au microscope à force atomique. Nos résultats montrent que ces papilles sont plus molles que les papilles sauvages à un stade anthèse, suggérant que le phénotype spiralé des tubes polliniques pourrait être dépendant d'une modification des propriétés mécaniques de la paroi cellulaire. Nous avons ensuite testé une série de mutants de paroi, présentant pour certains une diminution de la rigidité de leur paroi, associée ou non à un défaut d'organisation des MTC. Etonnamment, les tubes polliniques sauvages ne font pas de spires sur ces papilles mutées. L'ensemble de ces résultats suggère que la KATANIN, en régulant l'organisation des MTC et conférant des propriétés mécaniques particulières à la paroi cellulaire, joue un rôle primordial dans le guidage des tubes polliniques lors de leur croissance dans les papilles stigmatiques.

De façon similaire à la croissance des tubes dans les papilles, les hyphes des pathogènes filamenteux pénètrent les tissus épidermiques de leur hôte. Lors d'une attaque par un pathogène, les cellules de l'épiderme de l'hôte réagissent rapidement pour

mettre en place une réponse appropriée. Cette réponse précoce est décisive sur le résultat de l'interaction plante-pathogène. La seconde partie de mon travail de thèse a eu pour objectif de comparer la réponse cellulaire des papilles stigmatiques suite à l'invasion par deux types d'organismes, le tube pollinique lors de la pollinisation et les hyphes de deux Oomycètes pathogènes, *Phytophtora parasitica* et *Hyaloperonospora arabidopsidis* durant leurs processus d'infection. Alors que *H. arabidopsidis* n'est pas capable de pénétrer la surface du stigmate, le tube pollinique ainsi que l'hyphe de *P. parasitica* ont la capacité d'envahir la paroi de la papille, provoquant chacun des réponses cellulaires spécifiques de cette dernière. Par exemple, les deux organismes invasifs ne déforment pas la membrane plasmique des papilles de la même manière. Grâce à un système d'imagerie en temps réel, nous avons mis en évidence une mobilisation de l'actine et des compartiments endosomaux tardifs dans la cellule stigmatique au site de contact avec le tube pollinique ou l'hyphe. Cependant, seul l'hyphe de *P. parasitica* entraîne une polarisation du réseau *trans*-Golgien au site d'infection. Ces résultats démontrent que la papille stigmatique est capable d'adapter sa réponse en fonction de l'identité de l'envahisseur.

Acknowledgements

I would like to thank Bénédicte Charrier, Herman Höfte, Naomi Nakayama and Nathalie Poussereau for accepting to review this thesis.

Remerciements

Tout d'abord, je remercie Isabelle et Thierry pour m'avoir donné ma chance malgré un parcours atypique et m'avoir fait confiance. Merci à Isabelle pour m'avoir encouragé, formé, et épaulé tout au long de ma thèse et ce depuis mon stage de fin d'études. Merci à Thierry pour m'avoir enseigné sa rigueur et son sens des détails (ainsi que des couleurs !). Merci à tous les deux pour m'avoir accompagné et permis de me faire plaisir et de m'amuser avec ce sujet !

Je remercie aussi Olivier Hamant et Yohann Boutté pour avoir pris part à mes comités de thèse.

Cette thèse, c'est avant tout une aventure humaine. J'aimerais remercier les membres du RDP ainsi que ceux qui ont collaboré à la réalisation de ma thèse et qui ont pris sur leur temps pour m'aider dès que j'en avais besoin. Merci à l'équipe Sice, ainsi qu'à l'équipe Biophysique et MechanoDevo pour tous leurs conseils. Un grand merci à Tchié Kodera pour son soutien et ses encouragements (et les chocolats), à Olivier Hamant pour sa positivité, sa bienveillance et ses précieux conseils qui ont participé au développement de ce travail de thèse.
Merci à Frédérique Rozier pour ses conseils techniques ainsi que pour les qPCR ; à Virginie Battu, Arezki Boudaoud, Simone Bovio et Pascale Milani, les rois et reines de l'AFM. Merci à Vincent Bayle, Elodie Chatre, Claire Lionnet et Christophe Chamot, qui m'ont appris l'art d'utiliser un microscope sans le casser. La salle du MEB était un peu ma seconde maison. Merci aussi à l'équipe culture qui prend soin de nos plantes au quotidien ainsi qu'à Hervé Leyral et Isabelle Desbouchages pour tous ces milieux qu'ils nous préparent toujours dans la bonne humeur. À Nice, merci à Agnès Attard et Sophie Hok ainsi que les autres membres de l'équipe plantes – pathogènes; aux physiciens/nes de Grenoble, Catherine Quilliet et Karin John ainsi qu'à Denis Bartolo à Lyon, merci pour ces collaborations qui ont apporté cette note de multidisciplinarité à ma thèse que j'ai tant apprécié.

Un merci tout particulier à ceux qui ont partagé mon quotidien durant cette thèse, et pour tous les bons moments passés ensemble. Merci à Nathan pour les nombreuses

pauses café / discussions mémorables sur les marches du RDP ; pour les «11h30 » détente avec Virginie et Léa, que je remercie bien sûr pour la superbe escapade grecque ainsi que pour leurs soutiens tout au long de cette thèse ; à Marie-France, Jérôme et Jekaterina pour ces inoubliables soirées jeux (et les gâteaux !). Merci à tous pour votre amitié et votre soutien. Tous ces moments ont été précieux et vont énormément me manquer.

Merci aussi à Hanh Nguyen et Florian Massinon pour m'avoir initié au rôle d'encadrante que j'ai franchement adoré.

Je souhaiterais aussi remercier le département de biologie de l'ENS et les enseignants qui m'ont accueilli durant mes trois années de monitorat. Ce fut une expérience humaine et scientifique vraiment très enrichissante. Un merci tout particulier à Christine Miège pour la confiance qu'elle m'a accordé au début de mon monitorat, merci aussi Aurélie Vialette, Nathalie Depège Fargeix et Christophe Trehin pour les bons moments passés lors du TP physio. Merci également à David Busti, Jean-Pierre Moussus, Marc Coudel, et Régis Thomas de la prépa agreg pour ces supers sorties botaniques.

Et comme il n'y a tout de même pas que le RDP dans la vie, merci à mes amis, ma famille et Loïc qui m'ont permis de m'extraire de ma thèse pour mieux y revenir :

Comment ne pas remercier Amandine, pour les heures passées au téléphone à refaire le monde, les moments passés à Toulouse, à Gap ou à Lyon. Merci de m'avoir soutenu et sorti de ma bulle pour me ramener sur terre de temps en temps. Merci aussi à Amélie pour sa bonne humeur et son humour communicatif.

Enfin, un immense merci à mes parents pour m'avoir donné l'opportunité de m'épanouir et m'avoir encouragé sans relâche depuis toujours ; merci à Nono et Loulou d'être toujours là pour moi eux aussi. Pour leur soutien sans faille et surtout pour m'avoir toujours épaulé dans mes choix. J'ai beaucoup de chance de vous avoir.

Pour finir, ces dernières lignes sont destinées à Loïc, merci d'être là pour moi tout simplement, pour ton soutien, tes encouragements quotidiens et pour m'avoir appris à relativiser durant ce long fleuve pas toujours tranquille qu'est la thèse. Merci pour l'équilibre que tu m'apportes dans la vie en général.

List of main abbreviations

AFM: Atomic force microscopy
ATP : Adenosin triphosphate
BFA : Brefeldin A
bp : Base pair
CESA : Cellulose synthase
CMF : Cellulose microfibril
CMT : Cortical microtubule
Col-0 : Colombia
CSC : Cellulose synthase complex
Da : Dalton
DMSO : Dimethyl sulfoxyde
DNA : deoxyribonucleic acid
EHM : Extrahaustorial membrane
ER: Endoplasmic reticulum
FESEM : Field Emission Scanning Electron Microscopy
GFP : Green fluorescent protein
HC : Hemicellulose
HG : Homogalacturonan
KEGG : Kyoto encyclopedia of genes and genomes
LE : Late endosome
LoC : Lab-on-chip
PM : plasma membrane
PME : Pectin methylesterase
PMEI : Pectin methylesterase inhibitor
PTI : Pathogen associated molecular pattern - triggered immunity
RFP : Red fluorescent protein
RG : Rhamnogalacturonans
RLK : Receptor-like kinase
RNA : Ribonucleic acid
s.e.m. : Standard error of mean
SEM: scanning electron microscopy
T-DNA : Transfer deoxyribonucleic acid
TEM : Transmission Electron Microscopy
TGN : *trans*-Golgi Network
WT : wild-type

Table of contents

Table of figures

Table of supplementary figures and tables

1

Introduction

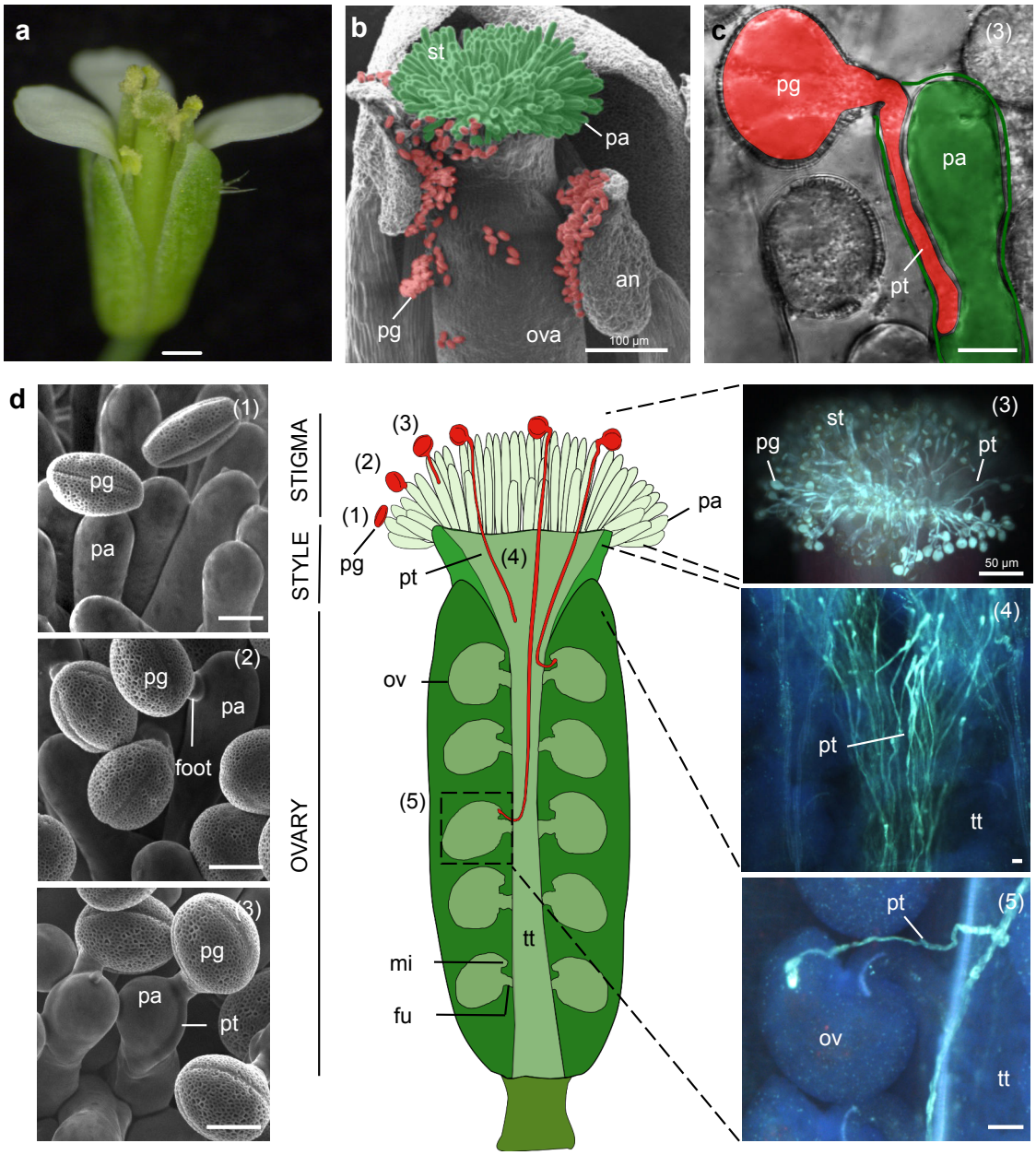

Fig. 1 / Pollen tube path within the pistil in *Arabidopsis thaliana*.
a, *A. thaliana* flower. Bar, 5 mm. b, Scanning Electron Microscopy (SEM) view of the upper part of the flower. In green, the stigma composed of unicellular papillae (pa). In red, the pollen grains (pg). c, Confocal image of a pollen grain germinated on a papilla. The pollen tube penetrates the papilla external wall layer (green line) and is growing towards the base of the stigma. d, Pollen tube pathway within the female partner. (1) Dehydrated pollen grains are deposited on the stigmatic papillae. (2) Pollen grains hydrate and stay attached to the papilla by the formation of an interface made up of compounds derived from both partners, called the “foot”. (3) The pollen grain emits a pollen tube that penetrates the papilla cell wall. (4) The pollen tube grows within the transmitting tract (tt) from the style to the ovary, to reach (5) the ovules (ov). (1-3, left) are SEM images. (3-5, right) are aniline blue staining images allowing the visualization of pollen grains and pollen tubes in bright blue. Bars, 10 µm when not specified on the images. Legends: Female partner: st = stigma, pa = papilla, tt = transmitting tract, ova = ovary, ov = ovules, fu = funiculus, mi = micropyle. Male partner: an = anther, pg = pollen grain, pt = pollen tube. Personal images.

The epidermis is the outer layer of plant and animal organisms acting as a boundary with the environment. In plants, the epidermis protects the internal tissues from outside chemical or mechanical damages associated with biotic or abiotic stresses, while specifically controlling exchanges with the environment and preventing water loss. In most cases, plant epidermis consists of a continuous and monolayer of cells that are structurally and functionally different depending on the organ they cover. For instance, tubular epidermal cells of the roots, called root hairs, are involved in water and nutrient absorption, guard cells of stomata at the surface of the leaves regulate gas exchanges and bulliform cells of *Ammophila arenaria* leaves mediate leaf rolling in stress condition to limit evapotranspiration. In flowers, epidermal cells play major roles in the reproduction process, such as the petal conical cells that accumulate scent to attract pollinators or the stigmatic cells at the extremity of the female organ that capture the male gametophytes.

I. The stigmatic epidermis, the first barrier to overcome to access the ovules

Success of fertilization is tightly linked to the result of the early communication event occurring at the female epidermal surface. Indeed, the first interaction that happens between male and female partners is the contact between the pollen grain, carrying the immotile sperm cells and the epidermal cells of the female organ (pistil). The upper side of the pistil terminates with a very specific tissue, the stigma, which in *Brassicaceae* species is composed of hundreds of unicellular elongated epidermal cells, called stigmatic cells or papillae (Heslop-Harrison and Shivanna, 1977). Once deposited on a stigmatic cell, a pollen grain adheres to the papilla surface and hydrates. After hydration, it germinates and produces a pollen tube that penetrates the stigma surface and then grows within the female tissues through the transmitting tissue of the style and the ovary to transport the male gametes towards the ovules where fertilization occurs. Fig. 1 illustrates the male – female interactions during the reproduction process that will be discussed in this introduction part.

I.1. An active interface

In Angiosperms, depending on plant families and species, stigmas have been classified into two groups: wet and dry stigmas (Heslop-Harrison and Shivanna, 1977). Wet stigmas, as in tobacco, are covered with viscous surface secretions containing proteins, lipids, and polysaccharides on which pollen grains hydrate spontaneously (Fig. 2a). On the contrary, in the *Brassicaceae* family, including for instance *Arabidopsis*

thaliana, *Arabidopsis lyrata*, *Brassica oleracea* and *Brassica napus*, stigmas are dry, which refers to the absence of abundant surface secretions, allowing early pollen selectivity by the female partner (Fig. 1, Fig. 2b). Binding assays suggest that the initial step of pollen adhesion onto the stigma surface is mediated by the pollen outer cell layer (Zinkl et al., 1999). Following adhesion, proteins and lipids from the pollen surface, composing the pollen coat, spread out and intermix with components of the stigma surface to establish a meniscus, called “foot”, required to create a hydrophilic environment essential for pollen hydration (Chapman and Goring, 2010). Formation of this interface is extremely rapid, within minutes after the first pollen contact in *A. thaliana*, and requires components of both surfaces. On the pollen side, pollen grains of *eceriferum (cer)* mutants, which are impaired in long-chain lipid synthesis normally present in the pollen coat, fail to hydrate on the stigma surface (Fiebig et al., 2000; Hulskamp et al., 1995; Preuss et al., 1993). Likewise, pollen hydration defects have been reported in mutants for the Glycine-Rich Protein 17 (GRP17), one of the most abundant pollen coat proteins (Mayfield and Preuss, 2000), as well as for Pollen Coat Protein (PCP)-class A and PCP-class B, both belonging to the small Cysteine Rich Protein family (Doughty 2000; Wang et al. 2017). On the stigma side, the papilla cell wall, covered with a waxy cuticle and a proteinaceous pellicle (Gaude and Dumas, 1986), exhibits unique properties compared with those of other epidermal cells. Mutant plants impaired in the *FIDDLEHEAD* gene, which encodes a protein that catalyzes elongation of fatty acids and affects cuticle function and water permeability, show abnormal pollen hydration and germination on leaf epidermis (Fig. 2c-d) (Lolle and Cheung, 1993; Lolle et al., 1992, 1997; Yephremov et al., 1999). Similarly, leaf epidermis of the *bodyguard* mutant supports pollen grain hydration and germination, normally restricted to stigma epidermis. BODYGUARD protein encodes an epidermis-specific extracellular hydrolase involved in cutin synthesis, the major biopolymers of the cuticle (Kurdyukov et al., 2006) (Fig. 2e). Taken together, these data suggest that the cuticle of papilla cells has unique water permeability generally not encountered in other epidermal cells. Moreover, Transmission Electron Microscopy (TEM) studies showed that the stigmatic cuticle is traversed by micro-channels proposed to represent an adaptation to allow water flow and transfer of nutrients towards the pollen grain (Elleman and Dickinson, 1994). Interestingly, immature stigmas, before papilla cells developed, are unable to support pollen hydration and germination suggesting that stigmatic factors required for successful early pollen-stigma interaction are synthetized during the course of stigma development (Ma et al., 2012).

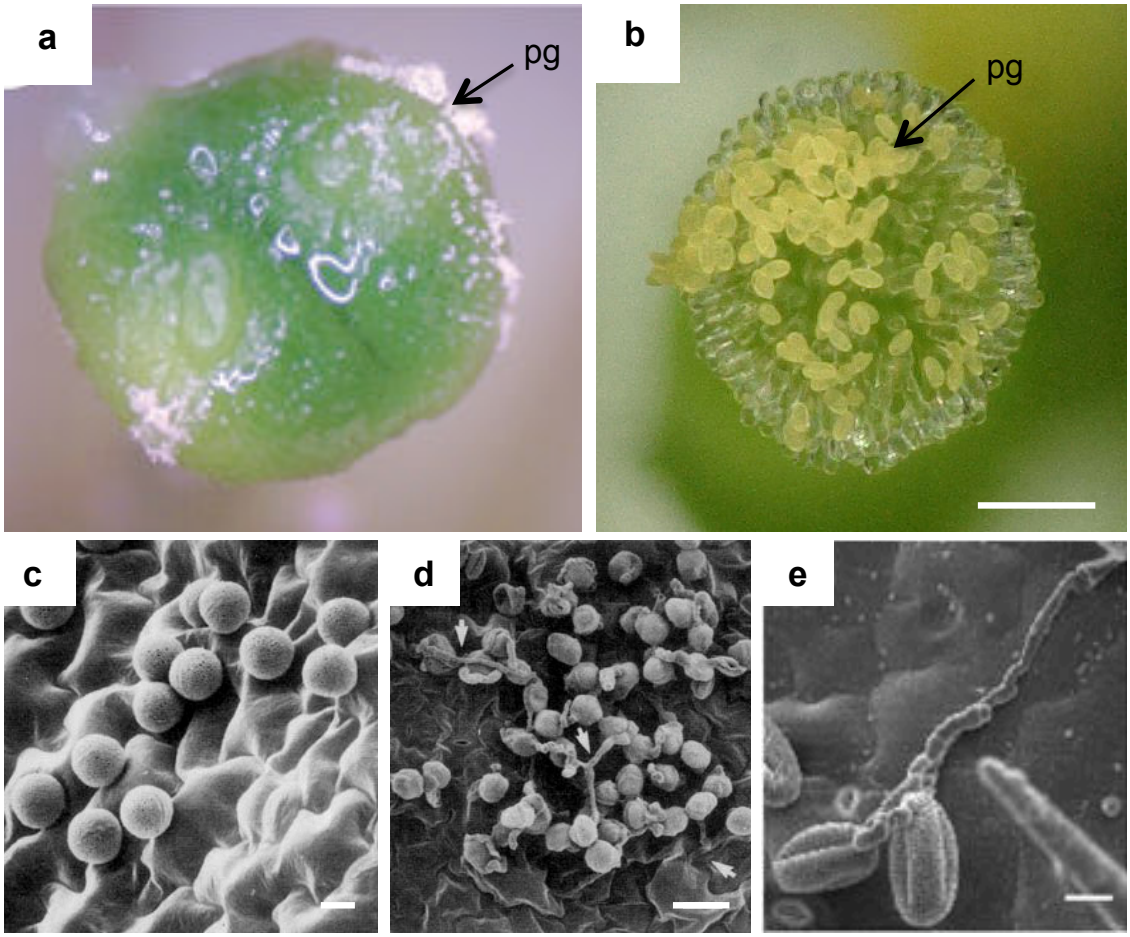

Fig. 2 / Stigma types and pollen hydration and germination.
a, Light microscopy top view of a wet *Nicotiana tabacum* stigma, with several pollen grains (pg); from https://www.imaging-git.com/science/electron-and-ion-microscopy. b, Light microscopy top view of the dry *A. thaliana* stigma pollinated with WT pollen grains (pg); personal image. c, SEM images of *A. thaliana* pollen grains on WT rosette leaf cells; some pollen grains adhere but do not germinate. Bar, 10 µm. d, SEM images of *A. thaliana* pollen grains on *fiddlehead* rosette leaf cells; some grains germinate (arrow). Bar, 20 µm; c-d, from Lolle and Cheung, 1993. e, Pollen grain germination on the *bodyguard* leaf epidermis; from (Kurdyukov et al., 2006).

I.2. Stigma papilla undergoes cytological changes following pollen tube penetration and growth

While the pollen starts to hydrate, some changes occur at the surface and within the stigmatic cells (illustrated in Fig. 3). One of the primary modification is the expansion of the stigmatic cell wall at the pollen contact point (Elleman and Dickinson, 1990, 1996; Elleman et al., 1992; Kandasamy et al., 1994). The papilla cell wall is divided into two sub-layers distinguishable by TEM: (i) the outer layer in contact with the cuticle is specific to the papillae and is expanded upon contact with the pollen grain and (ii) the inner layer homologous to a conventional cell wall (Elleman and Dickinson, 1994). The outer cell wall layer expansion is proposed to occurs by softening of the cell wall, permitting the pollen

tube entry and the pollen tube growth in a space generated between the two sub-layers (Elleman et al., 1992; Kandasamy et al., 1994). Concomitantly to the cell wall expansion, TEM studies showed that vesicles appear within the cell wall, beneath the pollen contact site (Dickinson, 1995; Elleman and Dickinson, 1994, 1996; Kandasamy et al., 1994). More recently, in Brassica, Goring and collaborators showed that multivesicular bodies (MVBs), an endocytic compartment normally destined to the vacuole for cargo degradation, are re-routed towards the stigmatic plasma membrane (PM) adjacent to the pollen grain (Safavian and Goring, 2013). MVBs are formed by invagination of the limiting membrane of late endosomes generating intraluminal vesicles, which are released into the extracellular space when MVBs fused with the plasma membrane. These extracellular vesicles, also named exosomes, are key players of the intercellular communication in animal cells (Maas et al., 2017). Vesicles detected in the stigmatic cell wall by early TEM studies may correspond to exosomes released from MVB fusion to the plasma membrane. Interestingly, neither MVBs nor exosomes were identified in Arabidopsis pollinated stigmas. Instead, secretory vesicles that fuse with the stigmatic plasma membrane were detected beneath the pollen grain (Indriolo et al., 2014; Safavian and Goring, 2013). Thus, extracellular vesicles in Brassica or secretory vesicles in Arabidopsis may participate in the exocytosis of material towards the pollen grain, such as cell wall enzymes, aquaporin for water transfer or other nutrients necessary to support the pollen activity (Goring, 2018). Interestingly, an Arabidopsis Ca^{2+} pump, ACA13, present in intracellular vesicles before pollination, accumulates at the plasma membrane at the contact site with the emerging pollen tube. Ca^{2+} export is required for pollen acceptance and ACA13 represents a putative transported cargo via the secretory pathway towards the stigmatic plasma membrane (Iwano et al., 2004, 2014).

While the involvement of polarized secretion in pollen acceptance has been clearly demonstrated, the way vesicles are specifically targeted to the plasma membrane region beneath the attachment site of the pollen grain remains unclear. In yeast, two subunits of the exocyst complex, Sec3 and Exo70, serve as spatial landmarks demarcating target PM domains as exocytic hotspots (Munson and Novick, 2006; Pleskot et al., 2015). The exocyst complex, conserved from yeast to mammals and plants, is composed of eight subunits and functions in tethering exocytic vesicles to the plasma membrane (Žárský et al., 2013; Zhang et al., 2010). Interestingly, this protein complex has been implicated in docking secretory vesicles in pollinated Brassica and Arabidopsis stigmatic cells (Safavian and Goring, 2013; Safavian et al., 2015; Samuel et al., 2009). Indeed, knockdown in *B. napus*, or knockout in *A. thaliana*, of exocyst subunit expression compromises pollen acceptance, and one component of the complex, the EXO70A1 protein, was found to be localised at the stigmatic plasma membrane (Safavian and Goring, 2013; Safavian et al.,

2015; Samuel et al., 2009). Several reports in yeast and animal cells showed that phosphatidylinositol (4,5)-bisphosphate (PIP2) together with small GTPases, contribute to the polarized localisation of the exocyst, notably the Sec3 subunit (He et al., 2007; Pleskot et al., 2015). Whether such components act as polarity determinants in pollination remains to be explored.

Secretory vesicles are typically transported along actin cables to reach the exocytic site (Ketelaar, 2013; Onelli et al., 2015; Thomas, 2012). The actin cytoskeleton of stigmatic cells was first showed by immunostaining to be unchanged following pollination in *B. napus* (Dearnaley et al., 1999). However, a more recent study contradicted this result (Iwano et al., 2007). By transient expression in *B. rapa* stigmatic cells of a GFP fused to the actin-binding domain of mouse talin, the authors described the formation of actin bundles focused at the pollen attachment site when pollen undergoes hydration. Moreover, treatment of the stigmatic cells with cytochalasin D, an actin-depolymerizing drug, significantly inhibits pollen hydration and germination. These observations are consistent with the assumption that polarized actin network might guide the vesicular secretion towards the pollen grain attachment site (Iwano et al., 2007).

Additionally, other cytosolic events triggered by pollination have been described. A pharmacological and genetic approach provided evidence that depolymerization of the stigmatic microtubule (MT) network is required for pollen acceptance in *B. napus* as well as in *A. thaliana* (Samuel et al., 2011). The authors hypothesized that MT breakdown beneath the pollen grain might facilitate and accelerate the delivery of resources from the stigmatic cell towards the pollen. In Brassica papillae, TEM and tomographic analysis revealed the presence of a large vacuole occupying the major volume of the cell, surrounded by tubular or smaller round vacuoles. Upon pollination, the vacuolar network is reorganised leading to the orientation of the large vacuole below the plasma membrane adjacent to the pollen grain (Iwano et al., 2007; Safavian and Goring, 2013). As the vacuole is the major storage compartment for inorganic ions and water, its extension towards the pollen grain may be involved in the delivery of vacuolar cargos necessary for pollen hydration and germination.

In conclusion, arrival of the pollen grain on the stigma surface releases cues that are sensed by the papilla cells and transduced into a variety of cellular modifications, such as active mobilization of the cytoskeleton, increased vesicular trafficking, and reorientation of the vacuole. These changes are necessary to hydrate the pollen grain, reactivate its metabolic activity and facilitate the entrance of the pollen tube.

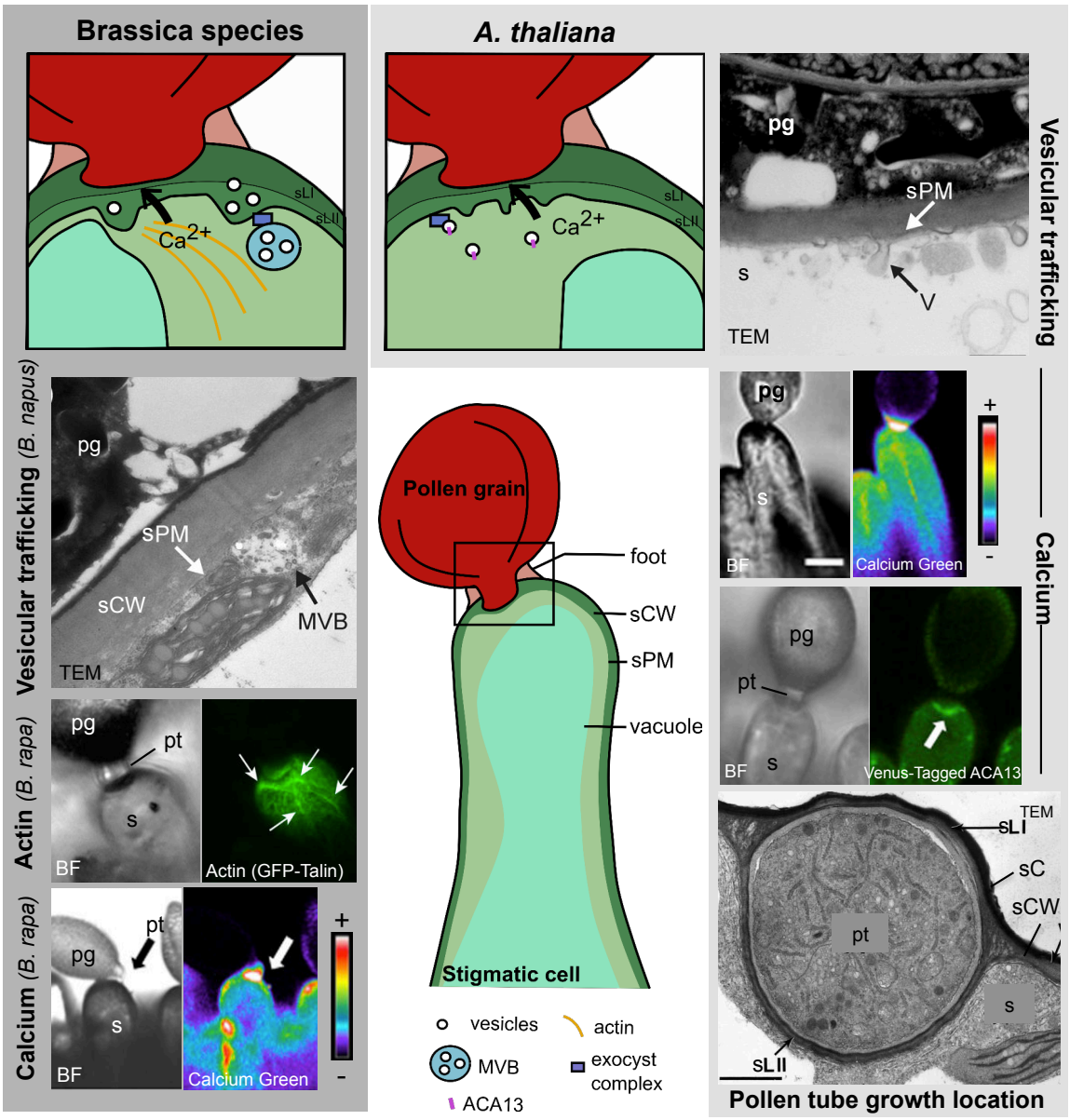

Fig. 3 / Papilla responses to pollen in Brassica species and *A. thaliana*.
The drawings represent cellular responses trigger by a pollen grain or an emerging pollen tube in Brassica or Arabidopsis papilla cells. Left (from top to bottom): MVBs (TEM images) accumulate at the pollen contact site in *B. napus* papilla, 5 minutes after pollination (map) (Safavian and Goring, 2013); Actin (GFP-Talin) bundle formation at the pollen tube contact site in *B. rapa*, 1.5 hours after pollen deposition (Iwano et al., 2007); Ca^{2+} export (calcium green assay) from the *B. rapa* papilla at the pollen germination contact site, 60 map (Iwano et al., 2014). Calcium Green images are shown in pseudo color with purple, low calcium concentration, and red, high calcium concentration (Iwano et al., 2014). Right (from top to bottom): Vesicles (TEM images) accumulate at the pollen contact site in *A. thaliana* papilla, 10 map (Safavian and Goring, 2013); Ca^{2+} export (calcium green assay) from the Arabidopsis papilla at the pollen germination contact site, 15 map (Iwano et al., 2014); The ACA13 (ACA13:ACA13-Venus), a Ca^{2+} pump, accumulates at the *Arabidopsis* papilla–pollen tube contact site (Iwano et al., 2014); *A. thaliana* pollen tube grows within the two layers of the stigmatic cell wall (TEM images) (Kandasamy et al., 1994). Legends: s = stigmatic cell, sCW = stigmatic cell wall, sPM = stigmatic plasma membrane, LI = outer layer of the stigmatic cell wall, LII = inner layer of the stigmatic cell wall, pg = pollen grain, pt = pollen tube, MVBs = multi-vesicular bodies, v = vesicles. BF = brightfield images, TEM = transmission electron microscopy

I.3. Female cues are necessary for proper pollen tube guidance within the pistil

After germination of the tube, the male partner has to properly find its way within the pistil tissues to deliver the sperm cells to the ovules, deeply hidden and protected in the ovary. The distance that the tube has to cover may be several tens of centimeters depending on the plant species. To reach its target, the pollen tube, which grows by tip-growth (see I.3.2.1), has to invade a series of tissues chemically and mechanically different. It has first to pass through the stigmatic cell wall and then it follows its journey in the extracellular matrix of the transmitting tract, a specialized secretory tissue of the style and ovary (Lennon et al., 1998). After emerging from this nutritive tissue, the tube has to progress along the surface of the funiculus, a structure that connects ovules to the ovary, and finally moves toward the ovule and enters the embryo sac through the micropyle (Mizuta and Higashiyama, 2018). Consequently, the pollen tube is continuously constrained during its path to the ovules, and both chemical as well as mechanical cues have to be taken into account to fully understand the pollen tube orientation and guidance within the female organ.

I.3.1. Chemical cues that direct pollen tube growth

Efforts have been made to identify molecules responsible for pollen tube guidance and several studies, at the end of the past century, showed that the embryo sac is the source of diffusive attractive signals (Higashiyama et al., 1998; Hulskamp et al., 1995; Ray et al., 1997). Consequently, for a long time, the stigma and style were considered as unnecessary for pollen tube guidance (Hulskamp et al., 1995; Sogo and Tobe, 2005). Work of Higashiyama group on *Torenia fournieri*, a unique plant with naked embryo sacs, contributed significantly to reveal the importance of the upper part of the pistil in pollen tube guidance. These authors developed a semi-*in vitro* assay wherein pollen tubes growing through a cut pistil emerge at the cut end of the style and continue to elongate in the medium (Higashiyama et al., 1998). In this assay, germination on the stigma and passage through the cut style were necessary to guide the pollen tubes towards isolated ovules placed in the medium, while pollen tube germinated directly on the medium never reached the naked embryo sacs. Thus, passage through the stigma/style tissues must activate the pollen tubes competency to perceive the ovule guidance signals. Pollen tubes of lily and *A. thaliana* are also attracted to ovules when passing first through the stigma/style tissues (Janson et al., 1993; Palanivelu and Preuss, 2006). Interestingly, in this latter work, some *A. thaliana* pollen grains germinated on the excised stigma and

produced tubes that did not penetrate the style but rather elongated directly on the medium towards the ovules. This observation suggested that contact with the stigma was sufficient to confer pollen tube guidance competency (Palanivelu and Preuss, 2006). Alternatively, guidance signals directly emitted by the upper part of the pistil may also exist. In 2005, Kim and collaborators, using an *in vitro* chemotropism assay coupled with biochemical and proteomic approaches, identified a lily (*Lilium longiflorum*) stigma chemotropic compound, the plantacyanin (Kim et al., 2003). The plantacyanin gene, strongly expressed in lily stigma, encodes a cell wall protein of unknown function that triggers the reorientation of pollen tube growth *in vitro*, a process known as chemotropism. *A. thaliana* plantacyanin, which is more abundant in the transmitting tract of the style and the ovary, has been proposed to similarly orient pollen tube growth *in vivo* (Dong et al., 2005). In lily, glycoproteins secreted in the transmitting tract of the style were found to mediate adhesion with the stylar matrix to guide the pollen tubes to the ovules (Mollet et al., 2000; Park et al., 2000). In addition, a stigma/stylar lipid transfer protein isolated in lily, SCA, cannot induce chemotropism by itself but is proposed to enhance the chemotropic activity of the plantacyanin by facilitating its access to the pollen tube to control its directional growth (Kim et al., 2003). In *A. thaliana*, the SCA-like small secreted peptide is also involved in pollen tube guidance (Chae et al., 2009). In conclusion, the stigma/style tissues are not only a route for the pollen tube but also have an active role in guiding the tubes to their final destination by either activating pollen tube competency to perceive deeper guidance signals or by directly secreting chemotropic or adhesive compounds.

After emerging from the transmitting tract, the pollen tube switches to ovular guidance. The most known ovular attractants are the LURE peptides, secreted by the two synergid cells of the embryo sac. *LURE* genes (*LURE1* and *LURE2*) were first identified in *T. fournieri* and encode cysteine-rich polypeptides (CRPs). Purified LURE peptides were shown to attract pollen tubes *in vitro* (Okuda et al., 2009). AtLURE1 peptides were identified in *A. thaliana* and have the capacity to attract *A. thaliana* pollen tubes *in vitro* and *in vivo* (Takeuchi and Higashiyama, 2012). Interestingly, *T. fournieri* and *A. thaliana* pollen tubes germinated *in vitro* do not reach the isolated ovules but become competent to LURE peptide attraction after passing through a cut pistil in a semi-*in vitro* assay (Okuda et al., 2009; Takeuchi and Higashiyama, 2012). Similarly, a methyl-glucuronosyl arabinogalactan (AMOR), synthetized by *T. fournieri* ovules induces competency of the pollen tube to LURE peptides after passing though the stigma/style tissues (Mizukami et al., 2016). Thus, these data reinforce the idea that passing through the entire pistil including the stigma is essential for pollen tubes to acquire capacity to sense ovular guidance cues.

At the final guidance step, the pollen tube passes through the micropylar gate to enter in one synergid cell where it bursts to release the sperm cells. Pollen tube burst is regulated by Receptor-Like Kinases (RLKs), among them the FERONIA (FER) protein has a central role. FER protein is localised at the plasma membrane of the synergid cells and in loss-of-function mutants, pollen tube fails to arrest its growth and never burst (Huck et al., 2003; Rotman et al., 2003). It has been proposed that FERONIA may recognize ligand from the pollen tube and triggers molecular cascade leading to proper pollen tube reception (Escobar-Restrepo et al., 2007). The molecular aspects of pollen tube burst and delivery of the male gametes into the embryo sac have been thoroughly described in a recent review by Mizuta and Higashiyama (2018).

The guidance of pollen tubes has been extensively studied during the past decades, and has exemplified above, most progress in this field has been done on other species than *A. thaliana*, such as lily for which pollen can easily germinate *in vitro*, or *T. fournieri*, which became a model plant due to is unique embryo sac protruding from the ovule. In addition, because pollen tube guidance is a dynamic process that takes place deep inside the female organ, most work was done *in vitro* or *in semi in vitro* conditions. The next challenges for the future will be to develop *in vivo* live-cell imaging taking into account the deepness of the interaction. Development of such methods seems required to better characterize guidance molecules but also to understand how the pollen tube responds to guidance signals to control its growth direction from the stigma to the embryo sac.

I.3.2. Biophysical aspects of pollen tube growth

As described above, most of the work on pollen tube guidance has been done using *in-vitro* systems, in other words, without the real constraints that the tube has to face while growing within the female organ. Indeed, during its travel, it has to pass through several barriers that likely exhibit different mechanical properties: (i) The stigmatic cell wall, although softened by the pollen tube secretions, constitutes a relatively stiff material, (ii) The transmitting tract, where the tube elongates, is a dense, stiff and fibrous extracellular matrix (Agudelo et al., 2012; Lennon et al., 1998), (iii) Emerging from the transmitting tract, the tube has to reach the funiculus and finally (iv) it has to penetrate one synergid cell to deliver the male gametes. This part is dedicated to deciphering the mechanical cues that permit a pollen tube to navigate through these changing landscapes.

I.3.2.1. Mechanism driving pollen tube elongation

The pollen tube is the fastest growing plant cell known. For instance, maize pollen tube can reach up to 1 cm per hour (Mascarenhas, 1993). The growth speed appears as a competitive factor for fertilization (Delph et al., 1998). Pollen tube growth has been extensively studied and is well documented (see Cameron and Geitmann, 2018; Heilmann and Ischebeck, 2016; Michard et al., 2017; Obermeyer and Feijó, 2017) and occurs by tip-growth, meaning that the expansion takes place exclusively at the apex of the tube (Fig. 4a) (Damineli et al., 2017).

Pollen tube tip growth is based on massive secretion that targets vesicles to the tube apex in a reverse fountain flow (Fig. 4b). Through constant exocytosis of vesicles containing cell wall precursors, enzymes and membrane material, new components are brought to the tip for cell wall and membrane expansion. Importance of the secretory machinery has been demonstrated thanks to drug treatments. Indeed, *Picea meyeri* pollen tubes treated with Brefeldin A, an inhibitor of secretion, where found to display an altered cell wall composition and a modified morphology of the tip associated with a wavy growth (Fig. 4c,d) (Wang et al., 2005). This polarized secretion was shown to depend on actin filaments, which are oriented towards the tube extremity (Fig. 4b) (Daher and Geitmann, 2011; Kroeger et al., 2009).

Pectin (see part II.2.2) are important components of the tip cell wall and secretion of flexible methyl esterified pectins towards the apex enhances wall softness, allowing its deformation by the turgor pressure, motor of the elongation (Rojas et al., 2011). At the opposite, deposition of callose as well as de-esterified pectins behind the tip region, at the shank, is proposed to rigidify the tube sides (Parre and Geitmann, 2005; Zerzour et al., 2009). Pectin modifications involved the action of pectin methylesterase enzymes (PME) (see part II.2.2) and de-esterified pectins, generated by PME, are cross-linked by calcium to rigidify the cell wall (Bosch et al., 2005). Thus, PMEs, affecting the mechanical properties of the wall, control the balance of esterified/de-esterified pectins limiting the expansion to the tip zone to maintain a cylindrical growth pattern. Additionally, these coordinated mechanisms confer resistance to tension stresses, preventing the tube to burst when embedded in the female tissue. Mechanical properties of the tip and the shank regions were shown to be different, with a softer apex compared to the shank, measured during pollen tube growth by micro-indentation (Zerzour et al., 2009).

A second characteristic of the pollen tube is its elongation via a pulsatile process, with periods of rapid growth separated by slower or stopped elongation periods. Interestingly, measurement of calcium gradient at the tip of Arabidopsis pollen tubes growing *in vitro* revealed that oscillations of calcium, mediated by Ca^{2+}-influx channels,

are correlated with growth fluctuations (reviewed in Feijó et al., 2001; Michard et al., 2017). However, this model is currently a matter of debate as Damineli et al. (2017), using high resolution measurements combined with computational methods found that Ca^{2+} oscillations are not necessarily couple with growth, calcium spikes being detected upon pollen tube growth arrest.

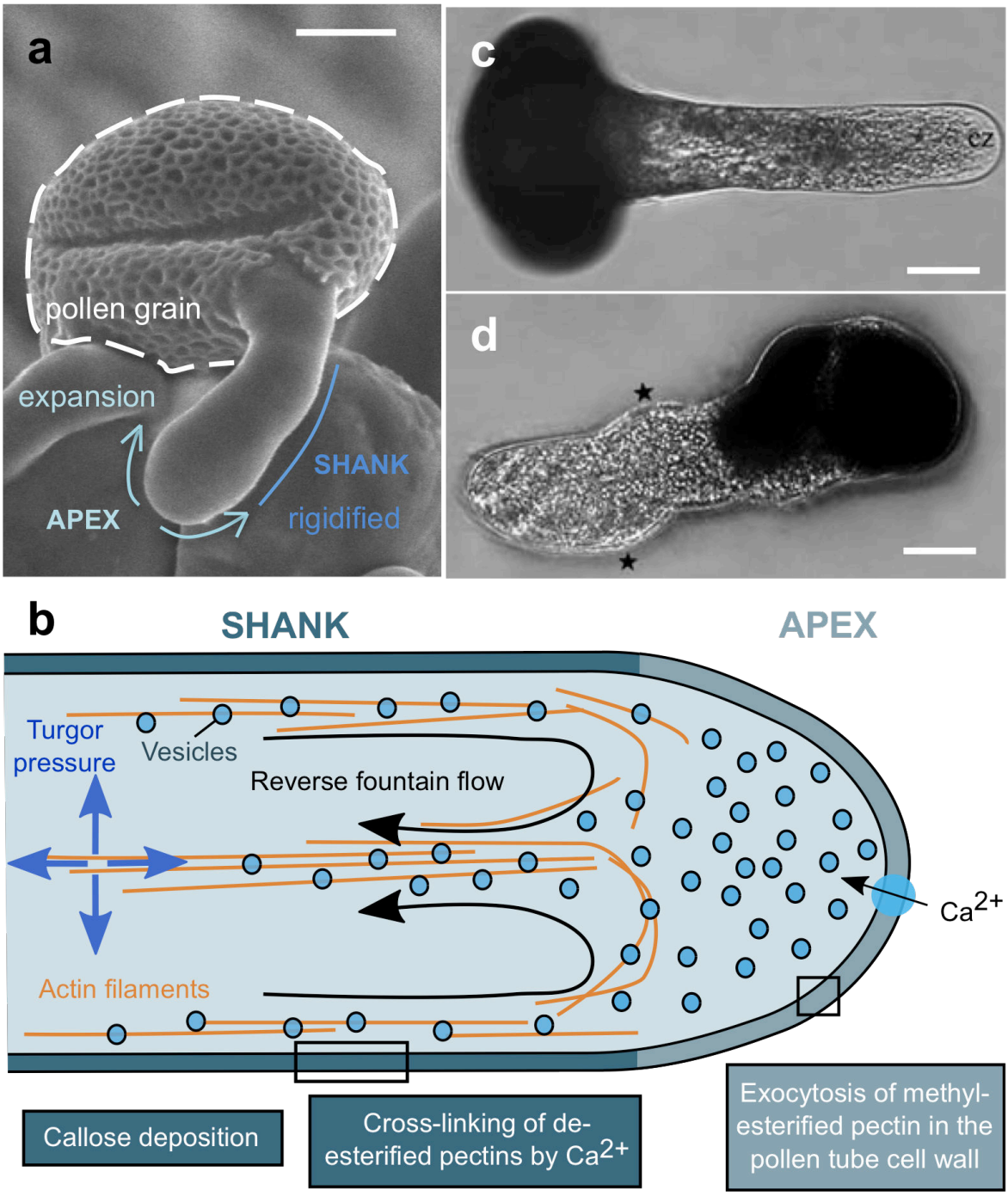

Fig. 4 / Mechanisms of pollen tube elongation.
a, *A. thaliana* pollen tube grows by expansion of its tip. Bar = 5 µm. Personal SEM image. b, Pollen tube elongation is mediated by turgor pressure and involves vesicle trafficking (in blue). Vesicles containing cell wall material and enzymes are secreted at the tip through actin filaments (orange). Pectins can be modified by pectin methyl-esterases (PMEs) and interaction with calcium confers different mechanical properties to the tube cell wall. The tip cell wall is soft and can deform; the

shank is rigid and resists to deformation. Adapted from (Cameron and Geitmann, 2018). c-d, Effect of Brefeldin A (BFA) inhibition on *Picea meyeri* pollen tube growth. Bars, 50 µm. From (Wang et al., 2005). c, *P. meyeri* pollen tube growth on standard medium during 36 hours leads to elongation of the tube at the apex. d, *P. meyeri* pollen tubes growing on BFA (5 µg/mL) containing medium have a larger tube and display aberrant wavy (asterisk) growth.

I.3.2.2. Pollen tubes are able to apply pushing forces and react to mechanical cues

Although pollen tube is able to secrete enzymes to soften the papilla cell wall, it also has to apply sufficient forces to penetrate it and elongate within various substrates. This pushing force exerted by the pollen tube is generated by the cytoskeleton and the hydrostatic turgor pressure (Sanati Nezhad and Geitmann, 2013). An *in vitro* assay of *Papaver rhoeas* pollen tubes, growing in different agarose concentration layers, demonstrated the importance of the pollen tube actin cytoskeleton in generating penetration forces. Indeed, depolymerization of actin filaments by latrunculin B decreased number of tubes able to penetrate the 1 to 3% agarose boundary (Gossot and Geitmann, 2007). The turgor pressure, which is characteristic of walled cells, such as plant cells, is created by water movement between the inside and the outside of the cell and relies on differences in concentrations of osmotically active molecules. Hydrostatic pressure, to generate pushing forces, can only act on a plastic cell wall, which, in the case of the pollen tube, corresponds to the apex, thus driving the pollen tip growth. Recently, the exerted force was recorded by a combination a cellular force microscope, force sensors and lab-on-chip devices (see next part), and was estimated at 3 µN in the apical part of the *A. thaliana* pollen tube (Burri et al., 2018).

To successfully find the path through complex matrix, ability to generate forces has to be coupled with the capacity to direct growth and avoid obstacles. Over the past few decades, many studies have highlighted the capacity of the pollen tube to perceive and quickly respond to mechanical obstacles. Microfluidic devices that originate from the Micro Electro Mechanical Systems field have been used, such as the lab-on-chip (LoC) or TipChip devices. These miniaturized platforms allow the monitoring of the ability of a single pollen tube to grow in individual microchannel with very different paths, designed to mimic the pollen tube *in vivo* microenvironment (Fig. 5a,b) (Agudelo et al., 2012, 2013; Ghanbari et al., 2014; Sanati Nezhad and Geitmann, 2013). These experiments revealed that a pollen tube is able to grow straight ahead if it does not encounter any mechanical obstacle and deviates immediately after contacting an obstacle, resulting in zigzag or curved trajectories through the microchannels (Fig. 5c). Moreover, when a pollen tube enters in collision with an obstacle, it adjusts its growth speed to reorient its direction,

depending on the collision angle (Agudelo et al., 2012) (Fig. 5d-e). When the pollen tube arrives perpendicularly (angle 90°) to the obstacle, its growth rate is dramatically decreased, whereas with a less pronounced angle (40°) its growth rate remains almost unchanged. This result is consistent with the fact that the tube has to make a higher turn when contacting an obstacle at 90°, which probably requires more time to the elongation machinery to reorient the tube growth (Agudelo et al., 2012). During its way to the ovules, the tube passes through narrow spaces, for example when it emerges from the transmitting tract. To mimic the compression stress that tubes can encounter during their growth, LoC system with microchannels containing narrow regions (microgaps) were designed (Fig. 5f) (Sanati Nezhad et al., 2013; Yanagisawa et al., 2017). Pollen tubes were able to adjust their width to enter in the microgap and return to their normal size when they get out from the narrow passage. Moreover, at the first contact with the microgap, the pollen tube growth rate decreases, then stays stable across the wider space. After passing the gap, the growth rate increases at the gap exit. These experiments reflect the flexibility of the pollen tube and demonstrate its ability to modulate its growth when it encounters an obstacle, slowing down when the constraint is too high.

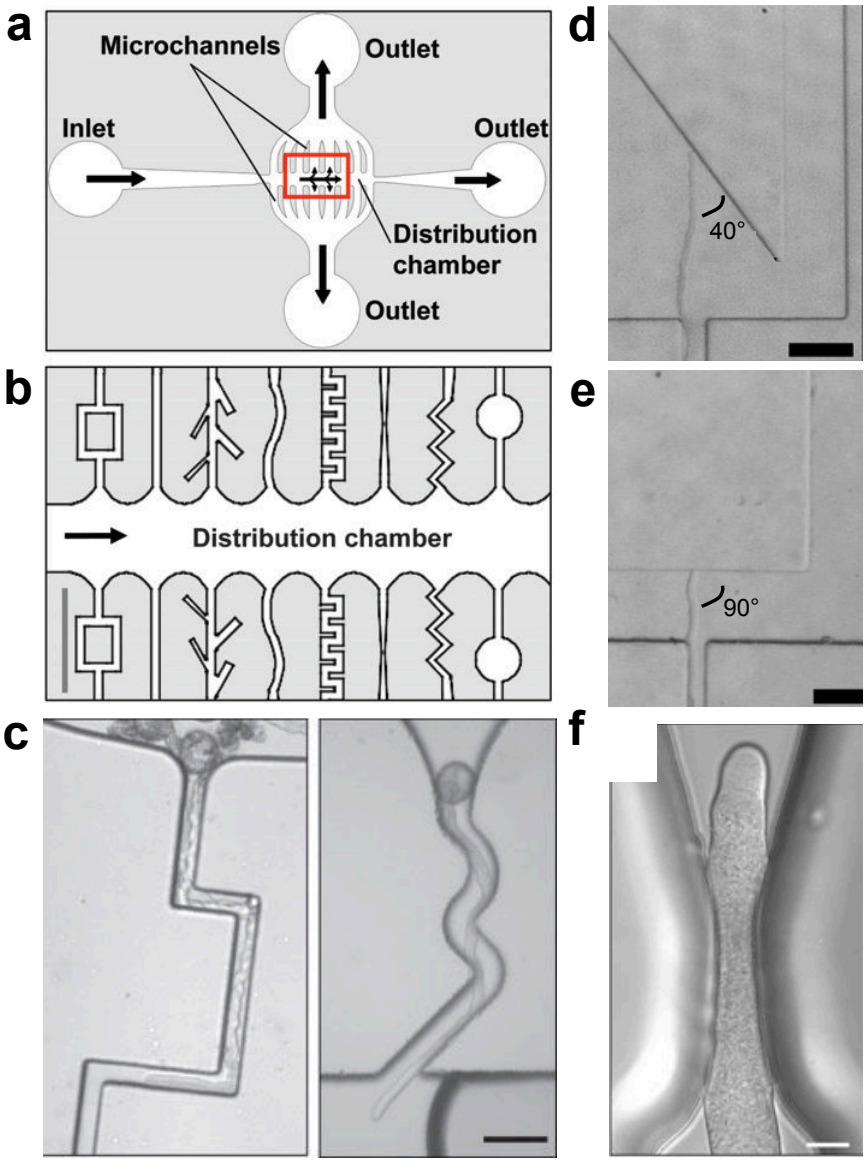

Fig. 5 / Pollen tube ability to face mechanical obstacles.
a-c. Microfluidic device used to monitor single pollen tube growth through microchannels; from (Agudelo et al., 2013). a, General design of the microfluidic network. Pollen tubes are deposited in the "inlet" part and move to the distribution chamber by means of a fluid flow. Pollen grains are then captured at the microchannel entries. b, Different microchannel geometries. c, Examples of camellia (*Camellia japonica)* pollen tubes path through microchannels with various geometries. Bar= 100 µm. d-f, Collision experiments, from (Agudelo et al., 2012). d-e, *A. japonica* pollen tubes collision with obstacles at (d) 40° and (e) 90° angles. Bars = 100 µm. f, Pollen tube passage through narrow gap; from (Sanati Nezhad et al., 2013).

Development of microfluidic platforms has improved our understanding of how a pollen tube is mechanically guided within a complex organ such as the pistil. The ability of the pollen tube to sense and react to the surrounding environment suggests that mechanosensitive receptors are likely to be present at the apex of the growing tube. Interestingly, two cell wall sensor receptors, ANX1 and ANX2, have been shown to

prevent early tube bursting out of the synergid (Miyazaki et al., 2009), and are localised to the apical region of the pollen tube (Boisson-Dernier et al., 2009). These two receptors belong to a protein family whose one member, FERONIA, functions not only in pollen tube reception (see section I.3.1.) but also controls root growth in response to environmental mechanical cues (Shih et al., 2014).

II. Mechanical properties influence cell behaviour

II.1. The cell wall properties reside in its structure and composition

As described above, mechanical properties of the medium in which the pollen tube grows play a crucial role in its behaviour. One of the most challenging aspects of the pollen tube growth is to bypass the stigmatic cell wall barrier whose main function is to protect the female organ against invaders. However, no clear data are available on the mechanical properties of the papilla cell wall, apart from TEM images showing papilla cell enlargement following tube growth, suggesting that mechanics may have a role in early pollen stigma interactions. Plant cell walls are divided into two classes; the primary cell wall deposited during cell growth and division and the secondary cell wall deposited when cells stopped growing and acquired specialized functions such as those from vessel. As papillae do not have specialized functions that required secondary cell wall synthesis, in this introduction part, we will focus only on structure and mechanical properties of the primary cell wall. Primary cell walls are thin and flexible, displaying many mechanical features such as strength, resistance to deformation, extensibility and anisotropy. The cell wall can resist to the high turgor pressure of the cell, pushing on the plasma membrane (Beauzamy et al., 2015). Wall mechanical properties reside in its structure and composition: a network of rigid cellulose microfibrils (CMFs) embedded in a viscous and cross-linked matrix of pectin and hemicellulose chains and proteins (Cosgrove, 2000). Many studies have decrypted the biochemical composition of cell wall components (see (Cosgrove, 2001; Park and Cosgrove, 2015) for further information). As illustrated in Fig. 6, the cell wall is a complex and dynamic network, where the various components can cross-link together and hence lead to a variety of networks with different mechanical properties. Here, I will only focus on the main components of the cell wall and their modifications that can affect or confer mechanical properties to the wall.

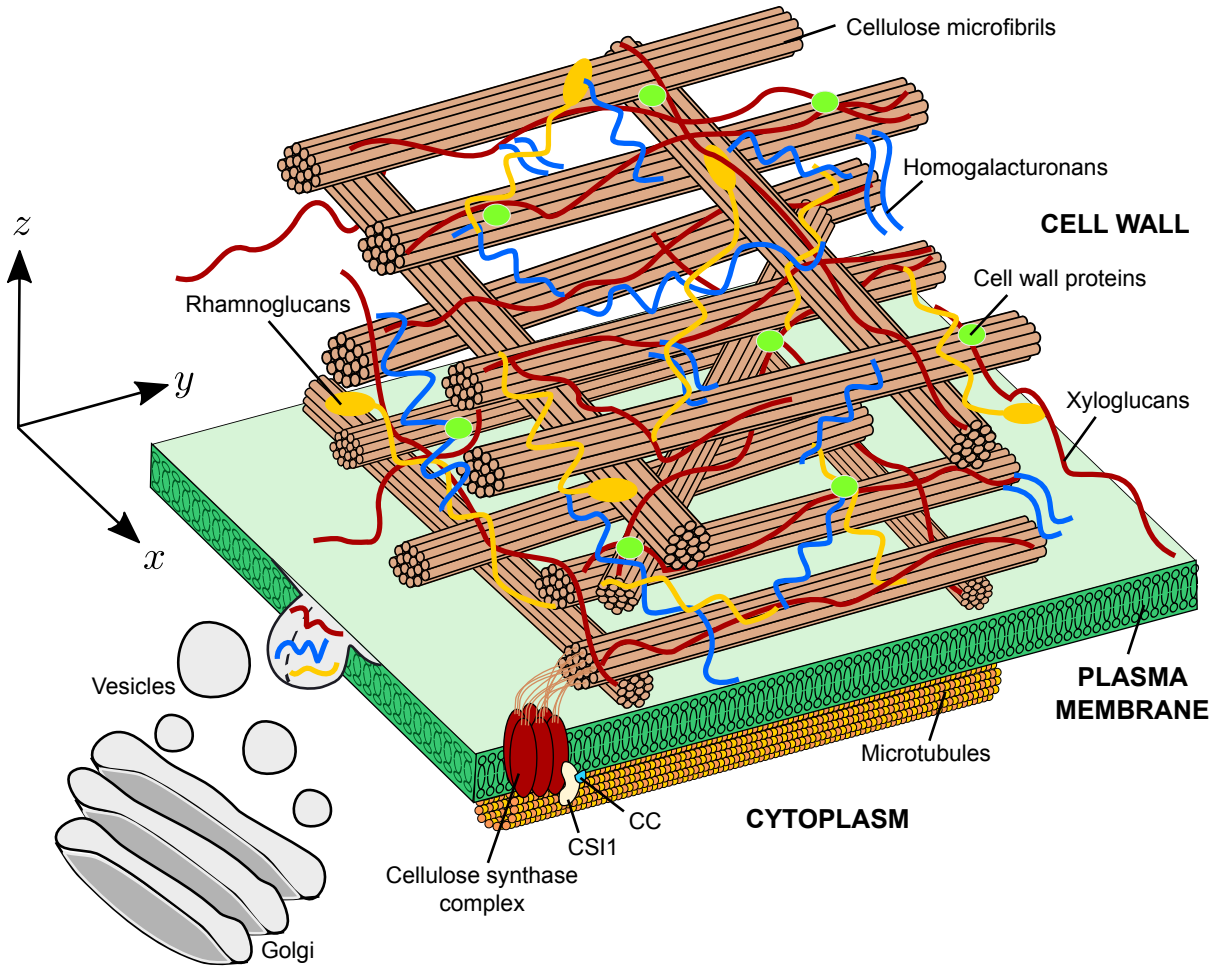

Fig. 6/ Schematic and simplified representation of the plant cell wall.
The main components are cellulose, hemicellulose (xyloglucans), pectins (homogalacturonans and rhamnogalacturonans) and proteins. Hemicellulose and pectins are synthetized in the Golgi and exocytosed to the cell wall. Synthesis of cellulose at the plasma membrane is achieved by the cellulose synthase complexes, linked to the microtubules via cellulose synthase interacting 1 (CSI1) and companion of cellulose synthase (CC). Inspired by (Lampugnani et al., 2018).

II.1.1. The cellulose microfibrils, the load-bearing elements of the cell wall

The cellulose, the most abundant polymer on Earth, is considered as the load-bearing element of the wall (Johnson et al., 2018). The crystalline cellulose microfibrils (CMFs) (Fig. 7a) are long polysaccharides made up of linked β-1,4-glucan linear chains, synthesised at the plasma membrane by cellulose synthase (CESA) proteins, which associate to form the cellulose synthase complexes (CSCs) generally organised in rosette (Arioli et al., 1998). It was previously established by TEM that a CSC is composed by 6 hexamer of 6 CESA subunits, producing therefore 36 individual cellulose chains to constitute one microfibrils (Herth, 1983). However, the number of CESAs by rosette and therefore the number of individual cellulose chains to constitute a CMF is under debate since the existing model has been revised to 18 or 24 (Nixon et al., 2016; Thomas et al.,

2013). In *A. thaliana*, 10 members compose the CESA gene family (Richmond and Somerville, 2000; Taylor, 2008). Genetic and biochemical studies have revealed a role for CESA1, CESA3, CESA6, CESA2, CESA5 and CESA9 in the biosynthesis of *A. thaliana* primary cell wall (Bringmann et al., 2012a; Desprez et al., 2007; Persson et al., 2007; Schneider et al., 2016; Turner and Kumar, 2018). Using CESA labelled with fluorescent proteins, Paredez et al. (2006) demonstrated that CESA complexes move along cortical microtubule (CMT) tracks (Fig. 6, Fig. 7b-d) (Paredez et al., 2006). CSCs migrate to the plasma membrane at around 200 to 350 nm/min (Desprez et al., 2007; Paredez et al., 2006). The newly synthetized CMFs are delivered into the extracellular space and then aggregate and interconnect with other wall components to form the cell wall structure.

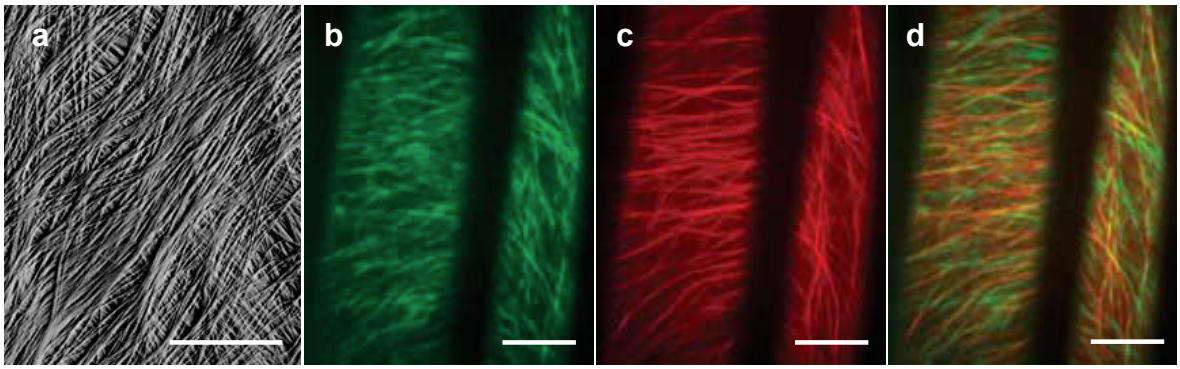

Fig. 7 / Interactions between cellulose and microtubules.
a, AFM image of the inner surface of onion epidermal cell showing the CMF organisation. Bar, 500 nm. From (Zhang et al., 2014). b-d, Alignment of CMTs and CSC trajectory in Arabidopsis etiolated hypocotyl cells. Bars, 10 µm. b, YFP:CESA6 for CESA trajectory labelling, c, CFP:TUA6 for labelling microtubules. d, Colocalisation of YFP:CESA6 and CFP:TUA6. From (Paredez et al., 2006).

The cellulose crystallinity and polymerisation degree of CMFs play a major role in influencing their mechanical properties (Johnson et al., 2018). Individual microfibrils, around 3.5 nm wide, can be detected by Atomic Force Microscopy (AFM) or Field Emission Scanning Electron Microscopy (FESEM), and are often oriented in a common direction, organised in a dense network, as observed in the cell wall of onion epidermal cells (Fig. 7a) (Cosgrove, 2014). The stiffness of cell wall is between 10 MPa to 10 GPa. When measured individually, the cellulose microfibrils are the stiffest components of the wall, with about 100 GPa, whereas hemicellulose (about 40 MPa) or pectin network (with 10 to 200 MPa) are softer (Mirabet et al., 2011). The CMF anisotropy is also crucial in wall reinforcement (Louveaux et al., 2016; Nakayama et al., 2012; Sampathkumar et al., 2014). Extensibility tests have been performed *in vitro* on onion epidermal cells, and they showed that extension of the cell wall is larger when the pulling force is applied transversally to the net CMF orientation, compared with when it is applied longitudinally to

it. This provides evidence that the wall mechanical anisotropy is conferred by the predominant orientation of CMFs, which is considered to orient cell growth direction (Suslov and Verbelen, 2006). The highly organised network of CMFs is also dynamic, microfibrils being deposited by layers. The newest ones are formed at the plasma membrane and move outward when new layers are synthesised, deplacing the oldest ones. Besides, CMF orientation can be subjected to shift between each layer depending on the wall tension and stretching (Cosgrove, 2018; Zhang et al., 2017). These variations of the CMF orientation lead to variations in the mechanical properties of the cell wall (Höfte and Voxeur, 2017; Johnson et al., 2018).

Modifications of cellulose can be performed by cellulases or endo-1-4-β-glucanases, such as KORRIGAN. Located at the membrane, KORRIGAN belongs to the glycoside hydrolase family9 (GH9) and has been reported to be associated with the CSCs (Vain et al., 2014). The *kor* mutant displays a dwarf phenotype with defects in the cell walls, notably a reduced cellulose content (Szyjanowicz et al., 2004). However, it remains unknown whether the GH9 enzymes have a direct role in wall loosening. Additionally, the *kor* mutant displays change in the pectin composition of cell walls of epidermal cells in *A. thaliana* (His and Driouich, 2001), reinforcing the idea that the cell wall is an intricate structure, regulated by feedbacks between its components.

II.1.2. Hemicelluloses and their roles in wall structure

Hemicellulose (HC) is a family of diverse polysaccharides composed of β-1,4 linked sugar backbones in an equatorial configuration. Sugar chains include xyloglucans (XyGs), xylans, mannans and glucomannans (Scheller and Ulvskov, 2010). Synthesised in the Golgi apparatus, they are transported to the cell wall by exocytosis (Fig. 6). The major hemicelluloses in dicot species are the xyloglucans, composed of α-(1-6)-xylosyl residues. It was firstly assumed that the major role of xyloglucans was to coat and tether CMFs together to constitute the load bearing network reinforcing the wall (Albersheim et al., 2010; Scheller and Ulvskov, 2010). This constitutes the “tethered” model of the primary cell wall structure (Fig. 8a) (Cosgrove, 2016). The xyloglucan xylosyltransferases (XXT) participate in xyloglucan biosynthesis in *A. thaliana.* The double loss-of-function mutant *xxt1 xxt2* have been shown to be deprived of xyloglucans and to exhibit a reduced hypocotyl cell wall stiffness and an aberrant cellulose organisation (Cavalier et al., 2008; Xiao et al., 2016). But strikingly, although lacking this key component of the cell wall, *xxt1 xxt2* plants display a mild growth phenotype (Cavalier et al., 2008; Johnson et al., 2018; Park and Cosgrove, 2012a; Xiao et al., 2016). It was suggested that this lack of xyloglucans could be compensated by other wall components. However, associated with

this apparent contradiction with the tethered model, nuclear magnetic resonance (NMR) results demonstrated that interactions between xyloglucans and cellulose are actually limited (Dick-Pérez et al., 2011). In cucumber (*Cucumis sativus*), an endoglucanase that hydrolyses both xyloglucans and cellulose and targets cellulose-xyloglucans polysaccharides, was found to promote irreversible extension of the cell wall by disassembling the microfibrils (Park and Cosgrove, 2012). On the contrary, specific cellulose or xyloglucan endoglucanases do not provoke such an irreversible extension of the cell wall (Park and Cosgrove, 2012a). Accumulating data on the relationship between cellulose, HC and the mechanical properties of the cell wall, have led to reconsider the established cell wall model. A new model, named the “biomechanical hotspot” model (Fig. 8b) was proposed by Cosgrove and collaborators, in which CMFs are directly linked to hemicellulose in a limited number of cross-links, hence reducing the enzyme accessibility to these hotspots. These hotspots would be the location of the action of endoglucanases and expansins, which would act to promote cell wall relaxation by separating CMFs (Cosgrove, 2016; Höfte and Voxeur, 2017).

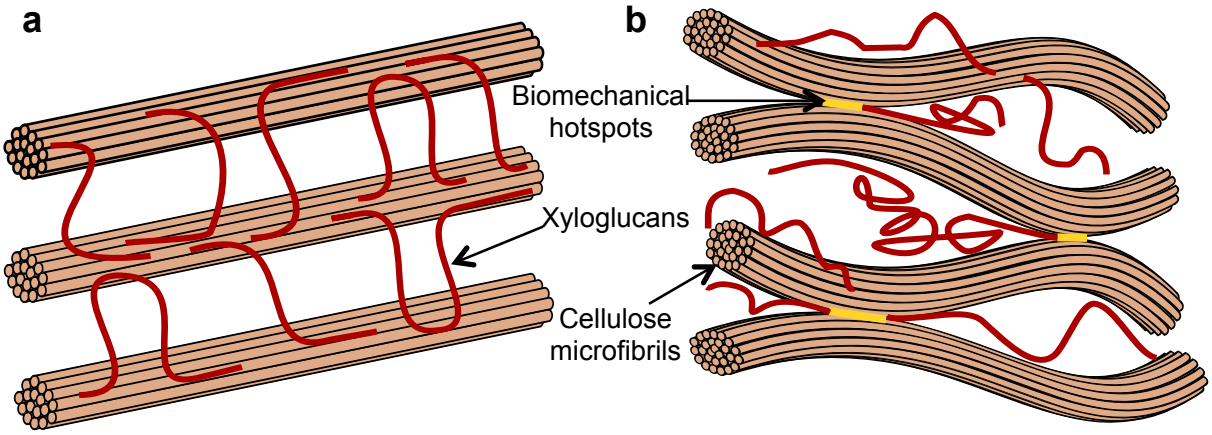

Fig. 8/ Two models for the structure of the primary cell wall.
a, The “tethered network”, where CMFs are separated by xyloglucans. b, The “biomechanical hotspots” model where a mix of cellulose – xyloglucans are present in a limited number of connections. These hotspots (yellow) permit a limited access to endoglucanases and expansins. Inspired by (Cosgrove, 2016).

Expansins are involved in cell wall loosening. The pH is crucial for many aspects of plant development and although clear enzymatic activity of expansins has not been demonstrated, many studies have suggested that low pH activates expansins, leading to dissociation between CMFs and xyloglucans and inducing wall loosening (Cosgrove, 2000, 2018; Lampugnani et al., 2018).

II.1.3. Pectins and their roles in mechanical properties

Pectins are a heterogeneous group of complex polysaccharides, enriched in galacturonic acid (Harholt et al., 2010). Synthesised in the Golgi apparatus in methyl-esterified forms, they are delivered to the wall by exocytosis (Fig. 6). Pectins form a network composed of homogalacturonans (HGs), the most abundant pectin, and rhamnogalacturonans (RGs) (Fig. 6). Various combinations of these elements covalently linked lead to formation of various specific pectin molecules (Atmodjo et al., 2013). Pectins have the capacity to link to proteins, forming a hydrogel network that stabilizes the cell wall (Tan et al., 2013). This network can be modified by enzymes such as pectate lyases, which cut homogalacturonans, or endo-/exo-polygalacturonases that hydrolyses pectin. Additionally, homogalacturonans, transported into the wall, undergo demethylesterification (removal of their methyl groups and exposing negative charges) by the pectin methylesterases (PMEs) (Wolf and Greiner, 2012). The *A. thaliana* genome contains 66 PMEs and 64 pectin methylesterase inhibitors (PMEIs) that negatively modulate PME activity (Pelloux et al., 2007). Catalytic activity of PMEs and PMEIs has been reported to play an important role in influencing wall mechanical properties and organogenesis, by either stiffening or loosening the cell wall depending on conditions. The pollen tube growth process represents a well-documented example of PME impact on wall mechanics (see section I.3.2.1.). When PME activity occurs in clusters, this will form blocks of free carboxyl groups that can interact with Ca^{2+} and create a stiff gel. If PMEs randomly esterify polymers of homogalacturonans, this leads to the release of protons, promoting the action of pectinase enzymes such as polygalacturonases or pectate lyases, severing the network and loosening the cell wall (Chebli and Geitmann, 2017; Höfte and Voxeur, 2017; Micheli, 2001). In addition, in the inflorescence meristem, overexpression of PME5, associated with a decrease of pectin methylesterification, leads to primordia formation, accompanied by a softer cell wall. At the opposite, PMEI3 overexpression leads to an increase of pectin methylesterification and inhibits primordia formation correlated with a stiffer wall (Peaucelle et al., 2008, 2011).

II.1.4. Cell wall proteins

Cell wall material is also regulated by proteins (see an overview in Albenne et al., 2014), and proteomic analyses of cell wall (Albenne et al., 2013; Duruflé et al., 2017) provided considerable insight into the variety of proteins trapped into the cell wall network. They play an important role in modifying cell wall components and participate in conferring the specific properties of the wall. Structural proteins such as arabinogalactan proteins

(AGPs), proline-rich proteins (PRPs), hydroxyproline-rich glycoproteins (HRGPs) or extensins have been identified. Some receptor-like kinases (RLKs) also known as cell-wall sensors, affect wall composition and dynamics. Interestingly, the mutation of the RLK THESEUS1 has been shown to partially restore growth defects of the *cesa6* mutant, such as alteration of hypocotyl elongation, even if it does not attenuate the cellulose synthesis defects (Hématy et al., 2007). Additionally, the FERONIA RLK was suggested to act as a regulator of the wall integrity (Höfte, 2015) and of mechanical signalling (Shih et al., 2014).

Finally, the cell wall is a complex and dynamic structure, where mechanical properties reside in the interaction and crosslinks between all its components. As mentioned earlier, the cytoskeleton, through the function of CMTs in orienting transport of CSCs to the plasma membrane, plays a crucial role in the construction of the cell wall. Mechanical anisotropy of the wall has been reported to mainly depend on the orientation of CMFs, which defines growth direction (Baskin, 2005; Baskin and Jensen, 2013; Bringmann et al., 2012; Sassi et al., 2014). In the next part, I will discuss the essential role of CMTs in cellulose orientation.

II.2. Microtubules and cell mechanics

II.2.1. CMTs and cellulose guidance

Although a high number of studies have reported that the orientation of CMFs aligns with that of CMTs in many tissues, other work has contradicted this statement, suggesting that CMT and CMF colinearity is not that strict. Indeed, transverse CMF deposition was observed in cases where CMT arrays were disorganised, for instance in the thermosensitive mutant *mor1-1* or in the XyG xylosyltransferases *xxt1 xxt2* mutant (Himmelspach et al., 2003; Xiao et al., 2016). Nevertheless, strong evidence supports the idea that CSCs are predominantly guided by CMTs, as CSCs were found to be physically linked to the CMT network via the CELLULOSE SYNTHASE INTERACTIVE 1 (CSI1) (Li et al., 2012) and the Companion of Cellulose Synthase (CC) proteins (Endler et al., 2015) (Fig. 6). In agreement with this observation, mutation in CSI1 leads to changes in CMT and CSC dynamics (Bringmann et al., 2012b; Mei et al., 2012). The close link between CMTs and CMFs suggests that CMF orientation can be modified via alterations of the CMT network. Indeed, disruption of the CMT pattern by the microtubule-depolymerising drug oryzalin disorganises CMF arrays (Baskin et al., 2004). But additionally, there is a feedback loop between cellulose synthesis and microtubule organisation, as following treatment with isoxaben, a drug that inhibits cellulose synthesis, disorganisation of CMT

pattern occurs in tabacco cells as well as conifer pollen tubes (Fisher and Cyr, 1998; Lazzaro et al., 2003). In this way, because the mechanical properties of the cell wall are strongly linked to the orientation of CMFs, the organisation of the CMTs is commonly used as a proxy to predict the cell wall anisotropy and mechanical properties of a cell (Hamant et al., 2008; Hervieux et al., 2016; Sassi et al., 2014). This raises the question of what controls CMT orientation.

II.2.2. Microtubule structures and functions

At the beginning of the 20th century, microtubules were detected and described as tubular or filamentous structures present in eukaryotic cells. With the emergence of improved transmission electron microscopy techniques in the 60s, these hollow tubes were found to be localised beneath the plasma membrane, parallel to cellulose microfibrils, and were called “microtubules” (Ledbetter and Porter, 1963). Despite their name, and with around 25 nm-diameter compared with 8 nm for actin filaments, microtubules are the largest type of filaments in the cell. They are formed from self-assembly of the GTP-binding α- and β-tubulin monomers (Goddard et al., 1994), organised in helix and forming 13 protofilaments assembled side by side around a hollow core to form the tubular microtubules. They are polar, the + end extremity elongates faster than the – one, and assembly and disassembly of tubulin heterodimers are mediated by GTPase activity (Desai and Mitchison, 1997). Organised in an extremely dynamic array, microtubules grow and shrink continuously (Mitchison and Kirschner, 1984). Microtubules cross other microtubules at crossover spots, and in function of the contact angle, they can depolymerize or polymerize. Events such as nucleation, severing, or bundling are critical for CMT dynamics and therefore crucial in assuring their functions.

To this end, CMTs are associated with various proteins, called Microtubule-Associated-Proteins (MAPs) that regulate their dynamic and organisation. Many MAPs exist in *A. thaliana* and their roles have been described in various reviews (Elliott and Shaw, 2018; Hamada, 2007, 2014). For instance, among other functions, MAP65 family proteins are known to promote CMT stability and regulate formation of bundles (Mao et al., 2006).

Orientation of CMT arrays results from the self-organisation of individual microtubules (Wasteneys and Ambrose, 2009) and involves severing activity, necessary to form an ordered CMT pattern (Lindeboom et al., 2013; Wightman and Turner, 2007; Wightman et al., 2013; Zhang et al., 2013). The KATANIN severing protein cuts microtubules at their crossover sites and plays a major role in their self-organisation. This heterodimeric protein is composed of a catalytic 60kDa and a regulatory 80kDa subunit

(McNally and Vale, 1993). The 60kDa subunit requires ATP hydrolysis to sever microtubules (Hartman and Vale, 1999). KATANIN plays a crucial role in plant growth, development and morphogenesis. Conserved in all eukaryotes, KATANIN is a well-studied severing protein, identified by several groups in *A. thaliana* under different names such as BOTERO1 (Bichet et al., 2001), KATANIN1 (Burk et al., 2001), FRAGILE FIBER 2 (Burk et al., 2001), KSS (McClinton et al., 2001), Atp60 (Stoppin-Mellet et al., 2002), LUE1 (Bouquin et al., 2003). Loss of KATANIN function leads to dwarf plants, which display aberrant cell growth associated with defects in most of the vegetative organs, such as round and thick leaves, and thick and shorter stems (Bichet et al., 2001; Bouquin et al., 2003; Burk et al., 2001; Panteris and Adamakis, 2012). The *katanin* phenotypes were shown to result from a reduced expansion of cells (Bichet et al., 2001; Burk and Ye, 2002) associated with defects in cell division (Panteris et al., 2011). Although *katanin* tip growing cells, such as pollen tubes, are not affected (Bichet et al., 2001), lower fertility and seed set were reported in *fra2*, *lue1* and *ktn1-2* (Luptovčiak et al., 2017). Anther and embryo development are altered, mutants exhibiting shorter anthers, shorter siliques, associated with a lower number of seeds than wild-type (WT) plants, highlighting a role for KATANIN in embryo and seed formation (Luptovčiak et al., 2017). At the cellular level, *katanin* mutants display a less dynamic and highly isotropic (disorganised) microtubule arrays in many tissues, such as root epidermal cells, stem cells, sepal or meristematic cells (Bichet et al., 2001; Burk and Ye, 2002; Hervieux et al., 2016; Uyttewaal et al., 2012). This isotropy of CMTs is accompanied by an isotropy of CMFs (Burk and Ye, 2002). Among the proteins that regulate KATANIN, the Rho-Of-Plant 6 (ROP6) and its interacting protein *ROP*-interactive CRIB motif-containing proteins 1 (RIC1) were identified as playing a key role in katanin activity during pavement cell morphogenesis (Lin et al., 2013).

As mentioned above, severing activity at crossover sites is crucial for the establishment of an ordered pattern, and this is also regulated by the microtubule-associated protein SPIRAL2 (SPR2). The *spr2* mutation was initially described to confer a specific morphology of the mutant plant, with leaf petioles, petals and hypocotyls twisting in right-handed helical growth (Furutani et al., 2000; Shoji et al., 2004). SPR2 was found to localise at the CMT crossover sites and it was suggested that it prevented severing activity, counteracting the function of KATANIN (Wightman et al., 2013). However, severing activity at crossover sites where SPR2 was present has been recently detected (Fan et al., 2018). However, in the *spr2-2* mutant, the lifetime of the crossover is decreased, hence reducing CMT severing. SPR2 has also been shown to localise to and to stabilize microtubule minus ends. Contrary to *katanin* mutants, in the *spr2* mutant the reorientation of CMTs is reduced, leading to an increase in the final anisotropy of CMT arrays (Fan et al., 2018; Nakamura et al., 2018).

II.2.3. CMT role in cell mechanics

Through its role in guiding CSCs, CMTs indirectly participate in the establishment of the cell wall properties. Indeed, in most cases, aligned CMTs induce a similar alignment of CMFs, and hence stiffen the cell wall. Additionally, CMTs also play a more direct role in conferring cell mechanical properties. To measure the role of CMTs in cell mechanics, independently of that of the cell wall, protoplasts were used and compressed between two plates at various forces (Durand-Smet et al., 2014). Treatment with oryzalin that depolymerizes CMTs, provoked a significant decrease of the protoplast rigidity, arguing for a direct role of CMTs in the mechanical properties of the cell. But how environmental conditions, and in particular mechanical stresses induced for instance by the growth of pollen tubes in stigma papillae or during an infection process, can affect cell mechanics and CMT organisation? Within the past decades, many studies have suggested a link between mechanical stress and the cytoskeleton, and especially the CMTs. It has been shown that cells are able to sense and react to mechanical stress by modifying their CMT network (Hamant et al., 2008). Pressing with a needle a cotyledon epidermal cell provokes a reorganisation of CMTs at the site of contact with the needle (Hardham et al., 2008), whereas compressing cells bundles the CMT network (Louveaux et al., 2016). Upon mechanical stress, CMTs reorient parallel to the maximal tensile stress direction in cells and tissues (Hamant et al., 2008; Landrein and Hamant, 2013; Uyttewaal et al., 2012). Mutants affected in CMT pattern and dynamics have been reported to display altered responses to mechanical stress, such as a slower response to mechanical stress in *katanin* mutants (Hervieux et al., 2016; Uyttewaal et al., 2012) or an enhanced one in *spr2-2* (Shoji et al., 2004; Buschmann et al., 2004; Hervieux et al., 2016), reinforcing evidence linking CMTs with mechanical stress.

II.2.4. Role of mechanical stress role in cell shape

Plant morphogenesis appears strongly dependent on the close relationship between CMTs, CMFs and mechanical properties of the cell. Indeed, cell growth is oriented by the anisotropy of the mechanical properties Fig. 9 and is regulated by feedback control where mechanical stress affects CMTs that in turn affect CMF orientation and growth direction. A highly anisotropic CMT pattern leads to an anisotropic CMF deposition (geometrically but also mechanically) and reinforces the cell wall in the direction of CMFs, orienting the growth direction perpendicularly to the CMFs. This modifies cell shape and can explain the *katanin* phenotype mentioned above.

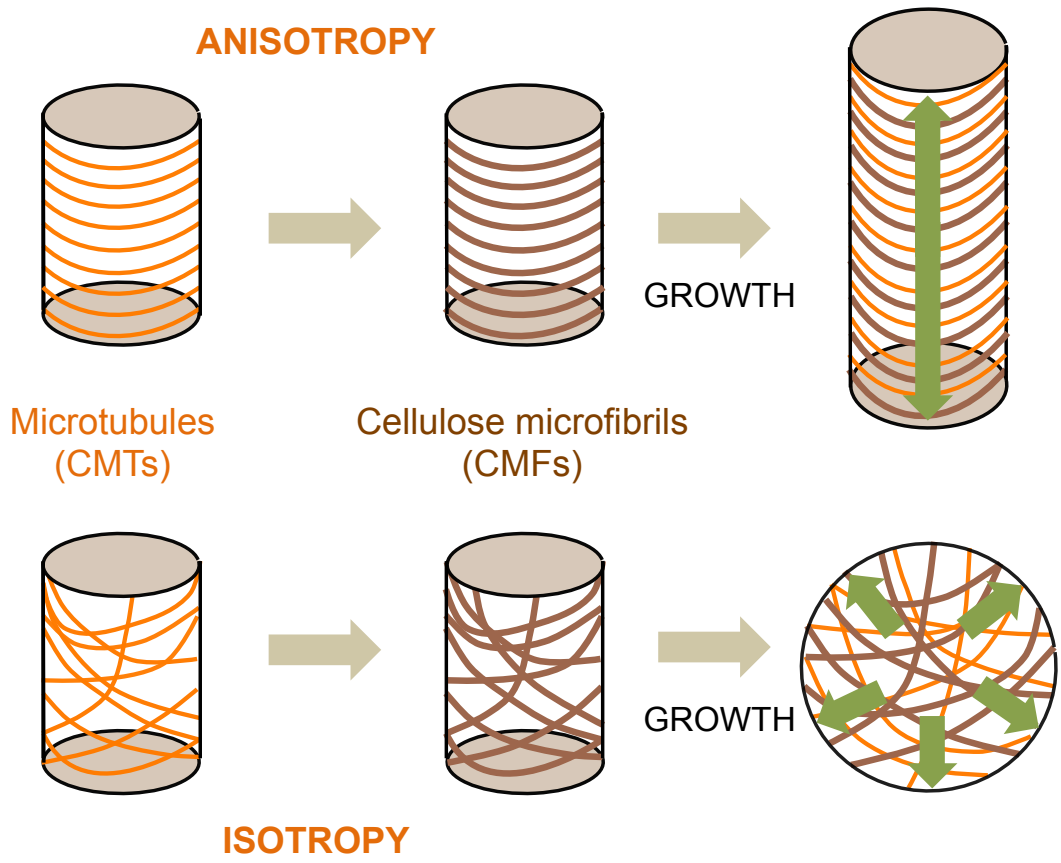

Fig. 9/ The main direction of cell growth depends on the CMT / CMF anisotropy.
Orientation of CMTs generally defines CMF orientation, through guiding the cellulose synthases along the CMTs. Anisotropic pattern reinforces the wall in the direction of CMFs and promotes growth, perpendicularly to the CMFs. On the contrary, in the case of randomly oriented CMFs, cell growth becomes isotropic.

At an organ level, differential growth between cells induces mechanical forces and conflicts between adjacent cells that impact their shape (Coen and Rebocho, 2016). One of the most evident examples of this is the pattern made by the jigsaw puzzle-like shaped cells at the epidermis of many plant leaves. At their initial stage of development, epidermal cells are polygonal with straight cell walls and then they acquire their specific shape composed of alternation of lobes and necks (Fu et al., 2005). To acquire this final geometry, coordination and communication between the neck of one cell and the lobe of its neighbouring cell is necessary, presumably by inhibition of outgrowth to form a lobe on one cell and deformation of the second cell. This involves feedback and various scale interactions of cell wall, cytoskeleton and their mechanical properties. A well organised CMT network has been shown to restrict expansion in the neck (Wasteneys and Galway, 2003), by regulating CMF deposition, while the presence of actin promotes lobe formation (Frank and Smith, 2002; Fu et al., 2002). The final shape has also been shown to be mediated by localised variations in the stiffness of adjacent cell walls. A correlation has been done between shape and mechanical properties, where cell wall of curved regions

was stiffer than straight ones. Alteration of cell wall mechanical properties modifies cell shape and also changes the lobe number (Majda et al., 2017). In the constitutively active *rop2* (CA-*rop2*) transgenic line, where pavement cells have partially lost their indented shape (Fu et al., 2002; Li et al., 2001), AFM measurements revealed that *CA-rop2* pavement cells have more homogeneous mechanical properties than WT (Majda et al., 2017). This is an example of how the mechanical properties of one cell can affect the shape of a neighbouring one.

Finally, thanks to the coordination of all the actors described here, the cell regulates its mechanical properties, and influences its surrounding environment.

2

Thesis objectives and strategies

The experimental work of my PhD thesis was divided into two main objectives, which both were focused on the same cellular model, the stigmatic epidermal cell. First, I investigated the role of the mechanical properties of stigmatic cells in pollen tube growth and guidance, and second, I explored how stigmatic cells respond to different types of invasive organisms, i.e., the pollen tube as a positive cell-cell interaction for the plant, leading to seed set, and Oomycete hyphae, as an example of negative interaction causing infection.

Role of the mechanical properties of stigmatic cells in pollen tube trajectory

The oriented growth of the pollen tube has been the object of numerous studies based on *in vitro* and semi-*in vivo* experiments. They allowed the discovery of chemical attractants produced by the pistil that function as guidance cues for the pollen tube progression. In addition, they demonstrated that pollen tube is able to perceive and react to mechanical constraints by modulating its growth, suggesting that mechano-perception plays a crucial role in regulating pollen tube path. Astonishingly, knowledge about the mechanical properties of the female tissues and on their possible impact on pollen tube growth are poorly documented.

The first challenge of my PhD work was to investigate the link between the mechanical properties of the stigmatic tissue and the pollen tube path *in vivo* in *A. thaliana*. As mechanical properties of plant cells are correlated with the microtubule network, we first asked whether CMT of papilla cells may act on pollen tube growth by analysing mutants impaired in microtubule pattern and dynamics. Secondly, as microtubules guide cellulose synthase complexes responsible for the production of cellulose microfibrils in the cell wall, we investigated the mechanical properties of the papilla cell wall in mutants affected in microtubule dynamics or cell wall composition and examined pollen tube path in these mutants.

Results of this work have been submitted to BioRxiv under the identification number BIORXIV/2018/384321.

Stigmatic epidermal cell response to Oomycete infection and pollen tube growth

Taking the stigmatic cell as “responding cell”, the aim of the second objective of my thesis was to compare the cellular response of stigmatic cells following infection by two Oomycetes (*Phytophtora parasitica* and *Hyaloperonospora arabidopsidis*) (“negative

interaction"), with that following interaction with pollen tubes ("positive interaction"). This later work was done in collaboration with the Interactions Plantes – Oomycètes (IPO) team of the Institut Sophia Agrobiotech in Nice Sophia Antipolis, France.

First, we investigated whether these two oomycetes were capable of infecting the female tissue, and we monitored the cellular events triggered by the papillae in response to infection and compared these cellular modifications with those observed with their natural host root cells. By setting up a live imaging system, we then monitored the subcellular reorganisation occurring within the stigmatic cell after both pollen tube and hyphal growth. Finally, taking advantage of transcriptomic data generated by our two groups, we made a comparative analysis of the molecular response triggered by each type of invasive organism and crossed the cellular with molecular findings. A manuscript describing this work is under preparation.

3

Role of the mechanical properties of stigmatic cells in pollen tube trajectory

KATANIN-dependent mechanical properties of the stigmatic cell wall regulate pollen tube pathfinding

Lucie Riglet[1], Frédérique Rozier[1], Chie Kodera[1], Isabelle Fobis-Loisy[1*] and Thierry Gaude[1*]

[1]Laboratoire de Reproduction et Développement des Plantes, Université de Lyon, ENS de Lyon, UCBL, INRA, CNRS, 46 Allée d'Italie, 69364 Lyon Cedex 07, France
*e-mail: thierry.gaude@ens-lyon.fr ; isabelle.fobis-loisy@ens-lyon.fr

This article is the version of the article we deposited on BioRxiv the August 3, 2018.
(doi: https://doi.org/10.1101/384321)

Abstract

Successful fertilization in angiosperms depends on the proper trajectory of pollen tubes through the pistil tissues to reach the ovules. Pollen tubes start their path by progressing within the cell wall of the papilla cells, applying pressure to the wall. Mechanical forces are known to play a major role in plant cell shape by controlling the orientation of cortical microtubules (CMTs), and hence deposition of cellulose microfibrils (CMFs). Here, by combining cell imaging and genetic approaches, we show that isotropic orientation of CMTs in aged, *katanin1-5* (*ktn1-5*) or oryzalin-treated papilla cells is accompanied by a tendency of pollen tubes to coil around the papillae. In addition, using atomic force microscopy, we uncover that aged and *ktn1-5* papilla cells have a softer cell wall. Altogether, our results suggest that KATANIN-dependent control of microtubule dynamics, and associated mechanical anisotropy of stigmatic walls, mediate pollen tube growth directionality.

Introduction

Following deposition of dehydrated pollen grains on the receptive surface of the female organ, the stigma, pollen rehydrates, germinates and produces a pollen tube that carries the male gametes toward the ovules where the double fertilization takes place. This long itinerary through the different tissues of the pistil is finely controlled, avoiding misrouting of the pollen tube and hence assuring proper delivery of the sperm cells to the female gametes. In *Arabidopsis thaliana*, pollen tubes grow within the cell wall of papillae

of the stigmatic epidermis, and then through the transmitting tissue of the style and ovary (Lennon and Lord, 2000). The transmitting tissue has an essential function in pollen tube guidance, providing chemical attractants and nutrients (Crawford and Yanofsky, 2008; Higashiyama and Hamamura, 2008). In contrast to these accumulating data showing the existence of factors mediating pollen tube growth in the pistil, whether guidance cues exist at the very early stage of pollen tube emergence and growth in the papilla cell wall remains largely unknown. The cell wall constitutes a stiff substrate and hence a mechanical barrier to pollen tube progression. There are numerous examples in animal cells demonstrating that mechanical properties of the cellular environment, and in particular rigidity, mediate cell signalling, proliferation, differentiation and migration (Discher et al., 2005; Ermis et al., 2018; Fu et al., 2010). In plant cells, cell wall rigidity depends mainly on its major component, cellulose, which is synthesized by plasma membrane-localised cellulose synthase complexes (CSCs) moving along cortical microtubule (CMT) tracks (Paredez et al., 2006). While penetrating the cell wall, the pollen tube exerts a pressure onto the stigmatic cell (Sanati Nezhad and Geitmann, 2013). Such physical forces are known to reorganise the cortical microtubules (CMTs), which by directing CSCs to the plasma membrane, reinforce wall stiffness by novel cellulose microfibril (CMF) synthesis (Paredez et al., 2006; Sampathkumar et al., 2014). Hence, there is an intricate interconnection between CMT organisation, CMF deposition and cell wall rigidity (Xiao and Anderson, 2016; Xiao et al., 2016). A major regulatory element of CMT dynamics is the KATANIN (KTN1) microtubule-severing enzyme, which allows CMT reorientation following mechanical stimulation (Louveaux et al., 2016; Sampathkumar et al., 2014; Uyttewaal et al., 2012). Here we investigated whether the CMT network of papilla cells might contribute to pollen tube growth and guidance in stigmatic cells by combining cell imaging and genetic approaches. We found that CMT network of papilla cells is modified with ageing, CMT bundles being anisotropic at anthesis and becoming isotropic at later stages of stigma development. This change in CMT organisation was accompanied by a modification of the direction of pollen tube growth, which passes from predominantly straight to coiled. In the *ktn1-5* mutant, papilla cells exhibited a strong CMT isotropy associated with a marked tendency of wild-type (WT) pollen tubes to turn around the papilla. Coiled growth of pollen tubes was also observed on stigma papillae treated with the CMT-depolymerizing drug oryzalin, although at a lower extent. Faster growth of coiled pollen tubes was observed in aged WT as well as *ktn1-5* papillae, which both were found to exhibit softer cell walls. Additionally, we tested a series of cell wall mutants, including mutants having CMT disorganisation and decreased cell wall rigidity and, unexpectedly, none of them used as female induced coiled growth of WT pollen tubes. Altogether, our results strongly suggest that CMT organisation and cell wall mechanical

properties dependent on KTN1 have a major role in guiding early pollen tube growth in stigma papillae.

Results

CMT dynamic pattern and pollen tube growth during stigma development. To assess the functional role of stigmatic CMTs in pollen – papilla cell interaction, we first analysed their organisation in papillae at stages 12 to 15 of stigma development as described (Smyth et al., 1990) (Fig. 10a,b). We generated a transgenic line expressing the CMT marker MAP65.1-citrine under the control of the stigma specific promoter SLR1 (Fobis-Loisy et al., 2007). Before (stage 12) and at anthesis (stage 13), the CMTs were aligned perpendicularly to the longitudinal axis of papilla cells and were highly anisotropic (median value of 0.40) (Fig. 10c,d). At stage 14, when anthers extend above the stigma, the CMT pattern became less organised, with a higher variability in anisotropy values. Finally, at stage 15 when the stigma extends above anthers, CMT anisotropy had a median value of 0.09 indicative of an isotropic orientation of CMTs (Fig. 10c,d). These findings reveal that the papilla CMT cytoskeleton is dynamic during development, with a change of CMT array orientation from anisotropy to isotropy. We then wondered whether this change in CMT organisation could be correlated with pollen tube growth. To this end, we self-pollinated Col-0 papillae from stages 12 to 15 and examined pollen tube growth one hour after pollination by scanning electron microscopy (SEM) (Fig. 11a). At stage 12 and 13, we found most (~60%) pollen tubes to grow straight in the papillae, whereas about 30% and 10% of tubes made half-turn or one turn around stigmatic cells, respectively (Fig. 11b). At later stages of development, the tendency to coil around the papillae dramatically increased, with more than 35% of pollen tubes at stage 14 and more than 55% at stage 15 making one or more than one turn around papillae. These results suggest that CMT organisation in the papilla impacts the direction of growth of pollen tubes and that loss of CMT anisotropy is associated with coiled growth.

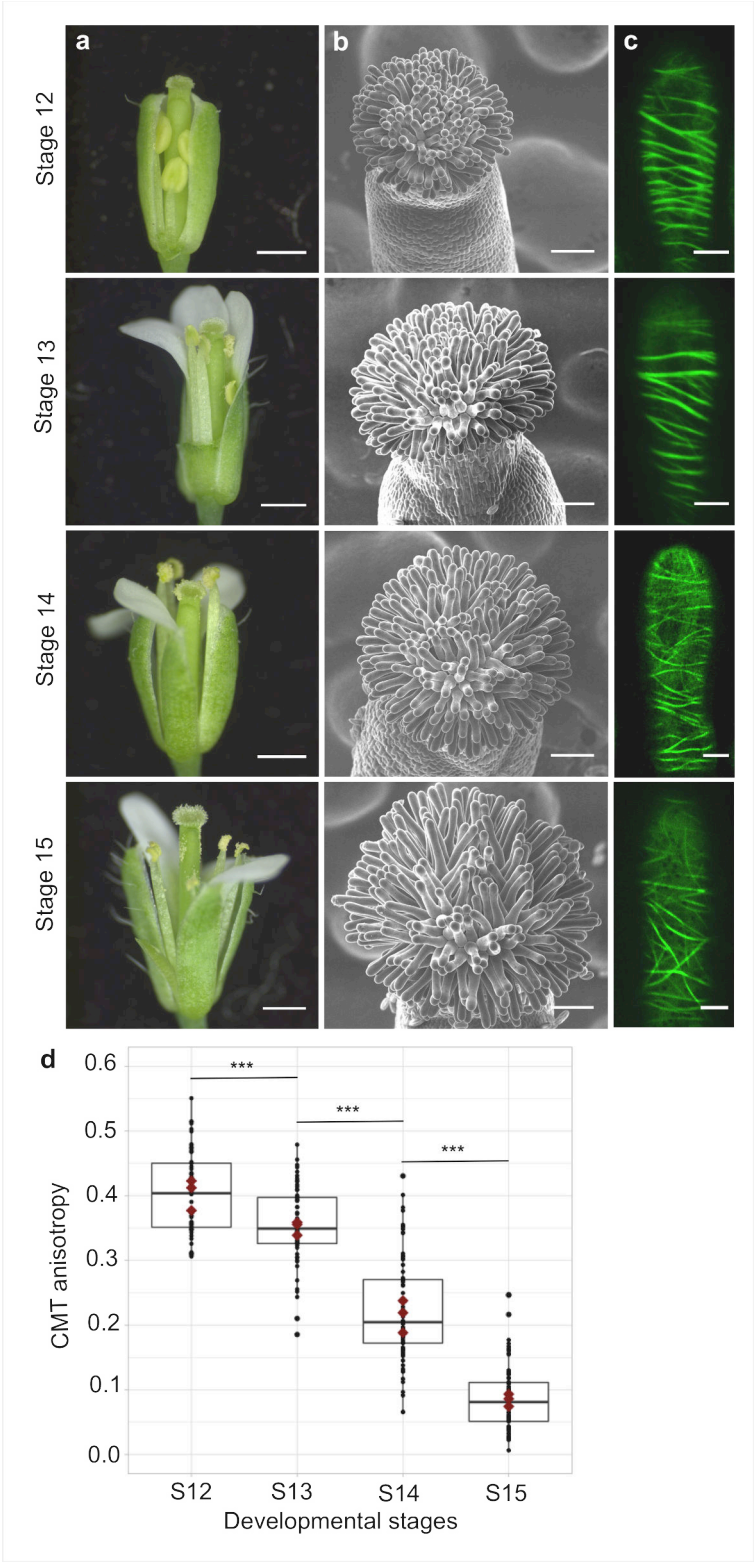

Fig. 10 / CMT organisation during papilla cell development.
a, Flower development of *A. thaliana* from developmental stages 12 to 15. Scale bar, 500 µm. b, Upper view of the stigma during development by SEM. Scale bar, 50 µm. c, Confocal images of papilla cells expressing MAP65-citrine at each stage of development. Scale bar, 5 µm. d, Quantitative analysis of CMT array anisotropy of papilla cells from stages 12 to 15. The red dots correspond to the mean values of the three replicates. Statistical difference were calculated using a Shapiro-Wilk test to evaluate the normality and then a Wilcoxon test, ***P < 0.01. N > 4 stigmas, n > 60 papilla cells for each stage.

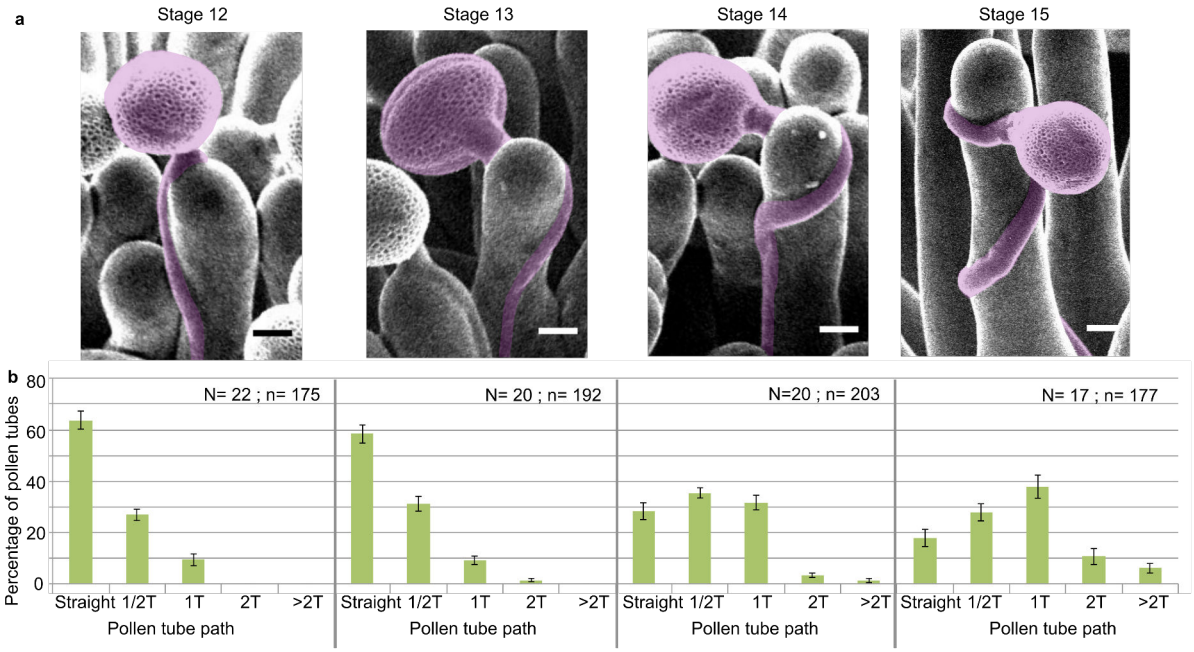

Fig. 11 / Pollen tube growth behaviour on papillae during development.
a, SEM images of Col-0 papillae pollinated with Col-0 pollen, one hour post pollination, from stages 12 to 15; pollen and tubes were artificially colorised. Scale bar, 5 µm. b, Quantification of the number of turns (T) made by the pollen tube on papillae from stages 12 to 15. Data are expressed as mean +/- s.e.m. A Chi-Square test for independence (at 6 degree of freedom) was used to compare all stages and demonstrated that the number of turns was significantly different between stages (***P < 0.01).

Impaired CMT dynamics of papillae affects pollen tube growth direction. To confirm the relation between stigma CMTs and pollen behaviour, we examined pollen tube growth on stigmas of the *katanin1-5* mutant, which is known to exhibit reduced CMT array anisotropy in root cells (Bichet et al., 2001; Burk and Ye, 2002; Burk et al., 2001). Because the CMT organisation in *ktn1-5* papillae is unknown, we crossed *ktn1-5* with the MAP65-1-citrine marker line and found that CMT arrays were more isotropic in *ktn1-5* papillae when compared with those of the WT (Fig. 12a,c). Using SEM, we then analysed Col-0 pollen behaviour on *ktn1-5* stigmatic cells at stage 13 (Fig. 12b). We observed that Col-0 pollen tubes acquired a strong tendency to coil around *ktn1-5* papillae, with above 60% of tubes making one or more than one turn around papillae, sometimes making up to 6 turns, before reaching the base of the cell (Fig. 12d and Supplementary Fig. 1). In some rare cases, pollen tubes even grew upward in the *ktn1-5* mutant and appeared blocked at the tip of the papilla (Supplementary Fig. 1b). To test the direct impact of stigma CMTs on pollen tube growth direction, we examined whether the destabilization of CMTs in Col-0 papillae could affect pollen tube growth. To this end, we treated stigmas by local application of the depolymerizing microtubule drug oryzalin in lanolin pasted around the style. After 4 hours of drug treatment, no more CMT labelling was detected in papillae,

while CMTs were clearly visible in mock-treated (DMSO) stigmas (Fig. 13a). Stigmas were then pollinated with Col-0 pollen and one hour later, pollen tubes were found turning on drug-treated but not on control papillae (Fig. 13b,c). However, the number of coils was significantly lower than on *ktn1-5* papillae. Indeed, 25% of the pollen tubes made at least 2 coils in *ktn1-5* papillae whereas this percentage represented only 4% on the oryzalin treated stigmas (Fig. 12d, Fig. 13c). Altogether, these results confirm that stigmatic CMTs contribute to the directional growth of pollen tubes in papilla cells.

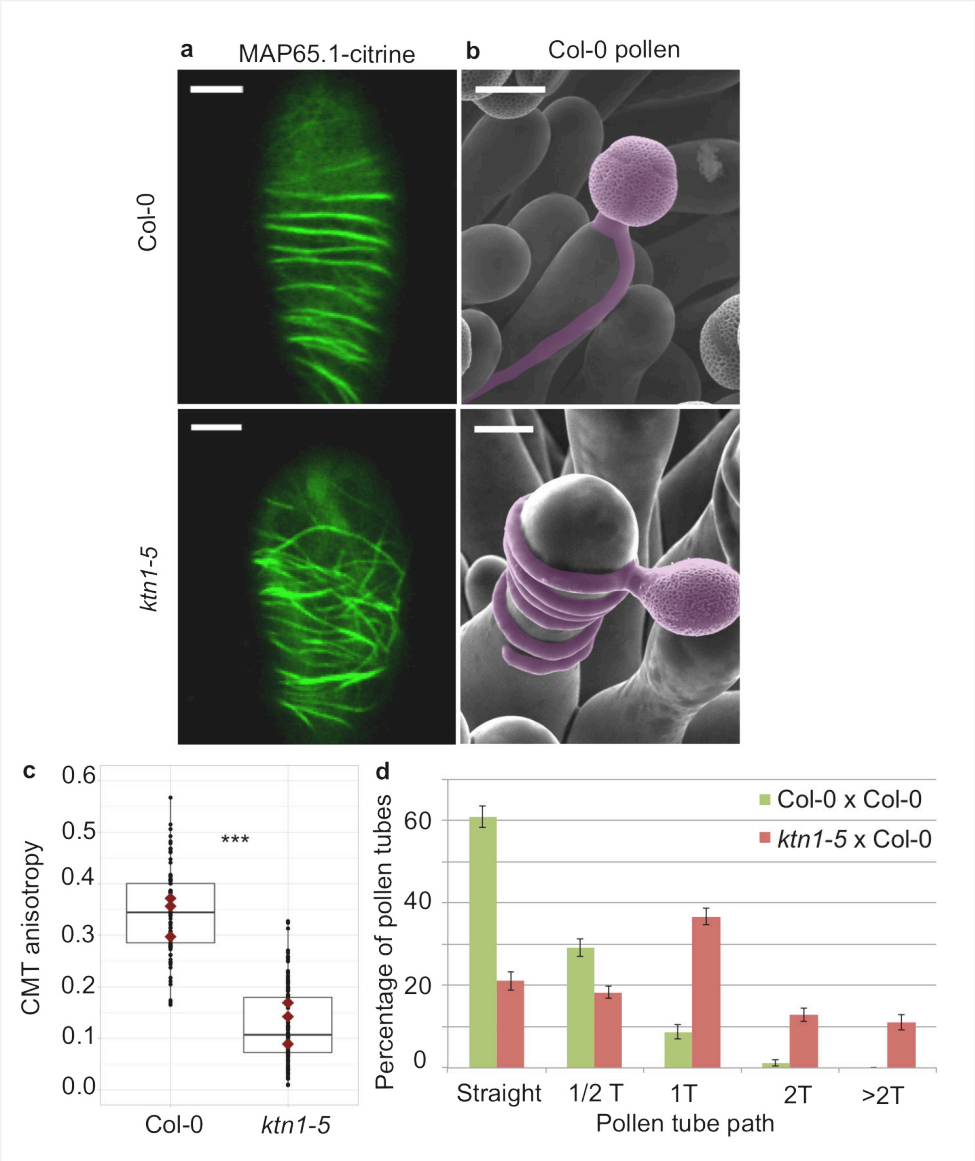

Fig. 12 / Effect of CMT organisation on pollen tube path.
a, Confocal images of papilla cells expressing MAP65.1-citrine in Col-0, *ktn1-5* at stage 13. Scale bars, 5 µm. b, SEM images of Col-0 and *ktn1-5* papillae pollinated with Col-0 pollen grains; pollen and tubes were artificially colorized. Scale bar, 10 µm. c, CMT anisotropy of Col-0 and *ktn1-5* papilla cells at stage 13. N(Col-0) = 10 stigmas, n(Col-0) = 106 papillae, N(*ktn1-5*) = 11stigmas, n(*ktn1-5*) = 114 papillae. Statistical differences were calculated using a Shapiro-Wilk test to evaluate the normality and then a Wilcoxon test with ***P < 0.01. d, Quantification of the number of turns (T) made by Col-0 pollen tubes on *ktn1-5* and Col-0 papillae. Data are expressed as mean +/- s.e.m. Statistical difference was found between pollen tube path within *ktn1-5* and Col-0 papillae

and was calculated using an adjusted Chi-Square test for homogeneity (2 degrees of freedom), ***P < 0.01. N(Col-0) = 27 stigmas, n(Col-0) = 251 papillae, N(*ktn1-5*) = 23 stigmas, n(*ktn1-5*) = 327 papillae.

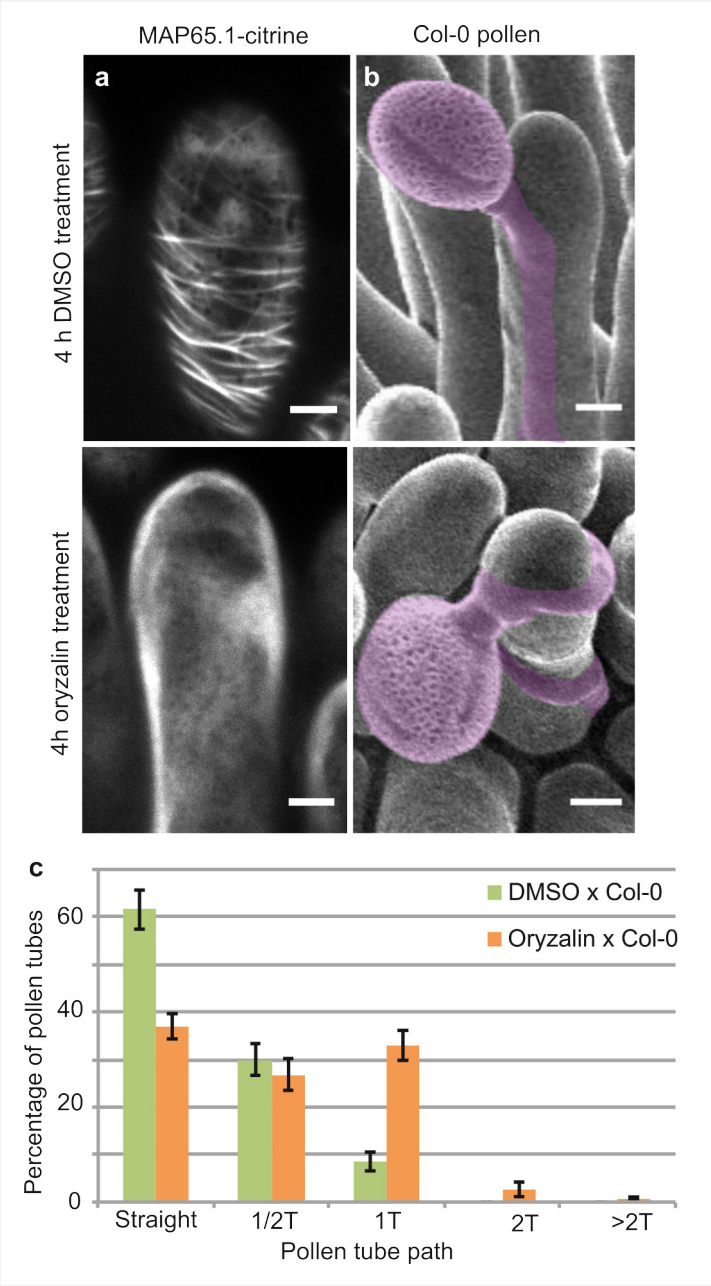

Fig. 13 / Local oryzalin application on Col-0 stigmas promotes MT destabilization and induces Col-0 pollen tube coils.

a, Col-0 papilla cells expressing MAP65.1-citrine after 4 hours of DMSO (top) or oryzalin (bottom) local treatment. b, SEM images of DMSO- (top) or oryzalin-treated (bottom) Col-0 stigmas pollinated with Col-0 pollen grains; pollen and tubes were artificially colorized. (a, b) Scale bars, 5 µm. c, Quantification of the number of turns(T) made by Col-0 pollen tubes on drug-treated and control papillae. Data are expressed as mean +/- s.e.m. Statistical difference was found between pollen tube path within DMSO (control) and oryzalin-treated papillae and was calculated using an adjusted Chi-Square test for homogeneity (2 degrees of freedom), ***P < 0.01. N(DMSO) = 12 stigmas, n(DMSO) = 117 papillae, N(oryzalin) = 16 stigmas, n(oryzalin) = 149 papillae.

Mechanical properties of the cell wall are disturbed in *ktn1-5* papilla cells. Because the main role of CMTs in plant cells is to guide the trajectory of CSCs, thereby impacting the mechanical anisotropy of the cell wall, we analysed the cell walls of Col-0 and *ktn1-5* papillae following pollination. First, using Transmission Electron Microscopy (TEM), we found Col-0 pollen tubes to penetrate the cuticle and to grow between the two layers of the papilla cell wall, as previously described (Kandasamy et al., 1994), in both Col-0 and *ktn1-5* papilla cells (Fig. 14a). We did not detect any significant difference in the ultrastructure of cell walls (Supplementary Fig. 2). Interestingly, as the pollen tube progresses through the papilla cell wall, it generates a bump (external deformation) and an invagination (internal deformation) in the cell wall. As such deformations could reflect differences in wall properties, we quantified the external (extD) and internal (intD) deformation following pollination of Col-0 and *ktn1-5* stigmas. To visualize more clearly this deformation, we pollinated stigmas expressing the plasma membrane protein LTI6B fused to GFP (LTI6B-GFP) with pollen whose tube was labelled with the red fluorescent protein RFP driven by the ACT11 promoter (Rotman et al., 2003) (Fig. 14b). We found that Col-0 pollen tubes grew with almost equal extD and intD values in Col-0 cell wall. However, the ratio between extD and intD was about 3 when Col-0 pollen tubes grew in *ktn1-5* papilla cells (Fig. 14b,c,d). These quantitative data are consistent with the observation of major protuberances caused by pollen tubes on *ktn1-5* stigmatic cells using SEM (Fig. 12b and Supplementary Fig. 1). Assuming that stigmatic cells are pressurized by their turgor pressure, this may reflect the presence of softer walls in *ktn1-5* papillae. To test this hypothesis, we assessed the stiffness of Col-0 and *ktn1-5* papilla cell walls using Atomic Force Microscopy (AFM) with a 400 nm indentation. We found that cell wall stiffness in *ktn1*-5 papilla cells was about 30% lower than that in stage 13 WT cells (Fig. 14e,f). To confirm this result, we investigated the stiffness of the papilla cell wall on WT stigmas at stage 15, where increased coiled pollen tubes were detected (Fig. 11a,b). We found the cell wall to be softer than that of papillae at stage 13 but stiffer than that of the *ktn1-5* (Fig. 14e,f). We then reasoned that the presence of softer walls should also affect the pollen tube growth rate, stiffer walls reducing growth. We thus monitored the growth rate of Col-0 pollen tubes in Col-0 and *ktn1-5* papillae. We found that pollen tubes grew faster (~ x 1.8) within *ktn1-5* papillae (Fig. 14g). Similarly, we found that pollen tube growth on stage 15 papillae was faster (~ x 1.6) than on stage 13 papillae (Fig. 14h). Altogether, these results suggest that KATANIN-dependent mechanical properties of papilla cell wall impact pollen tube growth.

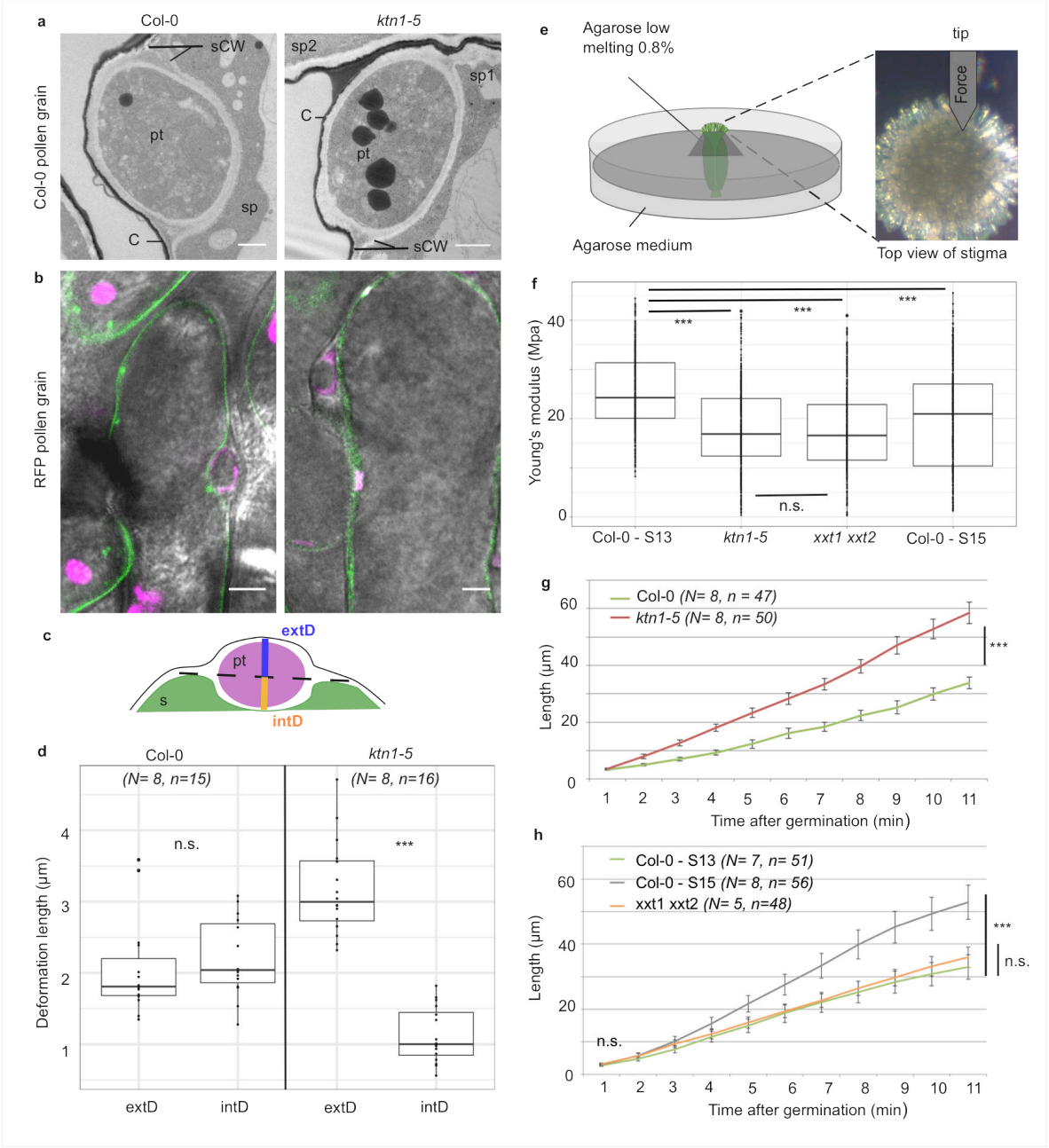

Fig. 14 / Mechanical properties of papilla cells.

a, Location of a Col-0 pollen tube in the cell-wall of Col-0 and *ktn1-5* papillae by TEM. pt = pollen tube, C = stigma cuticle, sCW = stigma cell wall, sp = stigma papilla. Scale bar, 1 µm. b, Confocal images of Col-0 and *ktn1-5* papillae expressing the plasma membrane marker LTI6B-GFP pollinated with an RFP-expressing pollen. Scale bar, 5 µm. c, Diagram showing the procedure used for evaluating the external (extD) and internal (intD) deformations made by Col-0 pollen tubes. d, External and internal deformations caused by Col-0 pollen tube growth in Col-0 and *ktn1-5* papillae. e, Drawing of the AFM experimental setup. Dissected pistils were inserted in agarose medium and fixed with low melting agarose for measurements. f, Young's modulus values of the papilla cell wall for Col-0 at stage 13 (N = 4 stigmas, n = 8 papillae), *ktn1-5* (N = 5 stigmas, n = 9 papillae), *xxt1 xxt2* (N = 4 stigmas, n = 11 papillae) and Col-0 at stage15 (N = 4 stigmas, n = 10 papillae. g, Mean of travel distances made by Col-0 pollen tubes in Col-0 and *ktn1-5* papillae. h, Mean of travel distances made by Col-0 pollen tubes in papillae of Col-0 at stage 13, Col-0 at stage 15 , *xxt1 xxt2* at stage 13. d-e and g-h, Statistical differences were calculated using a Shapiro-Wilk test to evaluate the normality and then a T-test. *** P < 0.01, n.s. = non significant. For h, we found

a significant difference (***P < 0.01) between Col-0 at stage 13 and 15, but non significant (n.s.) between Col-0 at stage 13 and *xxt1 xxt2* at stage 13.

Defects in papilla cell-wall composition are not sufficient to affect Col-0 pollen tube behaviour. The *katanin1/fra2* mutant was initially described as a mutant impaired in cell wall biosynthesis and CMT array organisation (Burk et al., 2001). This prompted us to test whether other mutants affected in cell wall biogenesis might exhibit the coiled pollen tube phenotype. Indeed, in the simplest scenario, the presence of softer walls, whatever the cause, may be sufficient to induce extra coiling due to faster pollen tube growth. We selected mutants impaired in the cellulose synthase complex (*kor1.1*, *prc1* and *any1*), hemicellulose biosynthesis (*xxt1 xxt2*, *xyl1.4*) and pectin content (*qua2.1*) (Supplementary Table 1). Strikingly, none of the 6 cell wall mutants displayed the coiled pollen tube phenotype (Supplementary Fig. 3). This suggests that the relation between CMT organisation, cell wall stiffness and pollen tube trajectory is stricter than anticipated. Because CMTs guide cellulose deposition, they also control the directional elongation of plant cells (Baskin, 2005). The contribution of stigmatic CMTs to pollen tube growth may thus be mediated by papilla cell shape only. For instance, wider cells in *ktn1-5* would promote pollen tube coiling. To check that possibility, we measured the length and width of papilla cells in Col-0 (at stage 13 and 15), *ktn1-5, xxt1 xxt2* and *any1* (Supplementary Fig. 4). We did not find any correlation between papilla length and the coiled phenotype. Indeed, coiled phenotype was observed in stage-15 WT papillae that were longer than those at stage-13, as well as in *ktn1-5* papillae that had a length similar to stage-13 WT papillae. The correlation between papilla width and coiled phenotype was also not clear-cut. As expected, *ktn1-5* mutant exhibited wider papillae than Col-0. Stage-15 WT papillae were also significantly larger than stage-13 WT papillae, where coils were observed. However, *xxt1 xxt2* and *any1* papillae were also wider than the WT but did not display the coiled phenotype. Altogether, this suggests that papilla morphology is not sufficient to explain the coiled phenotype. Because CMT disorganisation in papillae affects both wall stiffness and mechanical anisotropy, we next investigated the relative contribution of these two parameters in pollen tube growth. We focused our analysis on the *xxt1 xxt2* double mutant. Indeed, this mutant was reported to display CMT orientation defects and a softer cell wall in hypocotyl cells, when compared with the WT (Xiao et al., 2016). As the pollen tube phenotype on *xxt1 xxt2* stigmas was similar to the WT, we wondered whether the cell wall stiffness of stigmatic cells was actually affected in these mutant papillae. Using AFM, we found the papilla cell wall of the mutant to be about 30% softer than that of Col-0 papillae, i.e. very similar to that of *ktn1-5* (Fig. 14f). However, despite this similarity, the pollen tube growth rate in *xxt1 xxt2* stigmas was identical to Col-0 stigmas at stage 13 (Fig. 14h). In addition, contrary to *ktn1-5*, we did not observe external bumps on *xxt1 xxt2*

papillae when pollen tubes were growing (Supplementary Fig. 3g). These results indicate that alteration of the cell wall stiffness alone is not sufficient to induce the pollen tube coiled phenotype and promote tube growth speed, and suggest that, instead, the mechanical anisotropy of cell walls plays a key role in pollen tube trajectory.

Discussion

How the pollen germinates a tube and how pollen tube growth is regulated have been the object of many investigations (Mizuta and Higashiyama, 2018; Palanivelu and Tsukamoto, 2012). The use of *in vitro* pollen germination as well as semi-*in vivo* fertilization assays, together with the analysis of mutants defective in pollen or ovule functions, have rapidly expanded our knowledge of the mechanisms that sustain pollen tube growth, its guidance toward the ovule and the final delivery of male gametes within the embryo sac (Cameron and Geitmann, 2018; Dresselhaus and Franklin-Tong, 2013; Higashiyama and Yang, 2017). At the cellular level, cytoskeleton has been extensively studied during pollen tube elongation (Fu, 2015), highlighting the critical role played by the actin microfilaments in pollen-tube tip growth through delivery of materials for the biosynthesis of the plasma membrane and cell wall. By contrast, CMTs seem to have a lower importance in this process, drugs affecting CMT polymerisation having no significant effects on pollen-tube growth rate, yet altering the capacity of pollen tubes to change their growth direction (Gossot and Geitmann, 2007). Rearrangements of actin microfilaments (Iwano et al., 2007) and destabilization of CMTs (Samuel et al., 2011) have been described in stigmas following compatible pollination in Brassica species. However, CMT pattern and dynamics during papilla development have never been reported. Our data show that during the course of stigma maturation, which is associated with papilla cell elongation (Supplementary Fig. 4a,b), CMT bundles progressively move from perpendicular (anisotropic) to the elongation axis at stage 12 to disorganised (isotropic) at stage 15. This correlates with the known CMT dynamics during elongation in plant cells, where CMT arrays are highly anisotropic in young cells and become more isotropic as cells differentiate (Baskin, 2005; Landrein and Hamant, 2013). The progressive randomisation of CMT orientation in papilla cells is accompanied by an increased coiled growth of pollen tubes in papillae. Similarly, when CMTs are destabilized by the microtubule depolymerizing drug oryzalin, coiled pollen tubes are more frequently observed compared with untreated control stigmas. These results reveal a link between the stigmatic CMT cytoskeleton organisation and the trajectory that pollen tube takes while growing in the papilla cell wall. The fact that the most striking effect on pollen tube growth was found on *ktn1-5* mutant suggests that the coiled phenotype depends not only

on the CMT organisation but implicates other factors. Among various phenotypic alterations described in loss-of-function mutants for *KTN1*, are the impaired cell mechanical properties and cell elongation, defects in CMT organisation, cell wall composition and CMF orientation (Burk and Ye, 2002; Burk et al., 2001; Ryden et al., 2003). Interestingly, we found that the protuberance of pollen tubes at the surface of *ktn1-5* papillae was associated with a faster growth rate and a lower rigidity of the cell wall compared with Col-0. This places mechanics of the cell wall as a likely component involved in the coiled phenotype. Surprisingly, cell wall mutants, such as *xxt1 xxt2* and *prc1*, known to exhibit both abnormal CMT organisation and softer cell walls, and somehow that may share mechanical properties with *ktn1-5*, did not induce the coiled phenotype displayed by *ktn1-5* papillae. More remarkably, despite the similar stiffness of *xxt1 xxt2* and *ktn1-5* papilla cell walls measured in our AFM experiments, pollen tubes behaved differently on these two stigmas. This indicates that components other than cell wall stiffness are involved in the pollen tube coiled phenotype and that mechanical properties of the cell wall are likely not identical in the two mutants. Indeed, though sharing a similar alteration of cell wall stiffness, the global plant morphology of these mutants is clearly distinct. The *ktn1-5* mutant was described to have a severe reduction in cell length and an increase in cell width in all organs (Burk et al., 2001). This cellular phenotype was attributed to the distorted deposition of CMFs correlated with the isotropic orientation of CMTs, whereas in WT cells CMFs, like CMTs, are oriented perpendicularly to the elongation axis (Burk and Ye, 2002). We also found larger papilla cells for *ktn1-5* (Supplementary Fig. 4c,d), supporting the hypothesis that orientation of CMFs is also altered in *ktn1-5* papillae. Hence, we may assume that mechanical anisotropy, described as the cell wall anisotropy made by the orientation of the rigid CMFs (Sassi et al., 2014), is impaired in *ktn1-5* papillae. By contrast, the *xxt1 xxt2* double mutant, although deprived of xyloglucans in its cell walls, shows a growth phenotype (Cavalier et al., 2008; Park and Cosgrove, 2012) not as severe as *ktn1-5*. In etiolated hypocotyls, contrary to Col-0, CMFs are largely parallel to one another, straighter than in WT and oriented approximately transversely to the long axis of the cell (Xiao et al., 2016). Interestingly, we found the papilla cell shape of *xxt1 xxt2* stigmas to be similar to Col-0, though with slightly wider papillae (Supplementary Fig. 3g, Supplementary Fig. 4e,f). However, *xxt1 xxt2* papillae were less wide than *ktn1-5* papillae, which is consistent with an anisotropic growth of the papillae in the *xxt1 xxt2* mutant compared with *ktn1-5*. At the cell wall level, apart from a similar stiffness, the main differences between *ktn1-5* and *xxt1 xxt2* appear to be the cell wall composition, orientation of CMFs and possible changes in molecular connections between cell wall components and plasma membrane and/or cytoskeleton proteins. Indeed, a recent proteomic study revealed that loss of KATANIN function is associated

with the decrease in abundance of several cytoskeleton proteins, such as profilin 1, actin-depolymerizing factor 3 and actin 7 (Takáč et al., 2017), whereas targeted quantitative RT-PCR unveiled that Microtubule-associated protein (MAP) and wall signal receptor genes are downregulated in *xxt1 xxt2* (Xiao et al., 2016). In this latter study, KTN1 expression level was shown to be unchanged compared with Col-0. Altogether, our study suggests that KTN1, by maintaining the papilla mechanical anisotropy, has a key function in mediating early pollen tube guidance on stigma papillae.

The coiled phenotype was not only observed in *ktn1-5* but also in the WT Col-0 papillae at stage 15. This is likely to be related to isotropic orientation of CMTs and CMFs known to occur during cell elongation (Crowell et al., 2011; Zhang et al., 2014). At the organ level, it has been suggested that the mechanical anisotropy of the wall restrains organ emergence (Sassi et al., 2014). The authors propose that for the same wall stiffness, a cell wall with isotropic properties would lead to larger outgrowth than a wall with anisotropic properties. Our data are consistent with this hypothesis, albeit at the subcellular scale, since large protuberance of papilla wall following pollen tube growth is observed in *ktn1-5* papilla cells, exhibiting walls with isotropic properties.

It remains unclear how mechanical anisotropy guides pollen tube growth. We can hypothesise that as pollen tube grows inside the wall, it encounters recently deposited CMFs on the inner side of the wall (facing the cytoplasm) and older CMFs on the outer side. It is likely that these layers have different mechanical properties related to CMF orientation (Baskin, 2005). Pollen tubes may grow helically by default, as is the case for climbing plants around a cylindrical substrate but the presence of a mechanically reinforced inner wall may slow down and bias the trajectory of the pollen tube. It is worth noting that growth rate is slowed down when pollen tubes pass through a microgap of a microfluiding device, the tubes adapting their invasive force to the mechanical constraints (Sanati Nezhad et al., 2013). Our data show that the pollen tube tip, while progressing in the papilla wall, senses the mechanical features of its environment and reacts accordingly. Hence, it reveals some unanticipated internal and hidden properties of the cell wall. Interestingly, recent work showed that axons were capable of adapting their growth rate and direction according to mechanical constraints, growing straighter on rigid substrate underlining that mechanical signals are important regulators of pathfinding (Koser et al., 2016).

In the last decades, many studies pointed out that chemical but also mechanical components must be considered to be implicated in pollen tube growth direction (Cameron and Geitmann, 2018). Implication of chemical cues for pollen tube guidance in the stigma remains largely unknown, although the blue copper protein plantacyanin, when overexpressed in Arabidopsis stigmas, was reported to be a possible guidance factor

through an as yet undiscovered mechanism (Dong et al., 2005). However, no defect in pollen tube growth directionality was detected in a know-down plantacyanin mutant, questioning the actual role of this protein as a chemoattractant in Arabidopsis. In our study, we add mechanics as a key player in early pollen tube guidance in the papilla cell. Our results suggest that this role is mediated by a specific CMT organisation and mechanical anisotropy of the papilla cell, which both are dependent on KTN1. Importantly, KTN1 prevents emerging pollen tubes to grow upward on papilla cells and straightens pollen tube direction, helping the tube to find its correct path to the stylar transmitting tract. This highlights an yet unexpected role for KTN1 in pollen tube guidance, which was until now mostly known to be involved in plant development and stress-response regulation. In addition, our study also clearly unveils the fact that the mechanical properties of one single cell (e.g., the stigmatic papilla) impact the behaviour of its neighbouring cell (e.g., the pollen tube).

Materials and methods

Plant Materials and Growth Conditions. *Arabidopsis thaliana*, ecotype Columbia (Col-0), *Arabidopsis* transgenic plants generated in this study and *Arabidopsis* mutants were grown in soil under long-day conditions (16 hours of light / 8 hours of dark, 21°C / 19°C) with a relative humidity around 60%. *ktn1-5* (SAIL_343_D12), *xxt1xxt2*, *prc1.1, qua2.1*, *xyl1.4*, *kor1.1* and *any1* mutant lines were described previously (Cavalier et al., 2008; Fagard et al., 2000; Fujita et al., 2013; Lin et al., 2013; Mouille et al., 2007; Nicol et al., 1998; Sampedro et al., 2010; Shoji et al., 2004). All mutants were in Col-0 background except *kor1.1* which was in WS.

Plasmid construction. We used the Gateway® technology (Life Technologies, USA) and two sets of Gateway®-compatible binary T-DNA destination vectors (Hellens et al., 2000; Karimi et al., 2002) for expression of transgenes in *A. thaliana*. The DNA fragment containing the *Brassica oleracea SLR1* promoter was inserted into the pDONP4-P1R vector. The 165 bp-*LTI6B* fragment was introduced into the pDONR207 vector. *MAP65* gene spanning the coding region from start to stop codons was introduced into the pDONR221 vector. CDS from citrine or GFP were cloned into the pDONP2R-P3 vector. Final constructs, pSLR1::MAP65-citrine and pSLR1::LTI6B-GFP were obtained by a three-fragment recombination system (Life Technologies) using the pK7m34GW and the pB7m34GW destination vectors, respectively. We generated a pAct11::RFP construct by amplifying the promoter of the *A. thaliana Actin 11* gene and cloning it into the pGreenII gateway vector in front of the RFP coding sequence.

Generation of transgenic lines and crossing. Transgenic lines were generated by *Agrobacterium tumefaciens*-mediated transformation of *A. thaliana* Col-0 as described (Logemann et al., 2006). Unique insertion lines, homozygous for the transgene were selected. We introduced the pSLR1::LTI6B-GFP or pSLR1::MAP65-citrine construct in *ktn1-5* background by crossing and further selecting the progeny on antibiotic containing medium.

Microscopy

Confocal microscopy. Flowers at stages 12 to 15 (Smyth et al., 1990) collected from fluorescent lines were emasculated and stigmas were observed under a Zeiss LSM800 microscope (AxioObserver Z1) using a 40x Plan-Apochromat objective (numerical aperture 1.3, oil immersion). Citrine was excited at 515 nm and fluorescence detected between 530 and 560nm. GFP was excited at 488 nm and fluorescent detected between 500 and 550 nm. RFP was excited at 561 nm and fluorescent detected between 600 and 650 nm.

***Live imaging*.** Flowers from stages 12 to 15 were emasculated and pollinated on plants with mature pollen from the pACT11::RFP line. Immediately after pollination, stigmas were mounted between two coverslips. To maintain a constant humidity without adding liquid directly on the stigma surface, we use a wet piece of tissue in contact with the base of the stigma. Pollinated stigmas were observed under a Zeiss microscope (AxioObserver Z1) equipped with a spinning disk module (CSU-W1-T3, Yokogawa) using a 40x Plan-Apochromat objective (numerical aperture 1.1, water immersion). Serial confocal images were acquired in the entire volume of the stigma every 1 µm and every minute. Images were processed with Image J software and pollen tube lengths were measured.

***Atomic Force Microscopy*.** Pistils at stage 13 were placed straight in a 2% agar MS medium and 0.8% low-melting agarose was added up to the base of papilla cells. AFM indentation experiments were carried out with a Catalyst Bioscope (Bruker Nano Surface, Santa Barbara, CA, USA) that was mounted on an optical microscope (MacroFluo, Leica, Germany) equipped with a x10 objective. All quantitative measurements were performed using standard pyramidal tips (RFESP-190 (Bruker)). The tip radius given by the manufacturer was 8-12 nm. The spring constant of the cantilever was measured using the thermal tune method (Hutter and Bechhoefer, 1993; Lévy and Maaloum, 2002) and was 35 N/m. The deflection sensitivity of the cantilever was calibrated against a sapphire wafer. All experiments were made in ambient air at room temperature. Matrix of 10x10 measurements (step 500 nm) was obtained for each papilla, with a 1µN force. The Young's Modulus was estimated using the Nanoscope Analysis (Bruker) software, using the Sneddon model with a < 200nm indentation.

Environmental Scanning Electron Microscopy (SEM). Flowers from stages 12 to 15 were emasculated and pollinated on plants with mature WT pollen. One hour after pollination, pistils were cut in the middle of the ovary, deposited on a SEM platform and observed under Hirox SEM SH-3000 at -20°C, with an accelerating voltage of 15kV. Images were processed with ImageJ software and pollen tube direction was quantified by counting the number of turns made by the tube, only on papillae that received one unique pollen grain.

Transmission Electron Microscopy. Stage 13 flowers were emasculated and pollinated on plants with mature WT pollen. One hour after pollination, pistils were immersed in fixative solution containing 2.5% glutaraldehyde and 2.5% paraformaldehyde in 0.1 M phosphate buffer (pH 7.2) and after 4 rounds of 30 min vacuum, they were incubated in fixative for 12 hours at room temperature. Pistils were then washed in phosphate buffer and further fixed in 1% osmium tetroxide in 0.1 M phosphate buffer (pH 7.2) for 1.5 hours at room temperature. After rinsing in phosphate buffer and distilled water, samples were dehydrated through an ethanol series, impregnated in increasing concentrations of SPURR resin over a period of 3 days before being polymerized at 70°C for 18 h, sectioned (65 nm sections) and imaged at 80 kV using an FEI TEM tecnaiSpirit with 4 k x 4 k eagle CCD.

Anisotropy estimation. Flowers from MAP65 lines were emasculated and stigmas were observed under confocal microscope. Images were processed with ImageJ software and quantitative analyses of the average orientation and anisotropy of CMTs were performed using FibrilTool, an ImageJ plug-in (Boudaoud et al., 2014). Anisotropy values range from 0 to 1; 0 indicates pure isotropy, and 1 pure anisotropy.

Membrane deformation estimation. Flowers from LTI6B lines were emasculated and pollinated with mature pollen from the PACT11::RFP line. 20 minutes after pollination, stigmas were observed under confocal microscope. Serial confocal images every 1 µm encompassing the entire volume of the stigma were recorded and processed with ImageJ software. Plasma membrane deformation was estimated by choosing the slide from the stack that corresponded to the focus plan of the contact site with the RFP-labelled pollen tube. On the Bright field image corresponding to the selected slide, a line was drawn connecting the two ridges of the invagination of the papilla. Two perpendicular lines, one toward the exterior (ExtD) of the papilla to the maximum point of deformation, and the other toward the interior (IntD) on the GFP image were measured, respectively.

Statistical analysis. Graph and statistics were obtained with R software or Excel. Statistical tests performed are specified in figure legends.

Chemical treatment. To avoid contact of pollen grains with liquid, we performed local applications of oryzalin (Chemical service, Supelco) at 833 µg/mL (DMSO) in lanolin pasted around the style, just under the stigmatic cells, for 4 hours at 21°C. Oryzalin-treated pistils were pollinated with mature WT pollen and 1 hour after pollination observed under SEM.

Supplemental figures

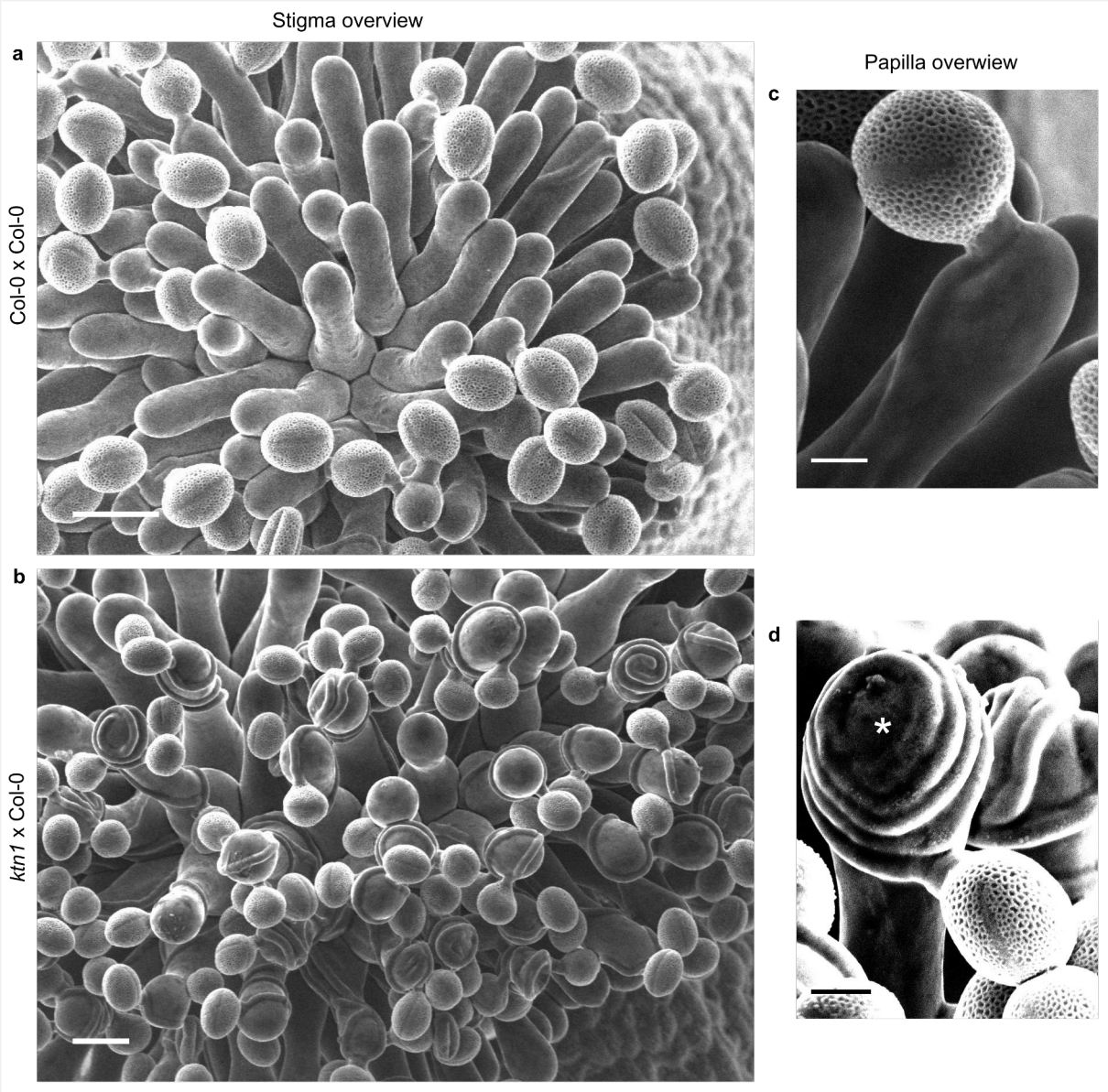

Supplementary Fig. 1 / Col-0 pollen tube behaviour on Col-0 and *ktn1-5* papillae at stage 13.
a-b, Top views of Col-0 (a) and *ktn1-5* (b) stigmas pollinated with Col-0 pollen grains. Scale bars, 20 µm. c-d, Magnification of pollinated papilla cells. c, Col-0 pollen tube grows mainly straight to the direction of the ovules on Col-0 papillae whereas d, it coils around and can even grow upward on *ktn1-5* papilla cells (*). Scale bars, 5 µm.

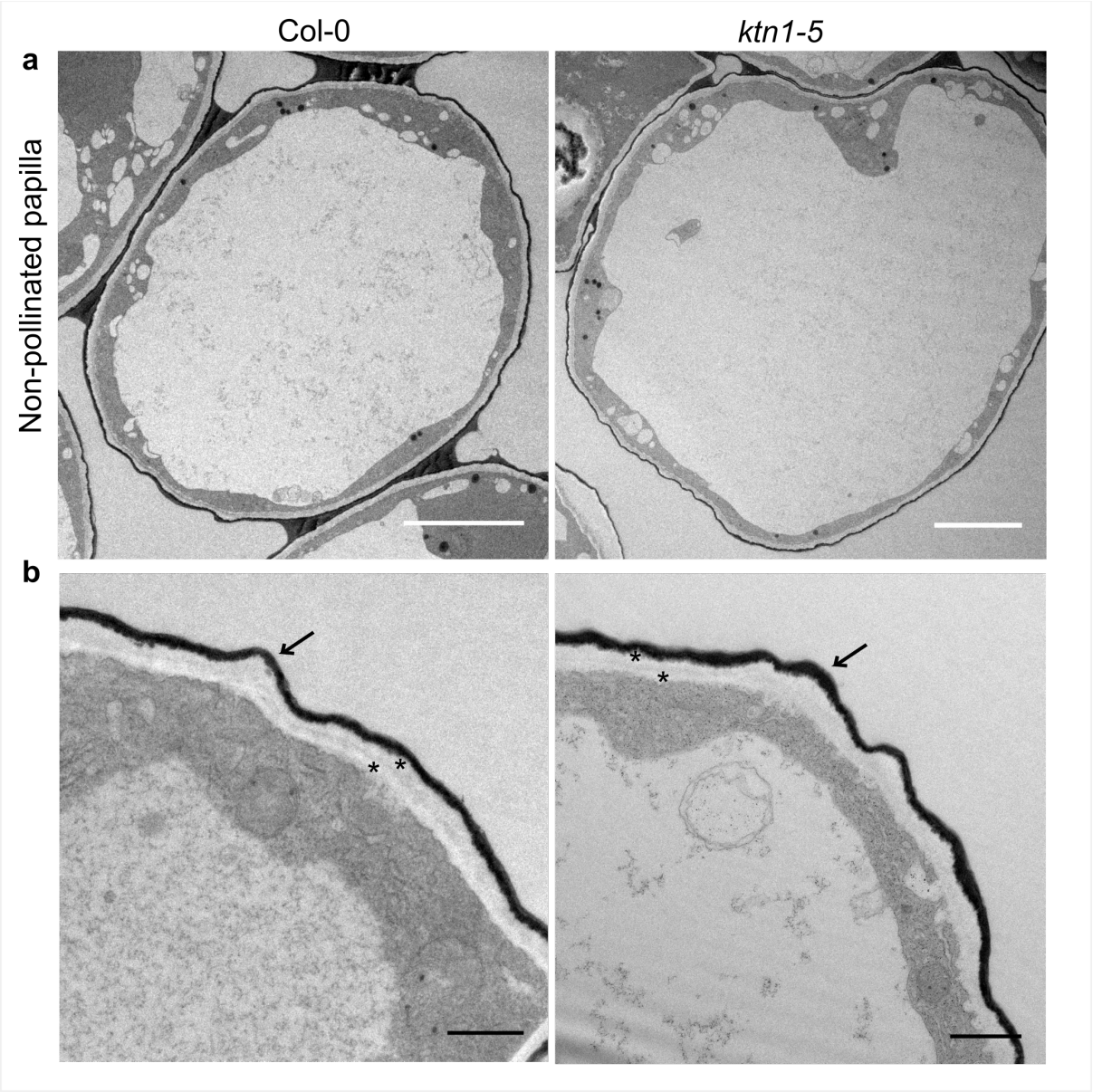

Supplementary Fig. 2 / Ultrastructure of Col-0 and *ktn1-5* papilla cells.
a, TEM images of non-pollinated Col-0 and *ktn1-5* papillae. Scale bar, 5 µm. b, Both Col-0 and *ktn1-5* papillae show a similar two-layered cell wall (*) delimited by a more electron dense thin layer (arrows) corresponding to the cuticle. Scale bar, 1 µm.

Cell wall component	AGI/Name	Function*	Mutant	References
Cellulose	AT5G49720 *KOR1*	Endoglucanase 25	*kor1*	(His and Driouich, 2001; Lei et al., 2014; Nicol et al., 1998)
Cellulose	AT5G64740 *PRC1*	Cellulose synthaseA catalytic subunit 6	*prc1*	(Fagard et al., 2000; MacKinnon et al., 2006; Panteris et al., 2014; Xiao et al., 2016)
Cellulose	AT4G32410 *ANY1*	Cellulose synthaseA catalytic subunit 1	*any1*	(Fujita et al., 2013)
Hemicellulose	AT3G62720 *XXT1* AT4G02500 *XXT2*	Xyloglucan 6-xylosyltransferase 1 Xyloglucan 6-xylosyltransferase 2	*xxt1 xxt2*	(Cavalier et al., 2008; Xiao et al., 2016)
Hemicellulose	AT1G68560 *XYL1*	Alpha-xylosidase 1	*xyl1.4*	(Shigeyama et al., 2016)
Pectin	AT1G78240 *QUA2*	Probable Pectin methyltransferase	*qua2.1*	(Abasolo et al., 2009; Mouille et al., 2007; Verger et al., 2018)

*From https://www.uniprot.org

Supplementary Table 1 / Cell-wall mutants tested

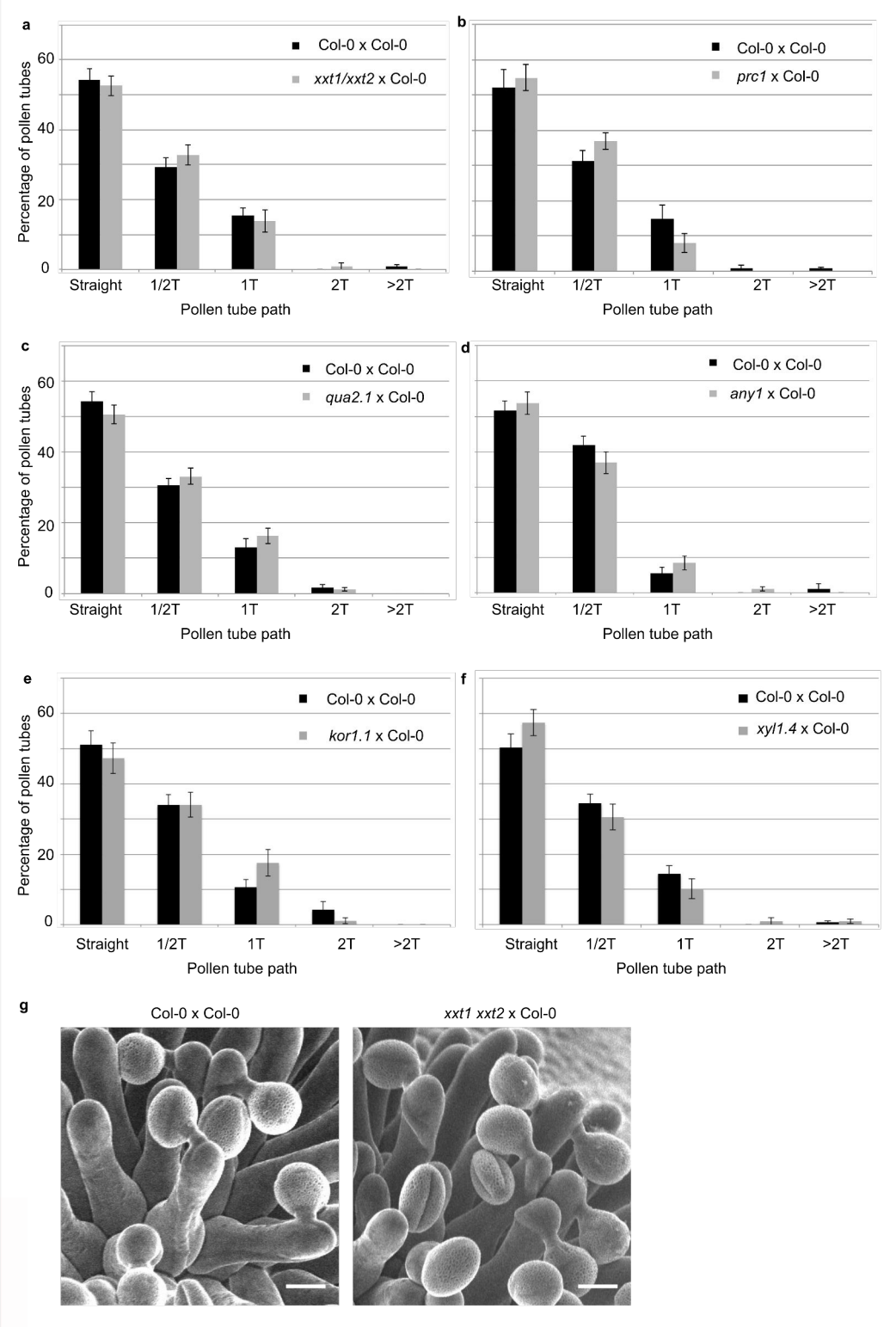

Supplementary Fig. 3 / Quantification of the number of coils made by Col-0 pollen tubes on papillae from cell-wall mutants at stage 13.

a, *xxt1 xxt2* x Col-0. N(Col-0) = 14 stigmas, n(Col-0) = 116 papillae, N(*xxt1 xxt2*) = 12 stigmas, n(*xxt1 xxt2*) = 116 papillae. b, *prc1* x Col-0. N(Col-0) = 14 stigmas, n(Col-0) = 115 papillae, N(*prc1*) = 12 stigmas, n(*prc1*) = 100 papillae. c, *qua2.1* x Col-0. N(Col-0) = 22 stigmas, n(Col-0) = 160 papillae, N(*qua2.1*) = 18 stigmas, n(*qua2.1*) = 162 papillae. d, *any1* x Col-0. N(Col-0) = 14 stigmas, n(Col-0) = 91 papillae, N(*any1*) = 14 stigmas, n(*any1*) = 95 papillae. e, *kor1.1* x Col-0. N(Col-0) = 14 stigmas, n(Col-0) = 141 papillae, N(*kor1.1*) = 11 stigmas, n(*kor1.1*) = 91 papillae. f, *xyl1.4* x Col-

0. N(Col-0) = 18 stigmas, n(Col-0) = 136 papillae, N(*xyl1.41*) = 16 stigmas, n(*xyl1.4*) = 108 papillae. Data are expressed as mean +/- s.e.m. No statistical difference was found between pollen tube path within the cell wall mutants and Col-0 papillae based on an adjusted Chi-Square test for homogeneity (2 degrees of freedom). g, SEM images of Col-0 and *xxt1 xxt2* stigmas pollinated with Col-0 pollen grains. Scale bar, 10 µm.

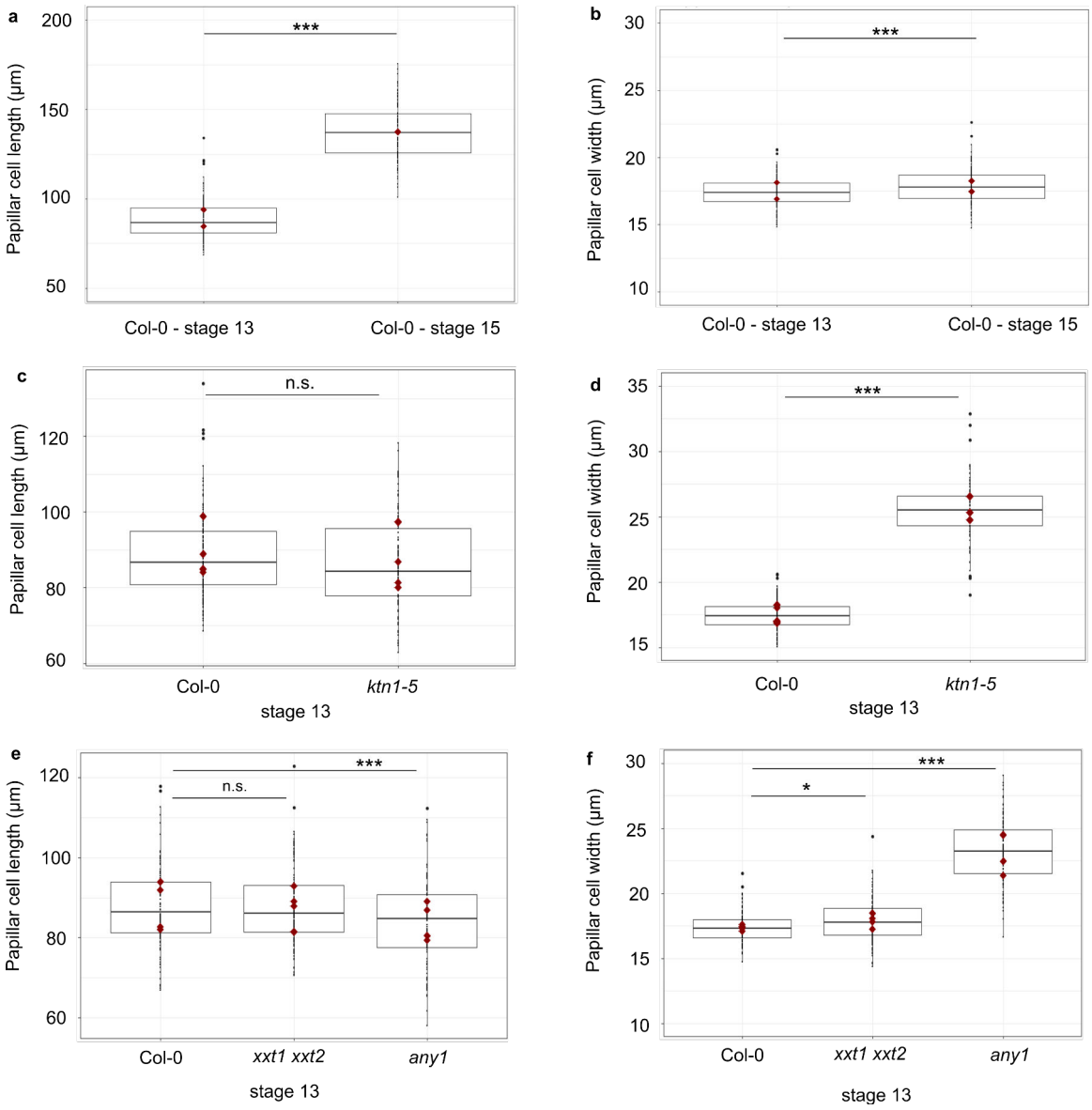

Supplementary Fig. 4 *I* Size of the papilla cells of Col-0 and cell wall mutants.
a, Papilla cell length of Col-0 at stage 13 and stage 15. b, Papilla cell width of Col-0 at stage 13 and stage 15. c, Papilla cell length of Col-0 and *ktn1-5* at stage 13. **d,** Papilla cell width of Col-0 and *ktn1-5* at stage 13. **e,** Papilla cell length of Col-0, *xxt1 xxt2* and *any1* at stage 13. **f,** Papilla cell width of Col-0, *xxt1 xxt2* and *any1* at stage 13. Statistical differences were calculated using a T-test. * P < 0.05, *** P < 0.01, n.s. = non significant. N=4 stigmas and n=120 papillae for each genotypes.

Acknowledgements

We thank O. Hamant for critical reading of the manuscript and fruitful discussion, A. Boudaoud, S. Bovio and V. Battu for advice on AFM experiments, and the Sice and MechanoDevo team members for discussion, P. Bolland, A. Lacroix and J. Berger for plant care and the PLATIM imaging facility of the SFR Biosciences Gerland-Lyon Sud. We thank the Bordeaux Imaging Centre especially L. Brocard and B. Batailler for TEM microscopy. We also thank the BioMeca® society and Pascale Milani for the AFM measurements. L.R. was funded by a fellowship from the French Ministry of Higher Education and Research. The work was supported by Grant ANR-14-CE11-0021.

Author contributions

L.R. performed all the experiments and the image analysis, except TEM and AFM, which were subcontracted. F.R. and C.K. contributed to cell imaging setup. L.R., T.G., and I.F.L., designed the study and analysed the data. L.R. and T.G. wrote the manuscript.

Competing interests

The authors declare no competing interests.

References

Abasolo, W., Eder, M., Yamauchi, K., Obel, N., Reinecke, A., Neumetzler, L., Dunlop, J.W.C., Mouille, G., Pauly, M., Höfte, H., et al. (2009). Pectin May Hinder the Unfolding of Xyloglucan Chains during Cell Deformation: Implications of the Mechanical Performance of Arabidopsis Hypocotyls with Pectin Alterations. Mol. Plant *2*, 990–999.

Baskin, T.I. (2005). Anisotropic Expansion of the Plant Cell Wall. Annu. Rev. Cell Dev. Biol. *21*, 203–222.

Bichet, A., Desnos, T., Turner, S., Grandjean, O., and Höfte, H. (2001). BOTERO1 is required for normal orientation of cortical microtubules and anisotropic cell expansion in Arabidopsis. Plant J. *25*, 137–148.

Boudaoud, A., Burian, A., Borowska-Wykręt, D., Uyttewaal, M., Wrzalik, R., Kwiatkowska, D., and Hamant, O. (2014). FibrilTool, an ImageJ plug-in to quantify fibrillar structures in raw microscopy images. Nat. Protoc. *9*, 457–463.

Burk, D.H., and Ye, Z.-H. (2002). Alteration of Oriented Deposition of Cellulose Microfibrils by Mutation of a Katanin-Like Microtubule-Severing Protein. Plant Cell *14*, 2145–2160.

Burk, D.H., Liu, B., Zhong, R., Morrison, W.H., and Ye, Z.-H. (2001). A Katanin-like Protein Regulates Normal Cell Wall Biosynthesis and Cell Elongation. Plant Cell *13*, 807–828.

Cameron, C., and Geitmann, A. (2018). Cell mechanics of pollen tube growth. Curr. Opin. Genet. Dev. *51*, 11–17.

Cavalier, D.M., Lerouxel, O., Neumetzler, L., Yamauchi, K., Reinecke, A., Freshour, G., Zabotina, O.A., Hahn, M.G., Burgert, I., Pauly, M., et al. (2008). Disrupting Two Arabidopsis thaliana Xylosyltransferase Genes Results in Plants Deficient in Xyloglucan, a Major Primary Cell Wall Component. Plant Cell *20*, 1519–1537.

Crawford, B.C.W., and Yanofsky, M.F. (2008). The Formation and Function of the Female Reproductive Tract in Flowering Plants. Curr. Biol. *18*, R972–R978.

Crowell, E.F., Timpano, H., Desprez, T., Franssen-Verheijen, T., Emons, A.-M., Höfte, H., and Vernhettes, S. (2011). Differential Regulation of Cellulose Orientation at the Inner and Outer Face of Epidermal Cells in the Arabidopsis Hypocotyl. Plant Cell *23*, 2592–2605.

Discher, D.E., Janmey, P., and Wang, Y. (2005). Tissue Cells Feel and Respond to the Stiffness of Their Substrate. Science *310*, 1139–1143.

Dong, J., Kim, S.T., Lord, E.M. (2005). Plantacyanin Plays a Role in Reproduction in Arabidopsis. Plant Physiol. *138*, 778–789.

Dresselhaus, T., and Franklin-Tong, N. (2013). Male–Female Crosstalk during Pollen Germination, Tube Growth and Guidance, and Double Fertilization. Mol. Plant *6*, 1018–1036.

Ermis, M., Antmen, E., and Hasirci, V. (2018). Micro and Nanofabrication methods to control cell-substrate interactions and cell behavior: A review from the tissue engineering perspective. Bioact. Mater. *3*, 355–369.

Fagard, M., Desnos, T., Desprez, T., Goubet, F., Refregier, G., Mouille, G., McCann, M., Rayon, C., Vernhettes, S., and Höfte, H. (2000). PROCUSTE1 Encodes a Cellulose Synthase Required for Normal Cell Elongation Specifically in Roots and Dark-Grown Hypocotyls of Arabidopsis. Plant Cell *12*, 2409–2423.

Fobis-Loisy, I., Chambrier, P., and Gaude, T. (2007). Genetic transformation of Arabidopsis lyrata: specific expression of the green fluorescent protein (GFP) in pistil tissues. Plant Cell Rep. *26*, 745–753.

Fu, Y. (2015). The cytoskeleton in the pollen tube. Curr. Opin. Plant Biol. *28*, 111–119.

Fu, J., Wang, Y.-K., Yang, M.T., Desai, R.A., Yu, X., Liu, Z., and Chen, C.S. (2010). Mechanical regulation of cell function with geometrically modulated elastomeric substrates. Nat. Methods *7*, 733–736.

Fujita, M., Himmelspach, R., Ward, J., Whittington, A., Hasenbein, N., Liu, C., Truong, T.T., Galway, M.E., Mansfield, S.D., Hocart, C.H., et al. (2013). The anisotropy1 D604N mutation in the Arabidopsis cellulose synthase1 catalytic domain reduces cell wall crystallinity and the velocity of cellulose synthase complexes. Plant Physiol. *162*, 74–85.

Gossot, O., and Geitmann, A. (2007). Pollen tube growth: coping with mechanical obstacles involves the cytoskeleton. Planta *226*, 405–416.

Hellens, R.P., Edwards, E.A., Leyland, N.R., Bean, S., and Mullineaux, P.M. (2000). pGreen: a versatile and flexible binary Ti vector for Agrobacterium-mediated plant transformation. Plant Mol. Biol. *42*, 819–832.

Higashiyama, T., and Hamamura, Y. (2008). Gametophytic pollen tube guidance. Sex. Plant Reprod. *21*, 17–26.

Higashiyama, T., and Yang, W. (2017). Gametophytic Pollen Tube Guidance: Attractant Peptides, Gametic Controls, and Receptors. Plant Physiol. *173*, 112–121.

His, I., and Driouich, A. (2001). Altered pectin composition in primary cell walls of korrigan, a dwarf mutant of Arabidopsis defcient in a membrane-bound endo-1,4-b-glucanase. 11.

Hutter, J.L., and Bechhoefer, J. (1993). Calibration of atomic-force microscope tips. Rev. Sci. Instrum. *64*, 1868–1873.

Iwano, M., Shiba, H., Matoba, K., Miwa, T., Funato, M., Entani, T., Nakayama, P., Shimosato, H., Takaoka, A., Isogai, A., et al. (2007). Actin Dynamics in Papilla Cells of Brassica rapa during Self- and Cross-Pollination. Plant Physiol. *144*, 72–81.

Kandasamy, M.K., Nasrallah, J.B., and Nasrallah, M.E. (1994). Pollen-pistil interactions and developmental regulation of pollen tube growth in Arabidopsis. Development *120*, 3405–3418.

Karimi, M., Inzé, D., and Depicker, A. (2002). GATEWAY^{TM} vectors for Agrobacterium-mediated plant transformation. Trends Plant Sci. *7*, 193–195.

Koser, D.E., Thompson, A.J., Foster, S.K., Dwivedy, A., Pillai, E.K., Sheridan, G.K., Svoboda, H., Viana, M., da F. Costa, L., Guck, J., et al. (2016). Mechanosensing is critical for axon growth in the developing brain. Nat. Neurosci. *19*, 1592–1598.

Landrein, B., and Hamant, O. (2013). How mechanical stress controls microtubule behavior and morphogenesis in plants: history, experiments and revisited theories. Plant J. *75*, 324–338.

Lei, L., Zhang, T., Strasser, R., Lee, C.M., Gonneau, M., Mach, L., Vernhettes, S., Kim, S.H., J. Cosgrove, D., Li, S., et al. (2014). The jiaoyao1 Mutant Is an Allele of korrigan1 That Abolishes Endoglucanase Activity and Affects the Organization of Both Cellulose Microfibrils and Microtubules in Arabidopsis. Plant Cell *26*, 2601–2616.

Lennon, K.A., and Lord, E.M. (2000). *In vivo* pollen tube cell of Arabidopsis thaliana I. Tube cell cytoplasm and wall. Protoplasma *214*, 45–56.

Lévy, R., and Maaloum, M. (2002). Measuring the spring constant of atomic force microscope cantilevers: thermal fluctuations and other methods. Nanotechnology *13*, 33.

Lin, D., Cao, L., Zhou, Z., Zhu, L., Ehrhardt, D., Yang, Z., and Fu, Y. (2013). Rho GTPase Signaling Activates Microtubule Severing to Promote Microtubule Ordering in Arabidopsis. Curr. Biol. *23*, 290–297.

Logemann, E., Birkenbihl, R.P., Ülker, B., and Somssich, I.E. (2006). An improved method

for preparing Agrobacterium cells that simplifies the Arabidopsis transformation protocol. Plant Methods *2*, 16.

Louveaux, M., Rochette, S., Beauzamy, L., Boudaoud, A., and Hamant, O. (2016). The impact of mechanical compression on cortical microtubules in Arabidopsis: a quantitative pipeline. Plant J. *88*, 328–342.

MacKinnon, I.M., Šturcová, A., Sugimoto-Shirasu, K., His, I., McCann, M.C., and Jarvis, M.C. (2006). Cell-wall structure and anisotropy in procuste, a cellulose synthase mutant of Arabidopsis thaliana. Planta *224*, 438–448.

Mizuta, Y., and Higashiyama, T. (2018). Chemical signaling for pollen tube guidance at a glance. J. Cell Sci. *131*, jcs208447.

Mouille, G., Ralet, M.-C., Cavelier, C., Eland, C., Effroy, D., Hématy, K., McCartney, L., Truong, H.N., Gaudon, V., Thibault, J.-F., et al. (2007). Homogalacturonan synthesis in Arabidopsis thaliana requires a Golgi-localized protein with a putative methyltransferase domain. Plant J. *50*, 605–614.

Nicol, F., His, I., Jauneau, A., Vernhettes, S., Canut, H., and Höfte, H. (1998). A plasma membrane-bound putative endo-1,4-beta-D-glucanase is required for normal wall assembly and cell elongation in Arabidopsis. EMBO J. *17*, 5563–5576.

Palanivelu, R., and Tsukamoto, T. (2012). Pathfinding in angiosperm reproduction: pollen tube guidance by pistils ensures successful double fertilization. Wiley Interdiscip. Rev. Dev. Biol. *1*, 96–113.

Panteris, E., Adamakis, I.-D.S., Daras, G., and Rigas, S. (2014). Cortical microtubule patterning in roots of Arabidopsis thaliana primary cell wall mutants reveals the bidirectional interplay with cell expansion. Plant Signal. Behav. *9*.

Paredez, A.R., Somerville, C.R., and Ehrhardt, D.W. (2006). Visualization of Cellulose Synthase Demonstrates Functional Association with Microtubules. Science *312*, 1491–1495.

Park, Y.B., and Cosgrove, D.J. (2012). Changes in Cell Wall Biomechanical Properties in the Xyloglucan-Deficient xxt1/xxt2 Mutant of Arabidopsis1. Plant Physiol. *158*, 465–475.

Rotman, N., Rozier, F., Boavida, L., Dumas, C., Berger, F., and Faure, J.-E. (2003). Female Control of Male Gamete Delivery during Fertilization in Arabidopsis thaliana. Curr. Biol. *13*, 432–436.

Ryden, P., Sugimoto-Shirasu, K., Smith, A.C., Findlay, K., Reiter, W.-D., and McCann, M.C. (2003). Tensile Properties of Arabidopsis Cell Walls Depend on Both a Xyloglucan Cross-Linked Microfibrillar Network and Rhamnogalacturonan II-Borate Complexes. Plant Physiol. *132*, 1033–1040.

Sampathkumar, A., Krupinski, P., Wightman, R., Milani, P., Berquand, A., Boudaoud, A., Hamant, O., Jönsson, H., and Meyerowitz, E.M. (2014). Subcellular and supracellular mechanical stress prescribes cytoskeleton behavior in Arabidopsis cotyledon pavement cells. ELife *3*, e01967.

Sampedro, J., Pardo, B., Gianzo, C., Guitián, E., Revilla, G., and Zarra, I. (2010). Lack of α-Xylosidase Activity in Arabidopsis Alters Xyloglucan Composition and Results in Growth Defects. Plant Physiol. *154*, 1105–1115.

Samuel, M.A., Tang, W., Jamshed, M., Northey, J., Patel, D., Smith, D., Siu, K.W.M., Muench, D.G., Wang, Z.-Y., and Goring, D.R. (2011). Proteomic Analysis of Brassica Stigmatic Proteins Following the Self-incompatibility Reaction Reveals a Role for Microtubule Dynamics During Pollen Responses. Mol. Cell. Proteomics MCP *10*.

Sanati Nezhad, A., and Geitmann, A. (2013). The cellular mechanics of an invasive lifestyle. J. Exp. Bot. *64*, 4709–4728.

Sanati Nezhad, A., Naghavi, M., Packirisamy, M., Bhat, R., and Geitmann, A. (2013). Quantification of cellular penetrative forces using lab-on-a-chip technology and finite element modeling. Proc. Natl. Acad. Sci. *110*, 8093–8098.

Sassi, M., Ali, O., Boudon, F., Cloarec, G., Abad, U., Cellier, C., Chen, X., Gilles, B., Milani, P., Friml, J., et al. (2014). An Auxin-Mediated Shift toward Growth Isotropy Promotes Organ Formation at the Shoot Meristem in Arabidopsis. Curr. Biol. *24*, 2335–2342.

Shigeyama, T., Watanabe, A., Tokuchi, K., Toh, S., Sakurai, N., Shibuya, N., and Kawakami, N. (2016). α-Xylosidase plays essential roles in xyloglucan remodelling, maintenance of cell wall integrity, and seed germination in Arabidopsis thaliana. J. Exp. Bot. *67*, 5615–5629.

Shoji, T., Narita, N.N., Hayashi, K., Asada, J., Hamada, T., Sonobe, S., Nakajima, K., and Hashimoto, T. (2004). Plant-Specific Microtubule-Associated Protein SPIRAL2 Is Required for Anisotropic Growth in Arabidopsis. Plant Physiol. *136*, 3933–3944.

Smyth, D.R., Bowman, J.L., and Meyerowitz, E.M. (1990). Early flower development in Arabidopsis. Plant Cell *2*, 755–767.

Takáč, T., Šamajová, O., Pechan, T., Luptovčiak, I., and Šamaj, J. (2017). Feedback Microtubule Control and Microtubule-Actin Cross-talk in *Arabidopsis* Revealed by Integrative Proteomic and Cell Biology Analysis of *KATANIN 1* Mutants. Mol. Cell. Proteomics *16*, 1591–1609.

Uyttewaal, M., Burian, A., Alim, K., Landrein, B., Borowska-Wykręt, D., Dedieu, A., Peaucelle, A., Ludynia, M., Traas, J., Boudaoud, A., et al. (2012). Mechanical Stress Acts via Katanin to Amplify Differences in Growth Rate between Adjacent Cells in Arabidopsis. Cell *149*, 439–451.

Verger, S., Long, Y., Boudaoud, A., and Hamant, O. (2018). A tension-adhesion feedback loop in plant epidermis.

Xiao, C., and Anderson, C.T. (2016). Interconnections between cell wall polymers, wall mechanics, and cortical microtubules: Teasing out causes and consequences. Plant Signal. Behav. *11*.

Xiao, C., Zhang, T., Zheng, Y., Cosgrove, D.J., and Anderson, C.T. (2016). Xyloglucan Deficiency Disrupts Microtubule Stability and Cellulose Biosynthesis in Arabidopsis, Altering Cell Growth and Morphogenesis. Plant Physiol. *170*, 234–249.

Zhang, T., Mahgsoudy-Louyeh, S., Tittmann, B., and Cosgrove, D.J. (2014). Visualization of the nanoscale pattern of recently-deposited cellulose microfibrils and matrix materials in never-dried primary walls of the onion epidermis. Cellulose *21*, 853–862.

Supporting information

Additional experiments were carried out to confirm some results or validate tools used in this work. The rational and outcomes of these experiments are presented below.

1. SLR1 promoter expression during stigmatic development

To follow the dynamics of CMTs during stigma development, we used the promoter region of the stigma specific *S-Locus Related gene 1* (*SLR1*) from *Brassica oleracea* (Lalonde et al., 1989). We checked the activity of the pSLR1 promoter with the pSLR1:GFP construct and found that it was active from stages 12 to 15, even though we noticed a decrease in GFP expression for the late stage 15 (Supplementary Fig. 5). These data are in accordance with a previous study in which activity of this promoter was analysed in *A. lyrata* stigmas (Fobis-Loisy et al., 2007) and where GFP fluorescence was found to decrease with flower ageing. This rather continuous expression of GFP under the control of pSLR1 allowed us to use pSLR1:MAP65-citrine as a marker of CMTs from stages 12 to 15.

Supplementary Fig. 5 / Expression of the pSLR1 promoter using pSLR1:GFP during developmental stages 12 to 15.
Confocal settings are identical for all images. GFP accumulates in the cytoplasm of stigmatic cells and enters spontaneously in the nucleus (n). Scale bar, 20 µm.

2. Stigmatic CMT dynamics confirmed with p35S:MBD-GFP marker line

Because MAP65 is known to bundle CMTs, we additionally analysed the CMT pattern during stigma development using the Microtubule Binding Domain (MBD) fused to GFP under the control of the 35S promoter (p35S:MBD-GFP). Like the MAP65-GFP marker, we found that CMT pattern was dynamic, changing from an anisotropic array to an isotropic one from stage 12 to 15 (Supplementary Fig. 6).

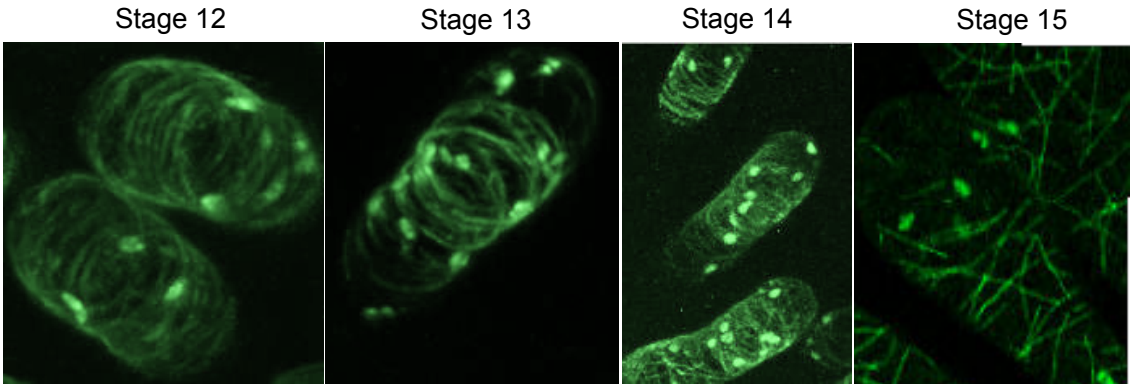

Supplementary Fig. 6 / Confocal images of papilla cells expressing MBD-GFP during stigma development.

3. Confirming the AFM measurements

We confirmed the difference of stiffness between Col-0 and *ktn1-5* papillae at stage 13 using another Atomic Force Microscope (JPK Nanowizard III), and using another method of curve analysis based on the retract curves. Results confirmed that apparent young modulus is significantly lower in *ktn1-5* than in Col-0 papillae (Supplementary Fig. 7).

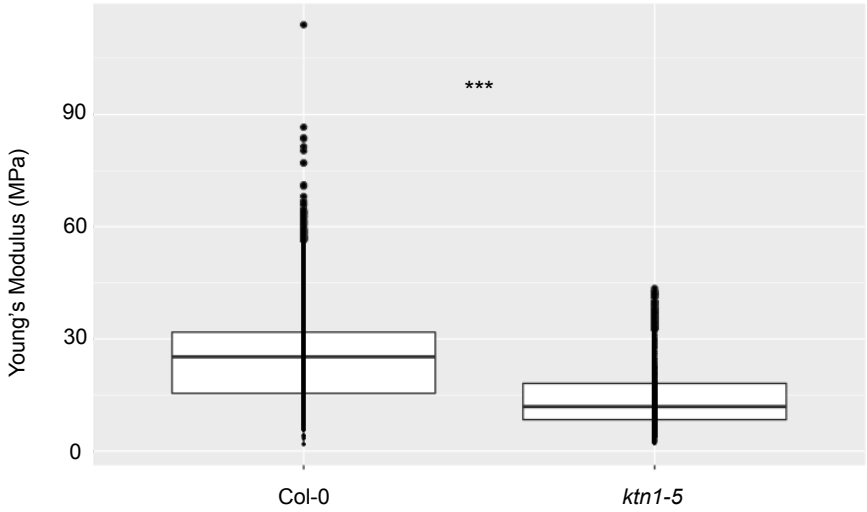

Supplementary Fig. 7 / Stiffness differences between Col-0 and *ktn1-5* papillae at stage 13.
Young's modulus values of the papilla cell wall for Col-0 at stage 13 (N= 7 stigmas, n= 33 papillae) and *ktn1-5* (N= 7 stigmas, n= 9 papillae). Statistical differences were calculating using a T-test, ***P<0.01.

4. Pollen tube guidance and fertility in *ktn1-5*

All the KATANIN mutants were described to have defects in seed yield and display shorter siliques (Luptovčiak et al., 2017). Given that WT pollen tube guidance is impaired on *ktn1-5* papillae, we investigated whether the *ktn1-5* pollen tube growth was affected on Col-0 papillae. Using Scanning Electron Microscopy, we found that *ktn1-5* pollen is able to hydrate, germinate and emit a tube that grows straight to the base of Col-0 papillae, hence behaving as a WT pollen on Col-0 stigma. By contrast, *ktn1-5* pollen tubes were mis-guided and turned around *ktn1-5* papillae, like Col-0 pollen tubes when placed on *ktn1-5* papillae (Supplementary Fig. 8a). Additionally, we analysed the fertility of the *ktn1-5* mutant and found a significantly lower number of seeds and shorter siliques when *ktn1-5* was self-pollinated (Supplementary Fig. 8b,c). Interestingly, *ktn1-5* pollen on Col-0 pistils gave a seed yield close to self-pollinated Col-0. Then, we checked whether Col-0 pollen tubes were capable of fertilizing *ktn1-5* ovules and found that although pollen tubes reached the ovules, only a very low seed set was counted (Supplementary Fig. 8d). Altogether, these results reveal that fertility of the female gametophyte is altered in *ktn1-5* mutant.

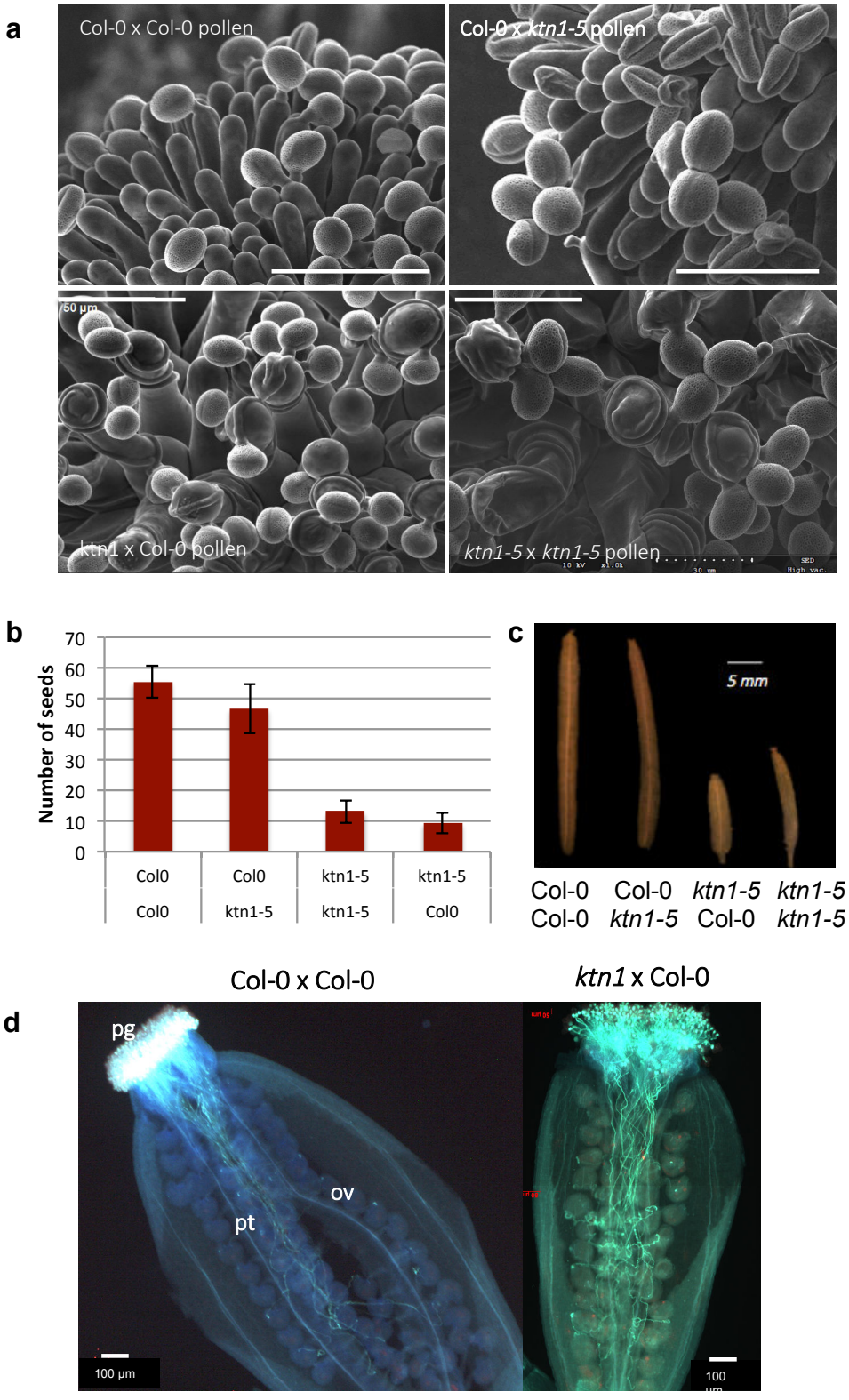

Supplementary Fig. 8 / *ktn1-5* is impaired in female fertility.
In all crosses, for example *ktn1-5* x Col0, the female partner is written first (*ktn1-5* in the example). a, Pollen grain behaviour using SEM. Scale bars, 50 µm. b, Seed set. c, Silique length. d, Aniline blue staining of Col-0 and *ktn1-5* pistils pollinated with Col-0 pollen grains, after 6 hours. pt=pollen tubes, ov=ovules.

5. Pollen tube growth behaviour on another KATANIN mutant, *botero1-7*

We checked whether the coiled phenotype could be observed in another KATANIN mutant, the *bot1-7* in WS background (Bichet et al., 2001). When we pollinated *bot1-7* papilla cells with WS pollen grains, growing pollen tubes coiled around the *bot1-7* papillae like they did on *ktn1-5* papillae (Supplementary Fig. 9).

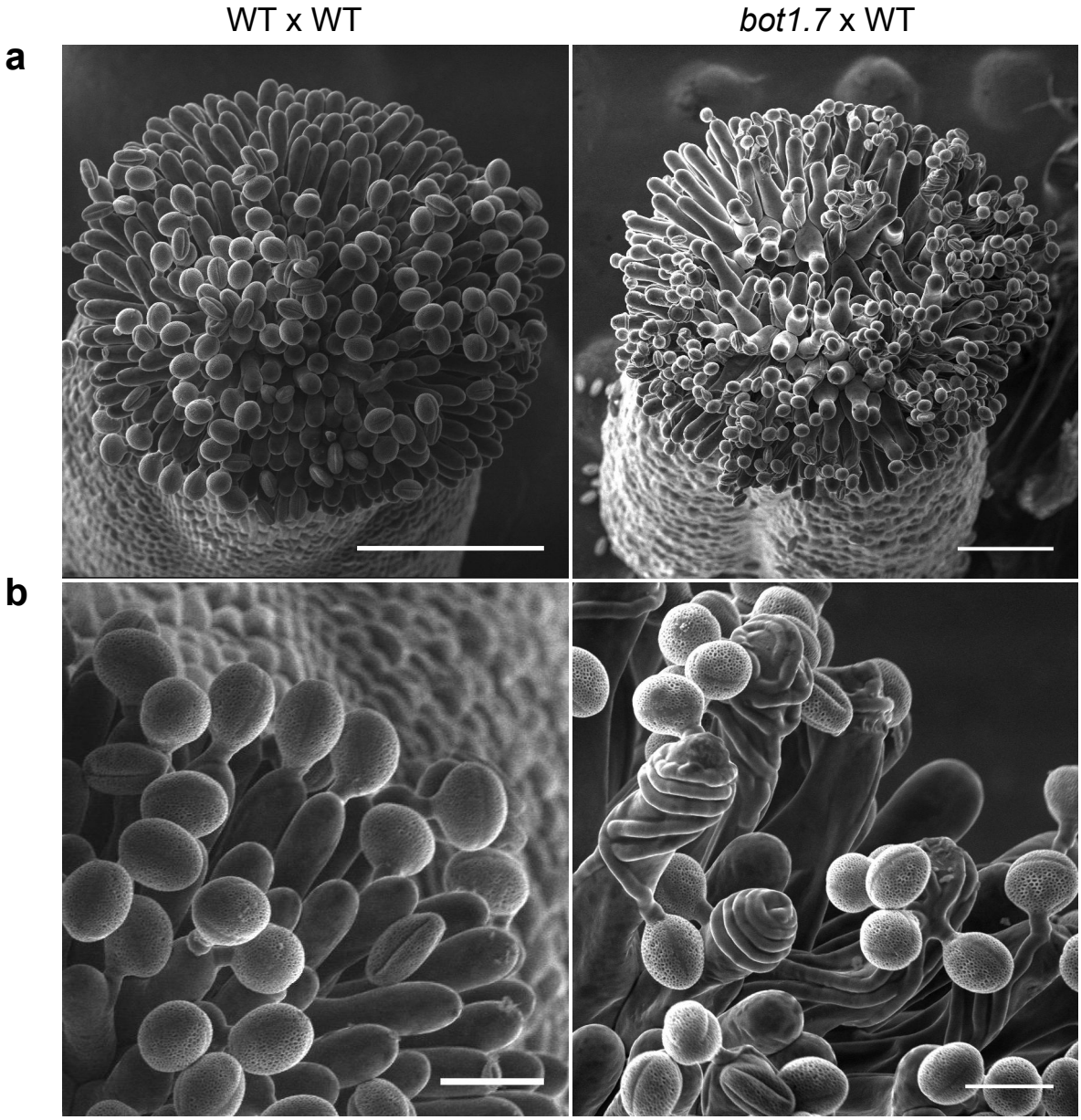

Supplementary Fig. 9 / WS pollen tube on *botero1-7* stigmas.
a, Overview of WS and *bot1-7* stigmas pollinated with WS pollen grains. Scale bar, 50 µm. b, Magnification of WS and *bot1-7* papillae pollinated with WS pollen Scale bar, 20 µm.

6. Effect of a highly anisotropic CMT pattern on pollen tube behaviour

To check whether the coiled pollen tube phenotype observed on *ktn1-5* papillae was linked to the particular CMT isotropy of mutant cells, we also tested the pollen tube response in a mutant predicted to have an increase of CMT array anisotropy. SPIRAL2 is a protein that prevents CMT severing at the microtubule crossing sites and acts in opposition to KTN1 activity. The *spr2-2* mutant exhibits more organised CMT arrays (Shoji et al., 2004). In the *spr2* mutant, microtubule reorientations are reduced, leading to an increase in the final anisotropy of the MT arrays (Fan et al., 2018; Nakamura et al., 2018) and a faster response to mechanical stress (Shoji et al., 2004; Buschmann et al., 2004; Hervieux et al., 2016). By expressing the MAP65.1-citrine marker in *spr2-2* papilla cells, we found an anisotropic pattern of CMTs resembling that of Col-0 papillae (Supplementary Fig. 10a,c). After pollination of *spr2-2* stigmas at stage 13 with Col-0 pollen grains, pollen tube growth was not significantly different from that observed with Col-0 stigmas, with a majority (above 50%) of pollen tubes growing straight in papilla cells (Supplementary Fig. 10b,d).

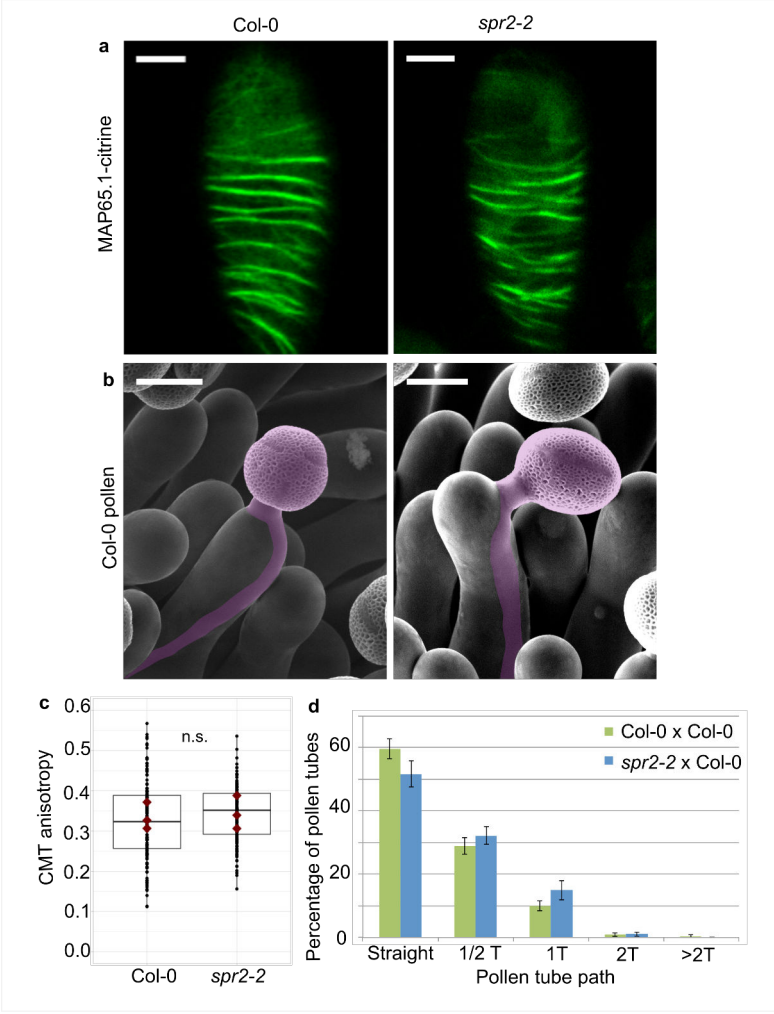

Supplementary Fig. 10 / Effect of highly organised CMT array on pollen tube path.

a, Confocal images of papilla cells expressing MAP65.1-citrine in Col-0 and *spr2-2* at stage 13. Scale bars, 5 µm. b, SEM images of Col-0 and *spr2-2* papillae pollinated with Col-0 pollen grains; pollen and tubes were artificially colorized. Scale bar, 10 µm. c, CMT anisotropy of Col-0 and *spr2-2* papilla cells at stage 13. Statistical differences were calculated using a Shapiro-Wilk test to evaluate the normality and then a Wilcoxon test, ***P < 0.01, n.s = non significant. N(Col-0) = 10 stigmas, n(Col-0) = 166 papillae, N(*spr2-2*) = 10 stigmas, n(*spr2-2*) = 145 papillae. d, Quantification of the number of turns (T) made by Col-0 pollen tubes on *spr2-2* and Col-0 papillae. Data are expressed as mean +/- s.e.m. No statistical difference was found between pollen tubes path within *spr2-2* and Col-0 papillae and was calculated using an ajusted Chi-Square test for homogeneity (2 degrees of freedom). N(Col-0) = 23 stigmas, n(Col-0) = 180 papillae, N(*spr2-2*) = 25 stigmas, n(*spr2-2*) = 238 papillae.

7. Cellulose organisation within stigmatic cells: comparison of Col-0, *ktn1-5* and *xxt1 xxt2* cell walls

Because of the importance of CMFs in the mechanical properties of the cell wall, we examined the CMF pattern of cell walls in papilla cells of Col-0, *ktn1-5* and *xxt1 xxt2* at stage 13. First, we used red Direct 23 staining, which was previously employed to reveal the CMF orientation in hypocotyl cells (Landrein et al., 2013). Because of the hydrophobic surface of stigma papillae, to facilitate penetration of the staining through the cuticle we treated stigmas with a solution of Adigor (Syngenta) (Hammami et al., 2014), an adjuvant previously used in leaves (Knoblauch et al., 2015). The stained cells were then observed by Total Internal Reflection Fluorescence (TIRF) or spinning disk microscopy. Our preliminary results (Supplementary Fig. 11) suggest differences between all genotypes. In Col-0, the CMFs seem to be straight like in *xxt1 xxt2*, although in this latter CMFs appear much thinner. In *ktn1-5* papillae, CMFs look more detached and isotropic. These very preliminary results are consistent with the hypothesis that mechanical anisotropy of the cell wall, which is observed in Col-0 and *xxt1 xxt2*, is necessary to direct pollen tube straight to the base of the papilla.

However, the difficulty we encountered in staining and observing a large number of papillae (e.g., on one stigma, only one or two papilla cells showed the cellulose staining) did not permit us to accumulate enough data to draw clear conclusion on CMF orientation.

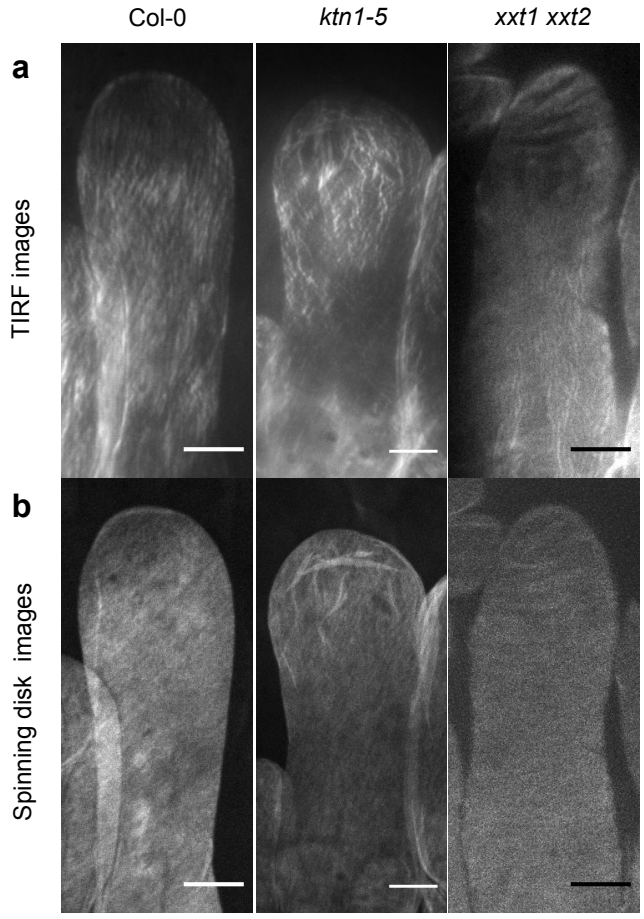

Supplementary Fig. 11 / Preliminary results of the cellulose pattern in stigmatic cells.
a, Col-0, *ktn1-5*, and *xxt1 xxt2* stigmatic papillae stained with Red Direct 23 and observed with TIRF microscopy. b, Col-0, *ktn1-5*, and *xxt1 xxt2* stigmatic papillae as in a, imaged with spinning disk microscopy. Scale bar, 10 µm

8. Plantacyanin expression in Col-0 and *ktn1-5* stigmas

In a previous work, coiled growth of pollen tubes was reported in Arabidopsis stigma papillae overexpressing the blue copper protein plantacyanin (AT2G02850), although the mode of action of this protein was not described and remains totally unknown (Dong et al., 2005). We checked whether the coiled phenotype in *ktn1-5* papillae could be explained by an increased plantacyanin expression in the stigma. By quantitative RT-PCR we found a relative plantacyanin expression of 2,21 for Col-0 and 0.80 in *ktn1-5*, indicating that the coiled phenotype in *ktn1-5* was independent of plantacyanin up-regulation.

Material & Methods

Plant Materials and Growth Conditions. *Arabidopsis thaliana*, ecotype Columbia (Col-0), *Arabidopsis* transgenic plants generated in this study and *Arabidopsis* mutants were grown in soil under long-day conditions (16 hours of light / 8 hours of dark, 21°C / 19°C)

with a relative humidity around 60%. The pSLR1::GFP construct has been previously described (Fobis-Loisy et al., 2007) as well as the p35S::GFP-MBD (Hamant et al., 2008). The *botero1-7* katanin mutant allele was previously described in Bichet et al., 2001, and the *spiral2-2* mutant in Shoji et al., 2004.

Cellulose staining. A droplet of Adigor was applied at 2.5% (v/v) solution on the stigma, during 4 hours. As described in (Landrein et al., 2013) for hypocotyls, emasculated pistils were incubated in 12.5% glacial acetic acid for 1 hour and dehydrated in 100% and then 5°% ethanol for 20 min each. Pistils were then washed in water during 20 min and stored in 1M KOH. Pistils were then stained using 0.01% (w/v) Red Direct 23 dye during 4 hours before imaging by TIRF microscopy.

Environmental Scanning Electron Microscopy (SEM). Flowers from stages 13 (Smyth et al., 1990) were emasculated and pollinated on plants with mature WT pollen. One hour after pollination, pistils were cut in the middle of the ovary, deposited on a SEM platform and observed under Hirox SEM SH-3000 at -20°C, with an accelerating voltage of 15kV. Images were processed with ImageJ software.

AFM Measurements. Pistils at stage 13 were placed straight in a 2% agar MS medium and 0.8% low-melting agarose was added up to the base of papilla cells. The experiments have been performed in air at room temperature. AFM indentation experiments were carried out using a JPK Nanowizard III microscope equipped with a CellHesion module driven by a JPK Nanowizard software 6.0. The CellHesion module allows the use of a 100µm-range Z piezo, located into the microscope stage, and increases the available Z range by several times compared to the head Z piezo (around 15 µm-ranged). All quantitative measurements were performed using standard pyramidal tips (Bruker RFESP-190), with a spring constant of 34,875 N/m. The tip radius given by the manufacturer was 8 nm. Matrix of 6 x 6 µm (144 points) was obtained for each papilla. The ramp size was 3 µm, approach and retraction speeds were 10 µm/s and the trigger force 1µN. The Young's Modulus was calculated using the JPK Data Processing software 6.0 by fitting the entire force versus the tip-sample distance curves. Due to the presence of a strong adhesion force (sometimes greater than 50% of the trigger force), a contact model including the adhesion was chosen, more specifically the DMT model for a cone-shaped indenter and retraction curves were analysed. The fit parameters were: tip shape, cone; half-cone angle: 18°; poisson ratio: 0,3.

RNA extraction and real-time quantitative PCR. 30 non-pollinated stigmas were dissected from stage 13-flowers and total RNA was extracted with the Arcturus®

PicoPure® RNA isolation kit (Life Technologies). 536 ng of total RNA were reverse-transcribed with the SuperScript® VILO™ cDNA Synthesis Kit (Invitrogen) and subjected to quantitative real-time PCR. Amplification of Plantacyanin (At2g02850) was performed with forward primer 5'- CTTTAACGCTGTGGGTTGGC -3' and reverse primer 5'-ACGTTGTGCATCCTCGGATT -3'. Real-time PCR was performed with SYBR green fluorescence and the iCycler iQ5 system (Bio-Rad, Hercules, CA). PCR efficiency of primers was estimated from calculation using the standard curve amplification and the equation E=10-1/slope. Quantitative analysis of real-time PCR results was performed using the 2-ΔΔCt method (Schmittgen and Livak, 2008) normalized to the endogenous reference Actin8 (forward primer 5'-TCAAGCTGTTCTATCACTTTACGC-3' and reverse primer 5'-GGAAGTGAGAAACCCTCGTAGATA-3').

Exploring the role of stigmatic cells in pollen tube guidance by modelling approach

How the mechanical anisotropy of the stigmatic cell can impact the pollen tube trajectory? How can we explain the loop phenotype observed on *ktn1-5* papillae?

One fascinating feature of the *ktn1-5* phenotype is the helical growth of wild-type (WT) pollen tubes on mutated stigmatic cells. To decipher this astonishing phenotype, we started a collaboration with Catherine Quilliet and Karin John, physicists from the "Laboratoire Interdisciplinaire de Physique" in Grenoble. Our objective is to create an in silico model for pollen tube growth on stigmatic cells. In this chapter, I will briefly explain the basis of this collaborative work, which is very preliminary.

To be able to model the pollen tube path, the first step is to create a virtual papilla, or papilla profile.

(i) Creation of a virtual papilla profile

The WT stigmatic cell has a characteristic elongated shape whereas the *ktn1-5* papilla has a shape that slightly diverges from the one of WT cells by its width (Supplementary Fig. 4a-d) and its "bottle" shape (Fig. 15a,b). To create the papilla profile, we decided to estimate the papilla cell shape based on to 5 representative points or distances of the papilla geometry (yellow points on (Fig. 15b): (i) the top of the papilla head, (ii and iii) the largest region of the papilla head and (iv and v) the narrowing region of the neck. We provided a series of images of WT and *ktn1-5* stigmas to our collaborators. They automatically measured lengths *L*, *l*, *B* and *D* (Fig. 15b) for 5 selected stigmatic cells from each genotype and based on these values developed a mathematical model for generating the papilla profile. The analytical model of the stigmatic geometry was obtained considering the papilla as an axisymmetric object. Briefly, the function *f(x)*, corresponding to a model of papilla profile, is the sum of three types of contributions: the top of the head (corresponding to the yellow-green curve in Fig. 15c), the upper part of the neck (blue curve) and finally, the lower part of the neck (corresponding to the green curve on the Fig. 15c), considered to be conical.

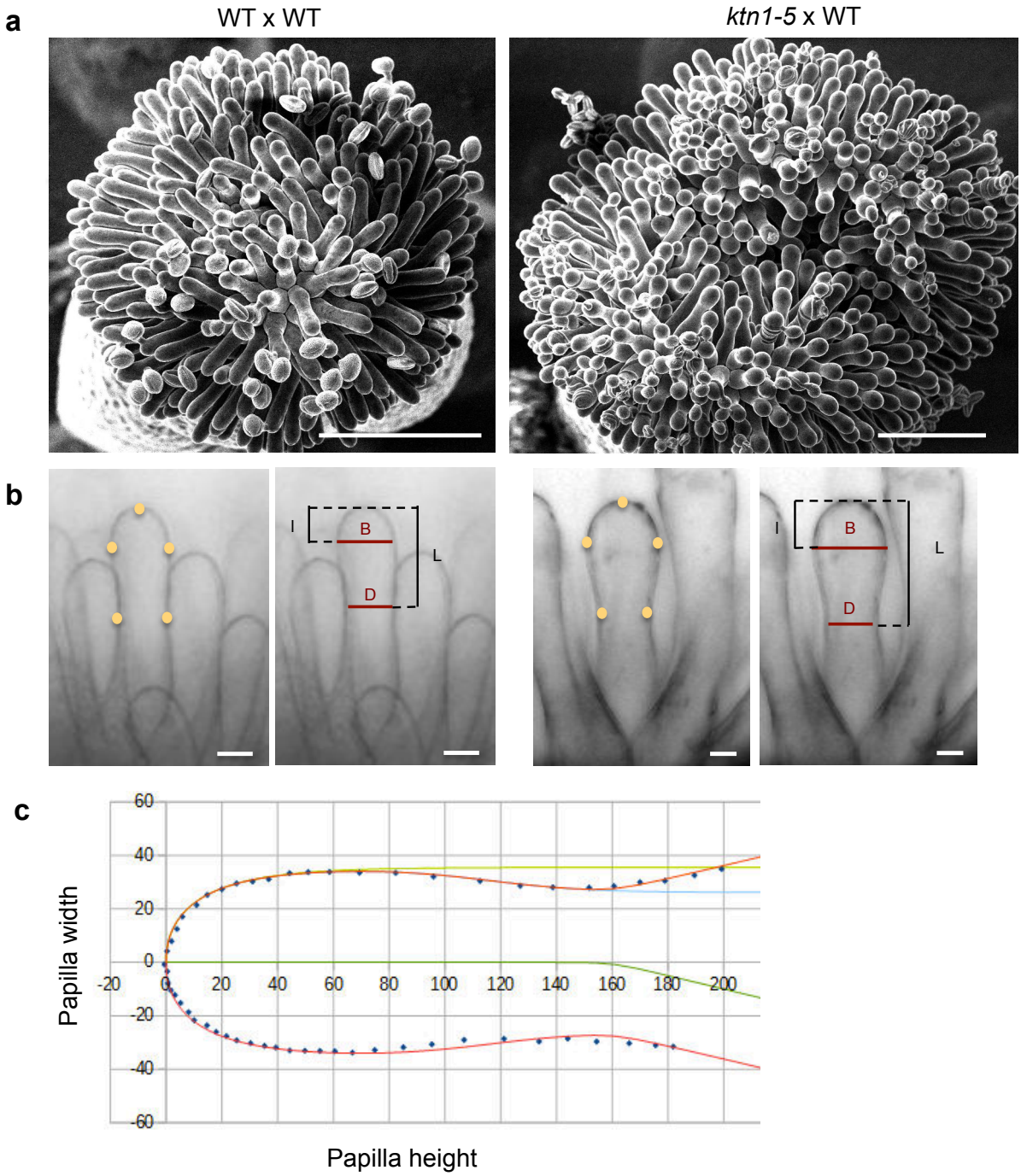

Fig. 15 / Papilla profile creation.
a, Scanning Electron Microscope (SEM) images of WT and ktn1-5 stigmas pollinated with WT pollen grains. Bars, 50 µm. b, Characteristic points of WT and *ktn1-5* papilla and lengths associated. Bars, 10 µm. c, Example of WT papilla profile. Yellow-green: model curve for top, blue: model curve for the head, dark-green: model curve for the base of the papilla. Red: sum of all the curves.

Having a first stigmatic cell profile, the next step was to define parameters allowing the modelling of pollen tube trajectories.

(ii) Defining pollen tube trajectory: parameters used

Based on biological observations I made during my PhD, we defined three important parameters that seem to be important for modelling the pollen tube path:

(i) The self-avoidance: observing pollinated *ktn1-5* papillae, I found that several pollen grains can germinate and emit a pollen tube on the same papilla, sometimes reaching up to 7 tubes by papilla. During its growth, a pollen tube rarely passes over another one, so that pollen tubes tend to self-avoid, as illustrated in Fig. 16a.

(ii) The position of the pollen grain attachment: on the WT or *ktn1-5* papillae, I did not observe any preferential site for pollen grain attachment, except that pollen grains do no attach to the lower third part of the papilla, probably due to the restricted space existing between the papilla bases. Thus, on the upper two thirds of the stigmatic cells, pollen tube seems to land randomly. In the model, the site where the pollen grain attaches is referred as the "starting position" corresponding to the ratio between the position of the pollen grain from the top of the papilla head (distance z, Fig. 16b) and the papilla size from the top (distance L, Fig. 15b, Fig. 16b).

(iii) The pollen tube entry angle: similarly, on WT or *ktn1-5* papilla, we did not observe any preferential angle for the direction taken by the growing pollen tube just after its germination, meaning that the tube can grow towards different directions, on the left, right, up or down. In the model, the angle made by the grain and the tube is referred as the "starting angle ϕ" (Fig. 16b)

Taking into account these parameters, our collaborators performed the first assay for pollen tube growth on the papilla profile. An example of this pilot model is shown on Fig. 16c.

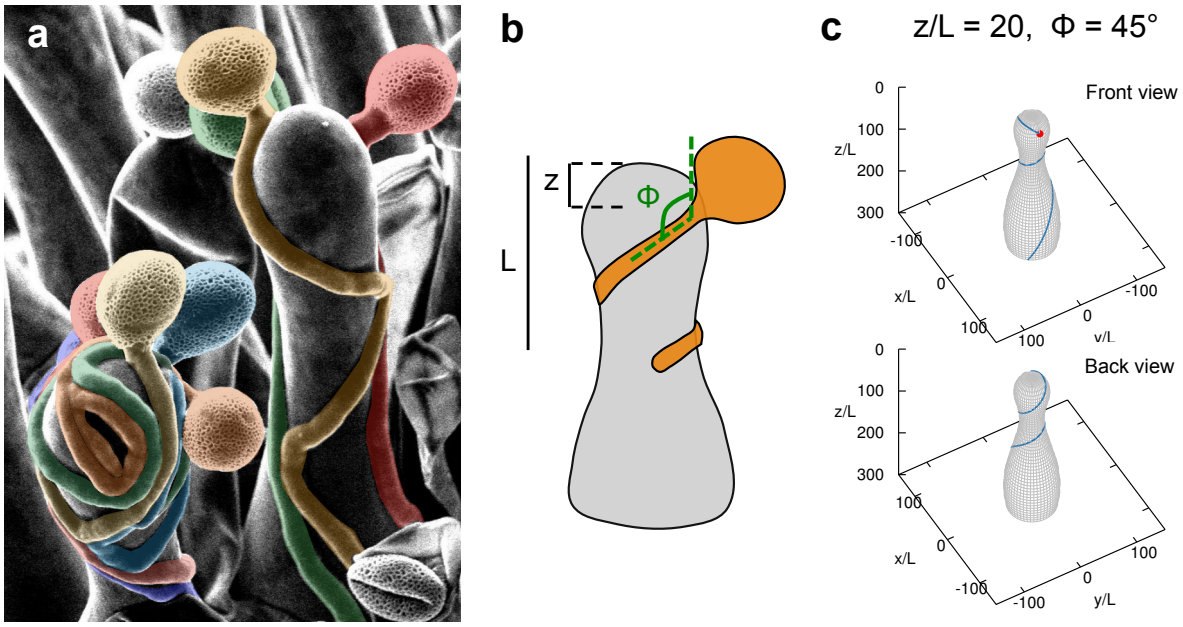

Fig. 16 / Example of pollen tube path.
a, Scanning Electron Microscope image (SEM) illustrating the self-avoiding behaviour of pollen tubes on *ktn1-5* papillae. b, representation of the pollen tube growth parameters: L, z and ϕ (see text) and c, Example of pollen tube path, starting position z/L= 20, starting angle ϕ = 45°.

(ii) Testing the pilot analytic model: does it explain the coiled phenotype observed on *ktn1-5* papillae

Our pilot model predicts that the number of coils is correlated with the starting position of the pollen grain and the starting angle of the tube. A phase diagram, presented in Fig. 17, illustrates this correlation for *ktn1-5* papillae. The horizontal axis corresponds to the starting position (z/L), the vertical axis to the starting angle (ϕ) and the color code to the number of predicted coils. When a pollen grain is deposited at the extremity of the papilla (z/L = 0), whatever the starting angle, the number of coils is predicted to be low. At the opposite, when a grain is deposited at the upper part of the stigmatic cell (z/L ranging from 10 to 50), the number of coils is maximal (>3) for starting angles ranging from 45° to 135°.

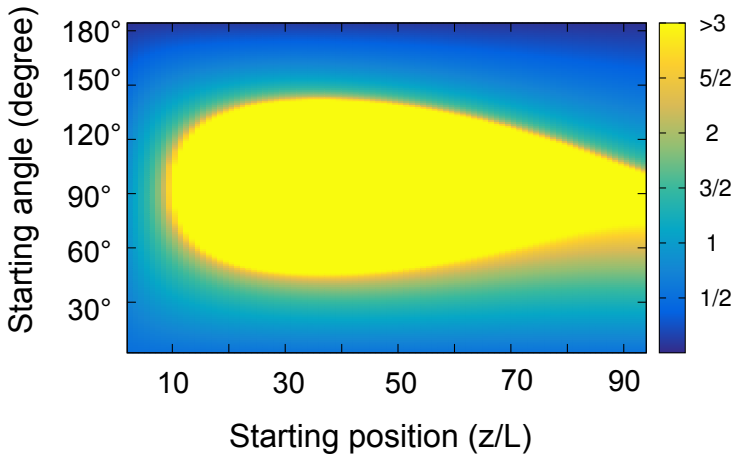

Fig. 17 / Phase diagram of the pollen tube behaviour depending on the initial angle and the starting position.
The color code indicates the number of predicted coils.

To validate this pilot model, only based on *ktn1-5* papilla shape (bottle shape) and our three selected pollen tube growth parameters, we measured on SEM images the starting position, starting angle and number of coils for about 20 pollen tubes on *ktn1-5* papillae. Our preliminary data reveal that there is no strict correlation between these three factors. This suggests that additional features are needed to reproduce the coiled phenotype exhibited by pollen tubes on *ktn1-5* stigmas.

In conclusion, we cannot fully correlate our biological data with the theoretical model. This fits well with our previous analysis showing that the stigmatic shape is not sufficient to explain the coiled phenotype observed on *ktn1-5* stigmas. Indeed, the stigmatic papillae of the *any1* mutant, which is impaired in cellulose synthase, have a shape similar to that of *ktn1-5* papillae but do not display the coiled phenotype. Other factors should be incorporated in the model, and we are currently thinking of how integrating anisotropy of the CMTs and mechanical properties of the stigmatic cell surface in it.

4

Epidermis responses to pathogen invading cells: the case of oomycete infection

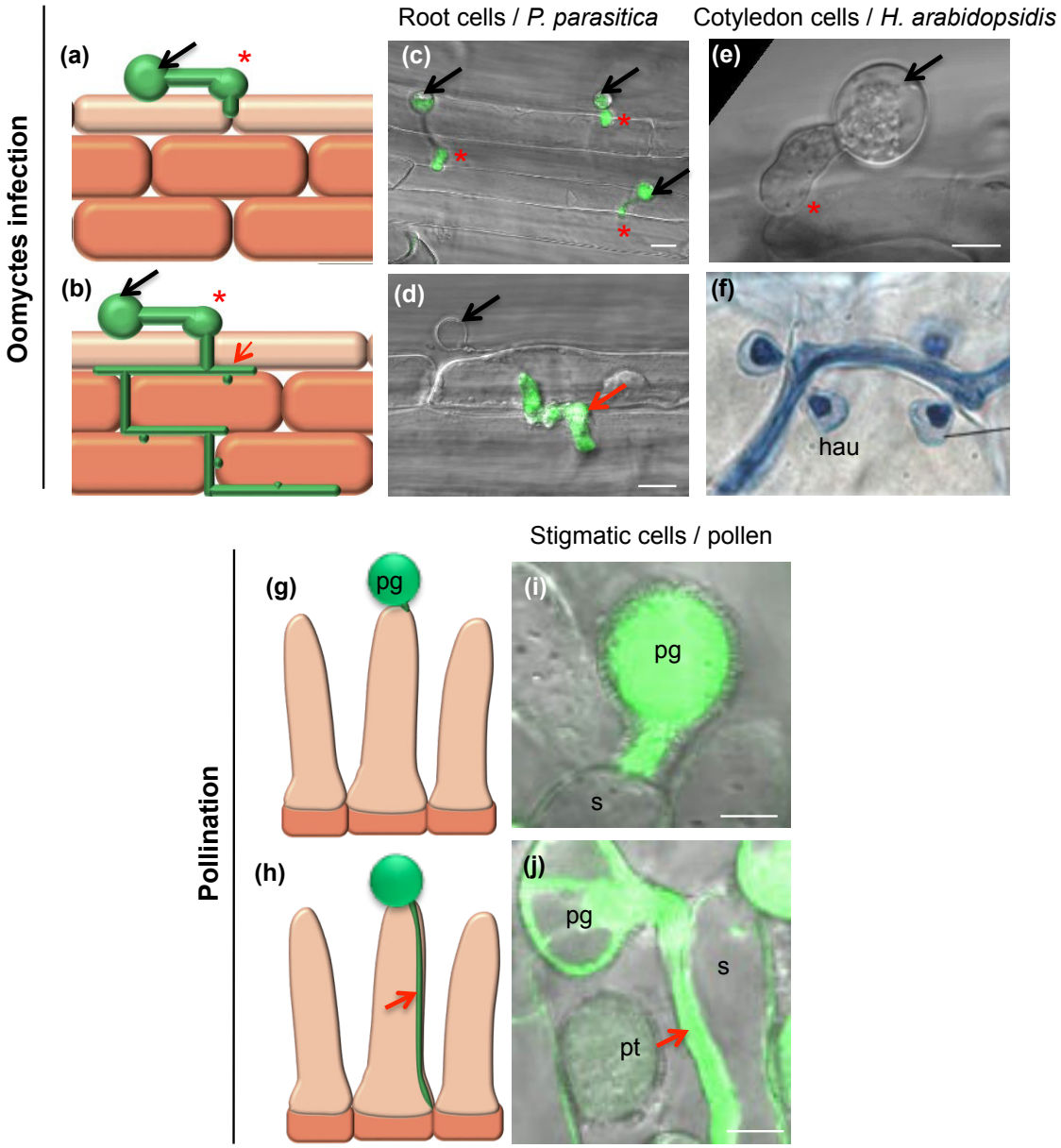

Fig. 18 / Oomycete and pollen interactions with plant epidermis surface.
(a-f) Oomycete infection of epidermal cells. (a,b) Schematic representation of interaction during oomycete infection. (a,c,e) Oomycete spores (black arrow) attach to the epidermis surface of the root (*P. parasitica*) (c) or the cotyledon (*H. arabidopsidis*) (e) and produce an appressorium (red *). (c) 2,5 hours after infection (hai), *P. parasitica* penetrates the root epidermal cells. (e) 8 hai, *H. Arabidopsidis* penetrates the cotyledon epidermal cells. (b, d ,f) Hypha (red arrow) grows through the epidermis and within the underlying tissues. (d) 6 to 10 hai for *P. parasitica.* (f) 24 hai for *H. arabidopsidis*. *H. arabidopsis* hyphae form feeding structures, haustoria (hau). *P. parasitica* zoospores express a GFP marker and *H. arabidopsis* spores express a GUS marker. (g-j) Pollination interaction with stigmatic cells. (g-h) Schematic representation of pollen – papilla interactions. (g,i) 10 min after pollination (map), pollen grain (pg) hydrates, germinates, and a short pollen tube starts to penetrate the stigmatic cells (s). (h,j) 60 map, pollen tube (pt, red arrow) grows though the epidermis and reach the underlying tissues. Pollen grain and pollen tube express a cytoplasmic GFP marker. Images from L. Riglet and A. Attard. Bars, (c,d,i,j) 10 µm, (e) 5 µm.

During the first part of this work, we extensively studied the role of the stigma epidermis as a boundary, facilitating the entrance of desirable pollen grains. Plant epidermis has also been shown to have crucial role in other cell-to-cell interaction processes such as pathogen attack. While the biological purpose of pollen-stigma and plant - pathogen interactions diverges, both processes exhibit several cellular and molecular similarities that led some authors to speculate that they may share common ancestry (Dickinson, 1995; Elleman and Dickinson, 1999; Nasrallah, 2005, Mondragón-Palomino et al., 2017; Zang et al., 2017). Vocabularies used in pollen–stigma interaction even borrow the one of the pathogen field, such as the foot also called appresoria-like structure (Elleman and Dickinson, 1990) or the pollen tube often assimilates as an invader (Sanati Nezhad and Geitmann, 2013). Comparing these two cell-to-cell interaction systems is of particular interest to decipher the cellular and molecular mechanisms underlying these phenomena that play key roles in plant biology.

When comparing pollen grain germination and pollen tube growth with the behaviour of filamentous pathogen (fungus and oomycetes) during infection, we found physiological similarities that led us to focus on this category of pathogens (Fig. 18). Besides, as the cell wall is an important layer at the interface between the invading cell and the plant tissue, we decided to restrict our analysis to oomycete pathogens which harbour a cell wall mainly composed of cellulose as plant cells (Latijnhouwers et al., 2003; Meng et al., 2014).

I. Oomycete lifestyles and invasive strategies

Oomycete pathogens cause most of the plant diseases in the world, damaging agricultural crops. The most notorious example was the Irish famine triggered by *Phytophtora infestans* between 1845 to 1851 that massively devastated the potatoes production, the main source of food, leading to about 1 million people died and a mass emigration of Irish to the USA (Alexopoulos et al., 1996; Ristaino, 2002).

Although oomycetes have been firstly classified as “lower fungi”, they differ from fungi in several characteristics. Molecular phylogenetic analysis has demonstrated that oomycetes and true fungi (as Ascomycetes and Basidiomicetes) have evolved independently, the oomycetes belonging to the Stramenipila phylum, including brown algae (Govers, 2001; Meng et al., 2014). Among their differences, they have different lifecycles; oomycetes are diploid during their vegetative stage contrary to fungi that are mostly haploid. Their cell wall composition also differs since the one of oomycetes mainly contains cellulose whereas the fungi wall is mostly constituted of chitin (Latijnhouwers et al., 2003; Meng et al., 2014). There are around 800 known oomycete species (Judelson,

2017) and they can display biotrophic, hemibiotrophic or necrotrophic lifestyles (Fawke et al., 2015). The biotrophic oomycetes are dependent of their host, maintaining them alive for survive throughout their lifecycle as do *Hyaloperonospora arabidopsidis* on leaves. Conversely, necrotrophic oomycetes kill their host and continue to feed from dead tissues. Between both, hemibiotrophic oomycetes, such as *Phytophtora parasitica*, have a biotrophic lifestyle at the early stage of their development and then switch to the necrotrophic lifestyle. Oomycete spores are single-nucleated cells without wall, specialized to disperse the pathogen, either by wind (as *H. arabidopsidis*) or water (as *P. parasitica*) (Savory et al., 2014). Spores can reach the plant surface directly when they are released on it (immotile spores or conidiospores) or swim towards the host (motile spores or zoospores). On the plant surface, the spore emits a germ tube that grows towards a suitable penetration site, before forming an appressorium necessary for epidermis breach. Following penetration, a tip-growing structure, called hyphae, is generated and grows through the epidermal cells and then intercellularly within the plant internal tissues. For biotrophic oomycetes or during the biotrophic phase of the hemibiotroph oomycetes, nutrients are acquired through the formation of haustoria. The development of such feeding structure involves the invagination of the plant plasma membrane that encircles the haustoria and forms a critical interface between the host and the pathogen (Bozkurt et al., 2015).

II. Cellular responses of infected epidermal cells

As other plant pathogens, when an oomycete successfully breaches the first physical barrier constituted by the plant cuticle and cell wall, it has to face the plant immune system response. The first level of plant resistance is triggered by recognition of pathogen derivate molecules (PAMP) or plant degradation products caused by the pathogen attack (DAMP). PAMPs and DAMPs induced a complex set of defence responses, known as PAMP-triggered immunity (PTI), such as production of reactive oxygen, synthesis of defence related proteins and antimicrobial compounds or cell wall reinforcement (reviewed in Bigeard et al., 2015). Furthermore, perception of PAMPs triggers host subcellular changes, which have been well documented in oomycete infections (Hardham 2007; Lu et al., 2012). One of the earliest responses of epidermal cells infected by oomycetes is the cytoplasmic aggregation beneath the penetration site. Observations of GFP-tagged Arabidopsis plants revealed a dense network of lamellar ER and concentration of Golgi stacks around the hypha penetration site (Takemoto and col., 2003). This re-organisation of the endomembrane system is proposed to be associated with materiel deposition to reinforce the physical (accumulation of callose) and chemical

(secretion of antimicrobial compounds) barriers to pathogen entrance. Cytoplasmic aggregation and polarized transport are dependent on the actin cytoskeleton as shown using drug treatments that delay or suppress several defence responses (Tomiyama et al., 1982; Takemoto et al., 1999). In addition to the pharmacological studies, a live imaging approach has shown a focalization of actin filaments around the penetration site in *A. thaliana* cotyledons cells infected with two Phytophtora species. By contrast, the behaviour of the cortical microtubules network is more variable. In some Arabidopsis epidermal cells, the network seems to be depolymerized, in other cells, CMTs are aligned surrounding the penetration site and in a third category, no apparent change occurs (Takemoto et al., 2003). Such variability in CMT behaviour led the authors to suggest a less important role for CMTs in plant defence than for actin microfilaments (Takemoto et al., 2004; Hardham, 2013).

III. Similarities between reproductive and defence responses

The first challenge for pollen or oomycete is to break the resistance of the outer epidermal cell walls. To this end, pollen grains or oomycete spores first attach to the epidermis surface and then produce structures, a “foot” for pollen or an appressorium for oomycetes that secrete cell wall degradation enzymes to soften the epidermal wall. Then, a penetrative tube, the pollen tube or the hypha, is emitted and elongates by tip-growth through the epidermal cell to reach the underlying tissues of their host. To penetrate and advance through the plant tissues, invading cells have to exert forces (Sanati Nezhad and Geitmann, 2013). For pollen tube and hypha, experimental data have suggested that penetrative forces are driven by the cytoskeleton and the internal turgor pressure. For example, in lily pollen tubes, actin depolymerization decreases the tube ability to invade stiff matrices *in vitro* (Gossot and Geitmann, 2007) and treatment of *P. infestans* hypha with latrunculin B, an actin-destabilization drug, leads to aberrant growth (Ketelaar et al., 2012). Additionally, early responses of epidermal cells to attempt penetration by an oomycete hypha or a pollen tube trigger reorganisation of subcellular components depending on a polarized actin network that might guide the vesicular secretion towards the invading growing cell.

Taken together, these resemblances between both invasive processes motivate us to develop a unique comparative system to investigate how epidermal cells sense and react to an invading cell. This comparative analysis constitutes the second part of my PhD work.

A stigmatic cell challenged by a pollen tube and oomycete hypha adapts its response to the invader's identity

Riglet Lucie[1*], Hok Sophie[2*], Le-Berre Jo-Yanne[2], Kebdani-Minet Naima[2], Keller Harald[2], Allasia Valérie[2], Gourgues Mathieu [2, 4], Rozier Frédérique[1], Bayle Vincent[1], Kodera Chie[1], Gaude Thierry[1], Attard Agnés[2+] and Fobis-Loisy Isabelle[1+]

[1] Laboratoire Reproduction et Développement des Plantes, Univ Lyon, ENS de Lyon, UCB Lyon1, CNRS, INRA, F-69342 Lyon, France

[2] Unité Mixte de Recherches Interactions Biotiques et Santé Végétale, INRA1301-CNRS6243-UNS, 400 route des Chappes, F-06903 Sophia Antipolis, France

[3] SPIBOC, Institut Sophia Agrobiotech, 400 route des Chappes, F-06903 Sophia Antipolis, France

[4] Bayer Crop Science France, 14, impasse Pierre Baizet CS 99163, F-69263 Lyon, France

* Authors contributed equally to this work

+ Corresponding authors : isabelle.fobis-loisy@ens-lyon.fr. (00) 33 4 72 72 89 85 / agnes.attard@inra.fr. (00) 33 4 92 38 64 05

(To be submitted to New Phytologist)

Summary

- The epidermis is the first barrier that protects organism from surrounding stresses. Similarly as the pollen tubes that germinate and grow within epidermal cells of the stigma, hyphae of filamentous pathogens penetrate the inner tissues of the host. Early response of the epidermal cells layer is therefore decisive for the result of these cell-cell interaction processes.
- Here, we aimed at comparing and characterizing how an epidermal cell can respond following intrusion by two types of invading cells, the pollen tube during pollination and the hyphae of two oomycetes: the hemibiotrophic pathogen *Phytophtora parasitica*, which infects roots, and the biotrophic pathogen *Hyaloperonospora arabidopsidis* infecting cotyledons.
- We found that contrary to *H. arabidopsidis*, *P. parasitica* is able to attach and penetrate the stigmatic cell as pollen tube does. The hypha and the pollen tube both

impose a mechanical pressure during penetration of the stigmatic cell wall that we found stronger for the pollen tube towards the interior of the cell. Additionally, *P. parasitica* induces the formation of a derived-stigmatic plasma membrane structure that encircled the hyphae, as observed in root.

- Using live imaging, we monitored the cellular events triggered in stigmatic cells following early penetration of *P. parasitica* hypha or pollen tube. We found that both invaders mobilized actin and late endosome compartments but, contrary to pollen tube, *P. parasitica* hypha also induces TGN focalization.
- Altogether, these results suggest that stigmatic epidermal cells are able to promptly react to the invader's identity, to adjust the most relevant responses.

Key words: Actin, *Arabidopsis thaliana*, *Hyaloperonospora arabidopsidis,* hyphae, *Phytophtora parasitica*, pollen tube, vesicular trafficking

Introduction

Epidermal cells are a layer of cells in direct contact with their environment. During a stress such as an intrusion by invading cells, they have to promptly react and mediate the most relevant responses. Invasive cell types exist in all eukaryotic kingdoms and include pollen tubes, fungal or oomycete hyphae. In plants, the first interaction that occurs between invasive pollen tubes and the epidermal cells of the stigma (also called papillae) is crucial for successful reproduction. Similarly, hyphae of filamentous pathogens penetrate the epidermal surface to reach the inner tissues of the host to complete their lifecycles. Early response of the first cell layers including epidermal cells is decisive for the result of these cell-cell interaction systems.

Many convergence points have already been reported between pathogen defence and pollen recognition, particularly during early cellular events triggered by these two cell-to-cell communication systems. Briefly, (i) there is a recognition of the external invader by the host, (ii) the pollen tube and the fungal/oomycete hypha secrete cell wall degradation enzymes to penetrate the host surface, (iii) both pollen tube and hypha grow first on the epidermal surface and then through the intercellular spaces of the host tissue, (iv) subcellular reorganisation of organelles and cytoskeleton occurs in the epidermal cell at the site of pollen or pathogen contact site (Hardham, 2007; Iwano et al., 2007, 2014; Samuel et al., 2009, 2011) and (v) both invader organisms take up resources from epidermal cells for their growth. Resemblances between pollen tube and hyphal growth have already led some authors to speculate that both processes share common ancestry (Dickinson, 1995; Dresselhaus and Márton, 2009; Nasrallah, 2005; Sanabria et al., 2008;

Zhang et al., 2017). Recently, transcriptomic analysis of *A. thaliana* pistils pollinated or infected with the fungus *F. graminearum* have shown that many differentially expressed genes are similarly regulated in response to both interaction processes (Mondragón-Palomino et al., 2017).

While similarities between these communication systems exist, a thorough comparative analysis of the early cellular events triggered in epidermal cells challenged by these two types of invasive organism has never been carried out. Here, we identified an epidermal cell type, the stigmatic cell that not only supports the growth of pollen tube but also promotes oomycete colonization. Using confocal, and electron microscopies, associated with comparative transcriptomic profiling, we showed that the hemibiotrophic oomycete *Phytophtora parasitica* (*P. parasitica*) attached to the stigma and infected the pistil whereas the biotrophic oomycete *Hyaloperonospora arabidopsidis* (*H. arabidopsidis*) did not. We also highlighted common as well as specific cellular processes triggered in the stigmatic cell invaded by a pollen tube or the *P. parasitica* hypha, revealing that the epidermis is able to adjust its response to the invader's identity.

Results

Infection of stigmatic cells by *P. parasitica* and *H. arabidopsidis*

To compare the cellular responses of stigmatic cells to invasive growth of a pollen tube or a oomycete hypha, we first tested the pathogenicity of two oomycete species exhibiting distinct lifestyles: the obligate biotrophic pathogen of *Arabidopsis thaliana, Hyaloperonospora arabidopsidis*, which develops on cotyledon and leaf cells and the hemibiotrophic pathogen *Phytophtora parasitica*, a typical root pathogen with a broad host range. *H. arabidopsidis* produces non-motile conidiospores that land on the leaves surface. To infect pistil tissues, we manually deposited *H. arabidopsidis* spores at the stigma surface. Spores started to germinate 4 hours after contact with the stigma but neither appressorium-like structures nor hypha penetration was observed, as expected if the oomycete penetrated the host cell. We also tested infection in liquid conditions, by dipping an entire flower in a conidiospores suspension. Similarly, spores germination at the stigma surface was observed but spores never differentiated any appressorium. Instead, *H. arabidopsidis* hyphae grew turning around papillae cells and never succeeded to penetrate them (Fig. 19a,b). *P. parasitica* zoospores are motile and were able to swim towards their host tissue. To infect pistil tissues, we dipped an entire flower or a naked pistil into a solution of *P. parasitica* GUS-expressing zoospores. Interestingly, in both cases, zoospores preferentially accumulated at the stigma surface (Fig. 19c,d). Petals and sepals did not seem to prevent zoospores to reach the stigma since we found similar

accumulation in an entire flower or a naked pistil. This reveals that *P. parasitica* has an affinity for the epidermal cells of the stigma. Likewise, when an entire root is dipped into a solution of *P. parasitica*, zoospores preferentially attached to a specific zone of the root that corresponds to the elongation zone (Fig. 19e) as previously described (Attard et al., 2007). Zoospores were able to attach to papillae and to infect them. Two hours after dipping, we observed the formation of an appressorium-like structure at the outer cell surface (asterisk, Fig. 19f) and the presence of a hypha within the cell (Fig. 19f) as described in infected root epidermis (Attard et al., 2007; Meng et al., 2014).

To go further in the characterization of pistil infection by *P. parasitica*, we infected *Arabidopis* transgenic plants expressing a GFP-tagged plasma membrane marker in stigmatic cells (LTI6B-GFP) and monitored the stigmatic plasma membrane during hyphal growth. Four hours after dipping, we observed an invagination on the plasma membrane (PM) that encircled *P. parasitica* hypha (Fig. 19g,h). In several examples of fungus or oomycete infections, the plant plasma membrane continuously encloses the advancing hypha and separates it from the invaded plant cell (Genre et al., 2005, 2009; Hardham, 2007; Yi and Valent, 2013). However, this plasma membrane invagination has never been described in epidermal cells infected with *P. parasitica*. We thus checked if such structure is formed when oomycete penetrates the root. Interestingly, using a transgenic *Arabidopsis* plant expressing an RFP-tagged plasma membrane located receptor kinase (PM-RK), we found that in the natural host cell, the hypha is surrounded by a plasma membrane derived structure (Fig. 19i,j) similarly as in the stigma epidermis.

In root, following penetration of the epidermis, the *P. parasitica* hyphae grow intercellularly to reach the root cortex and the vasculature (Attard et al., 2007; Fawke et al., 2015). In pistil tissue, 24 hours after the first contact, GFP-labelled hyphae were able to penetrate the entire pistil, to grow from the top to the inner tissues and succeeded to reach the ovary (Fig. 19k) similarly as pollen tubes did (Fig. 19l).

Altogether, these results demonstrated that, contrary to *H. arabidopsidis*, and even though the stigmatic epidermis is not its natural host tissue, *P. parasitica* is able breakdown the stigmatic barrier to develop a hypha within epidermal cells and invades the entire pistil. Furthermore, papillae react to the pathogen entrance, since the interaction provokes the invagination of the plasma membrane, encircling the hypha.

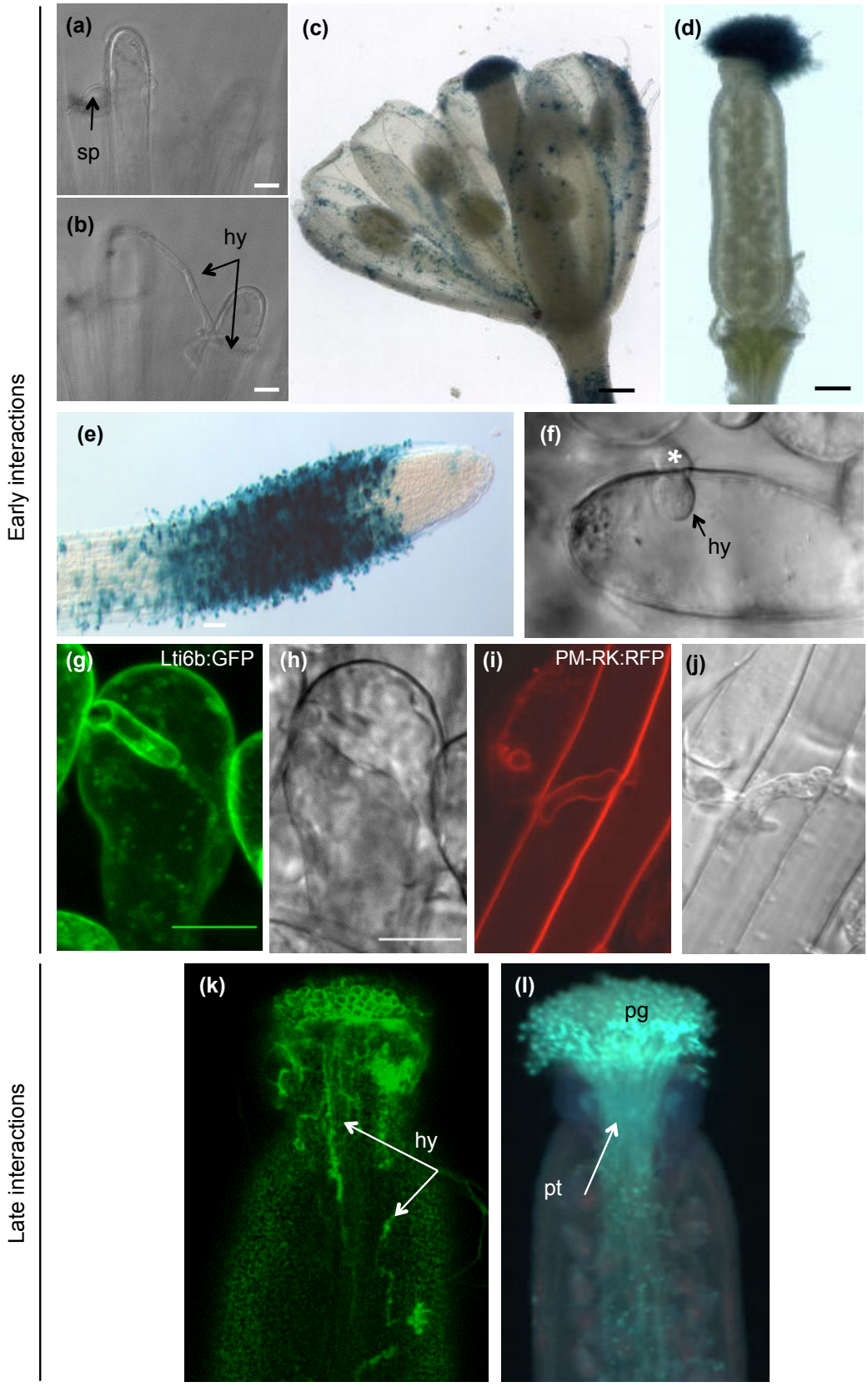

Fig. 19 / *P. parasitica* infects pistil tissues.
(a-b) *H. arabidopsidis* does not penetrate the papillae, and the hypha grows from cells to cells. Two images from the same stack. Bars, 10 µm. (c) Entire flowers or (d) naked pistils were dipped during 1 hour in a suspension of GUS-expressing zoospores of *P. parasitica*. *P. parasitica* preferentially attaches to the stigmatic epidermis. Bars, 200 µm. (e) Incubated roots in a suspension of GUS-

expressing *P. parasitica* zoospores, 2,5 hours after inoculation (hai). Zoospores attach to the elongation zone of the root. (f) *P. parasitica* is able to form an appressorium (2 hai) (*) on the papilla surface and to penetrate the external layer to a hypha within the cell. (g-h) Z-projection of serial confocal images showing stigmatic cells infected with *P. parasitica* (4 hai). The stigmatic plasma membrane, labelled with (g) LTI6B-GFP, or (h) in bright field, surrounds the penetrating hypha. Bars= 10 µm. (i-j) Z-projection of serial confocal images showing that after 6 hai with *P.parasitica*, root cell plasma membrane, labelled with (i) PM-RK, or (j) in bright field, surrounds the penetrating hypha. (k) Entire flowers were dipped in a suspension of *P. parasitica* GFP-expressing zoospores for 1 hour and maintained on the plant. Growing hyphae were detected in pistil tissues by confocal microscopy (24 hai). (l) Pollinated pistil (6 hours after pollen contact), the pollen tubes developed in pistil tissues. Legends: hy, hypha; pg, pollen grain; pt, pollen tube; sp, spore.

P. parasitica hypha and pollen tube grow within the external layer of the stigmatic cells

To obtain spatial information about the growth location of the *P. parasitica* hypha within the papillae, we performed Transmission Electron Microscopy (TEM) on infected stigmas. Images showed that hyphae are able to penetrate the cuticle, the electron-dense layer that covers the external surface of the aerial parts of land plants (Schreiber, 2010) (Fig. 20a). We found that the hypha can grow beneath the cuticle in close contact with the stigmatic CW (Fig. 20b) or directly in contact with the papilla plasma membrane, after cell wall degradation (Fig. 20c). We also noticed that the hyphal growth was responsible for an enlargement (asterisk, Fig. 20b,c) but it remains unclear whether it corresponds to a cell wall enlargement or to an accumulation of material around the hyphae. In some cases, probably corresponding to later infection stages, as stigmatic cell penetration is not synchronic, we observed *P. parasitica* hypha totally embedded in stigmatic cytoplasm, surrounded by the stigmatic plasma membrane (Fig. 20d). This could correspond to the invagination of the papilla plasma membrane observed by confocal microscopy (Fig. 19g,h). Because the location of *P. parasitica* hypha in root epidermal cells has not been previously reported, we investigated it by TEM. The Fig. 20e and d showed that hypha grows in contact to the root plasma membrane and digests the cell wall and the suberin, a multi-layered lamella deposited on the inner surface of root epidermal cell walls (Schreiber, 2010). Furthermore, beneath the invading hypha, some material accumulated outside the plasma membrane (asterisk, Fig. 20f). Such material deposition is known as wall apposition and occurred in response to oomycete infection and is suggested to play a role in penetration resistance (Hardham, 2007). Taken together, our results showed that *P. parasitica* hypha is able to invade the papilla in a similar way that it does in the root. The hypha triggers the digestion of the host cell wall and the lipophilic layer, the cuticle in stigmatic cell and the suberin in root cell, and grows in close contact with the plasma membrane without damaging it.

Finally, we further aimed at comparing the hyphal growth, to the natural invading cell of the stigma, the pollen tube. We found that the pollen tube digests the cuticle layer to grow beneath this layer. However, contrary to the hyphal growth, we did not observed a complete digestion of the stigmatic cell wall (Fig. 20g,h). Rather, the pollen tube induced separation of the inner and outer cell wall layers and grows in the space generated between these two layers. This invasive growth has been previously described and is characteristic of Brassicacea species (Elleman et al., 1992; Kandasamy et al., 1994).

In conclusion, whereas oomycete hypha and pollen tube were able to attach to the stigma surface and to penetrate the cuticle, their further growth depends on how they manipulate the stigmatic cell wall. While pollen tube is engulfed within the cell wall, the hypha is growing in a more free space under the cuticle or between the cell wall and the plasma membrane. This raises the question whether the constraint exerted by both invaders on the stigmatic single cell is similar, especially as it has been reported that to invade a plant tissue, an advancing cell has to exert a pressure on its host (Sanati Nezhad and Geitmann, 2013).

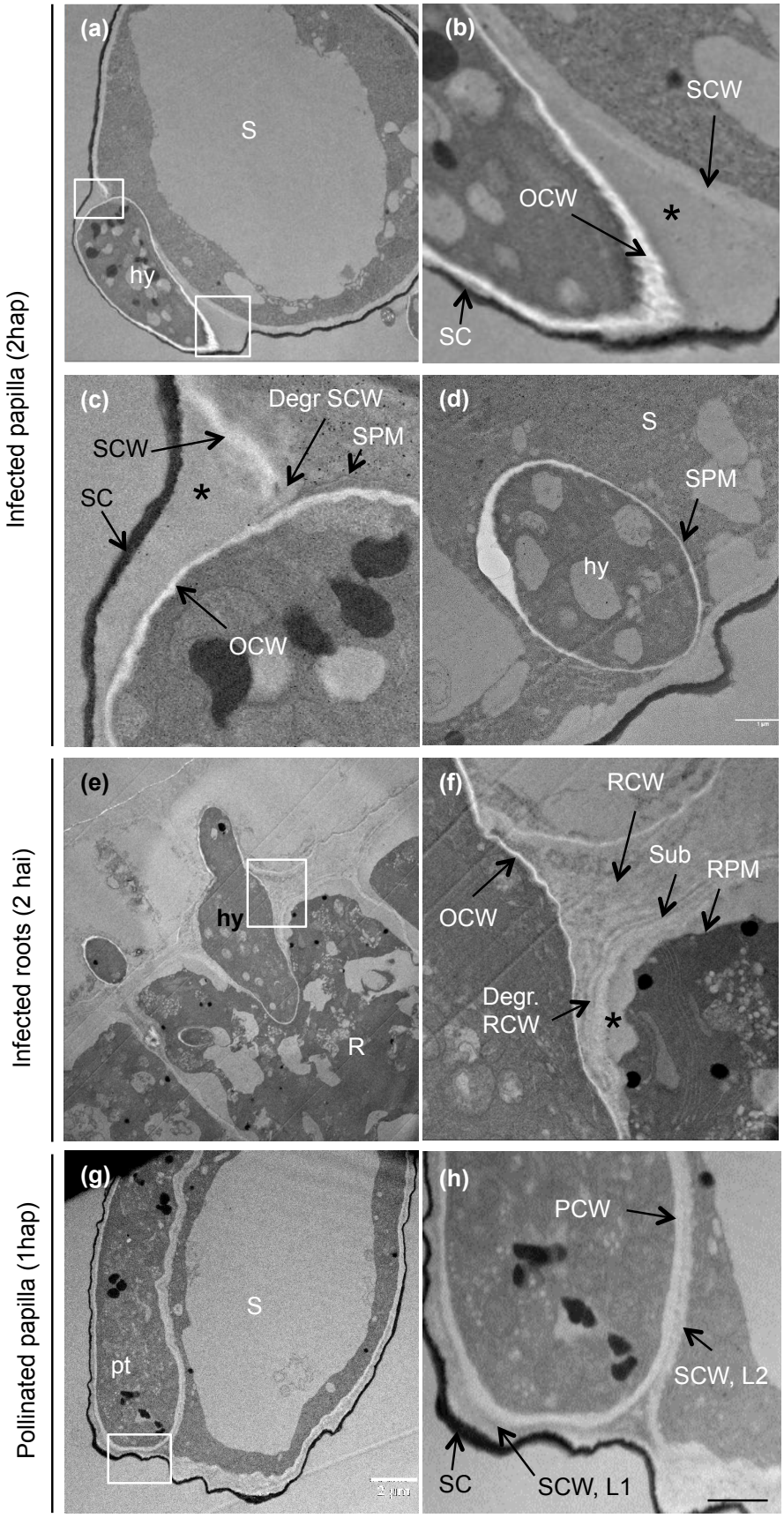

Fig. 20 / Penetration of the stigmatic cell external layer by the pollen tube or the *P. parasitica* hypha.

(a-d) Stigmatic cell infected with *P. parasitica* (2 hai). (b) Closer view of the hyphal growth under the cuticle. (c) Closer view showing degradation of the stigma cell wall. (b-c) The enlarged space (*) is from an unknown origin. (d) In some cases, *P. parasitica* hypha is surrounded by the stigmatic plasma membrane. (e-f) Root cells infected by *P. parasitica* (2 hai). (f) Closer view of the root cell wall degradation. (g-h) Stigmatic cell one hour after pollination (hap). (h) Closer view, pollen tube grows between the two cell wall layers: the outer layer L1 and the inner layer L2. Legends: pt, pollen tube; hy, hypha; OCW, oomycete cell wall; RPM, root plasma membrane; SPM, stigmatic plasma membrane; SC, stigmatic cuticle; SCW, stigmatic cell wall; L1, outer stigmatic cell wall layer; L2, inner stigmatic cell wall layer; PCW, pollen cell wall; S, stigmatic cell. Degr, degraded; R, root; Sub, suberin.

Deformation of stigmatic cell is higher after pollen tube penetration than hypha penetration

To evaluate mechanical constraints applied by both invaders on stigmatic cells, we measured the papilla deformations generated by their growth as previously described (Riglet et al., 2018). Briefly, two parameters were measured: (i) the deformation toward the interior of the cell, estimated by the plasma membrane invagination labelled with the LTI6B-GFP marker and (ii) the deformation towards the exterior of the cell using bright field images (Fig. 21a,b). We found that, although both pollen tube and hypha sizes were similar (Fig. 21c), the hypha created an external bump and slightly deformed the papilla plasma membrane, whereas external and internal deformations induced by the pollen tube are nearly equivalent (Fig. 21a-d). Thus, whereas pollen tube and hypha both penetrated and grew within the external layer of the papilla, they did not impact the stigmatic cell in the same manner and may be perceived differently by the invaded substrate.

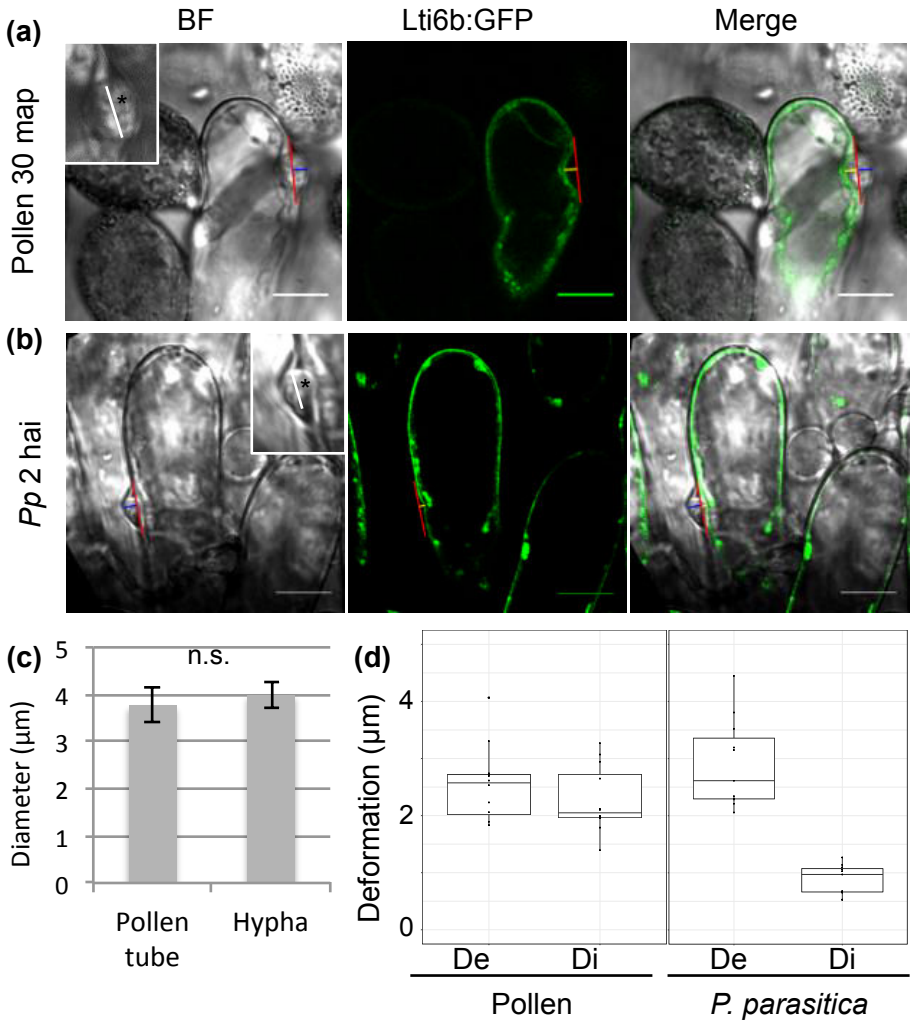

Fig. 21 / Both invaders do not deform the papilla in the same manner.
(a,b) Pollen tube or hypha diameters (white line *) were measured on Bright field (BF) images. To quantify the deformation, a line was drawn between the two external points of the deformation (red line), then, blue line corresponding to the external deformation (De) was measured. On GFP images (plasma membrane position visible thanks to LTI6B labelling), a yellow line corresponding to the internal deformation (Di) was drawn. Bars, 10 µm. (c) Measurement of pollen tube and hypha diameters. The error bars correspond to the s.e.m., n.s. = non significantly different, using a T-test. (d) Measurement of the external and internal deformations. n= 12 pollen tubes and n= 11 hyphae.

Cellular responses triggered in the stigmatic cell depends on the invader origin

It has been reported that invaded substrates are able to perceive mechanical forces generated during invasion by a tip-growing cell (Sanati Nezhad and Geitmann, 2013). Therefore, we investigated cellular events triggered within the papilla following pollen tube or hypha intrusion. Previous works have revealed a pivotal role for vesicular trafficking and cytoskeleton dynamics during filamentous pathogen infection (Hardham, 2007) and have also been proposed to act in pollen recognition (Iwano et al., 2007, 2014; Safavian and Goring, 2013; Safavian et al., 2015; Samuel et al., 2009, 2011). To have an overview of the trafficking routes and cytoskeleton dynamics in the papilla, we decided to focus on

(i) *TGN* movement (VHA-a1-GFP marker line), a compartment at the crossroad of secretion and endocytosis; (ii) late endosome (FYVE-GFP marker line), a compartment on the way to the lytic vacuole and (iii) actin rearrangements (LifeAct-Venus marker line) known to be involved in vesicular transport. Stigmas from these three marker lines were pollinated or infected with *P. parasitica* and cell dynamic was monitored by confocal microscopy in living papillae at early interaction time point (10 min after pollination (map) or 2 hai respectively (Fig. 22a). To quantify fluorescence changes, we designed an ImageJ plugin (available on demand) allowing to discriminate the papilla fluorescence at the contact site zone with both invaders (red arrow and yellow circles, Fig. 22a) from the outside contour, called surrounding zone (green circles, Fig. 22a). We obtained fluorescence mean values for both zones and subtracted them to obtain a mean fluorescence difference. Un-pollinated and un-infected papillae were used as controls (Fig. 22a). In stigmatic cells expressing the TGN marker, no fluorescence increase or decrease were detected at the contact point with the growing pollen tube; meaning that the fluorescence difference between contact and surrounding zones was equivalent in pollinated cells compare to non pollinated papilla (Fig. 22b). At the opposite, in papillae infected with *P. parasitica*, a huge positive fluorescence difference were detected compare to non-infected cells, corresponding to an increase of GFP fluorescence in the contact zone (Fig. 22b). Thus, VHA-a1 labelled-TGN-compartments are concentrated around the penetrating hypha compare to the rest of the cell. In stigmatic cells expressing the late endosome marker or the actin marker, we detected significant fluorescence difference in response to both invaders meaning that, in both interaction types, late endosomes migrate towards the contact point with the invader and actin filaments concentrate around the growing invading cell (Fig. 22b).

Taken together, our results suggest that the stigmatic epidermis does not respond in the same manner, depending whether is invaded by a pathogen or a pollen tube; some cellular pathways (LE trafficking, actin reorganisation) are trigger in both interaction types whereas others (TGN movement) are specifically activate.

The stigmatic cell is not the oomycete natural host cell. We wondered whether LE, TGN trafficking or actin reorganisation also occur in root cells after *P. parasitica* infection, which has not yet been investigated. To address this question, we infected TGN-, late endosome- and actin – labelled roots with *P. parasitica* and monitored cell dynamics by confocal microscopy. As previously, we quantified the fluorescence thank to our imageJ plugin (Fig. 23a). Interestingly, similarly as in papillae, TGN and late endosome compartments accumulated around the penetrating hypha as a clear positive fluorescence difference were measured (Fig. 23a,b). Unfortunately, the quantification of the actin

fluorescence was not possible using our ImageJ plugin because actin filaments highly concentrated in the cortical region of the entire root cell, which masked fluorescence difference between surrounding and contact zones (Fig. 23, actin infection1, *). However, by eyes, we detected accumulation of actin fluorescence close to the hypha tip for 11 cases out of 13 (Fig. 23a). In some infected cells, we clearly observed a focalization of actin cables towards the contact point with the penetrating hypha (Fig. 23a, actin infection 2).

In conclusion, TGN and late endosome movements as well as actin focalization observed in stigmatic cells in response to hypha penetration mimic the cellular responses trigger in natural host cell and are not linked to the oomycete / stigma artificial system we developed.

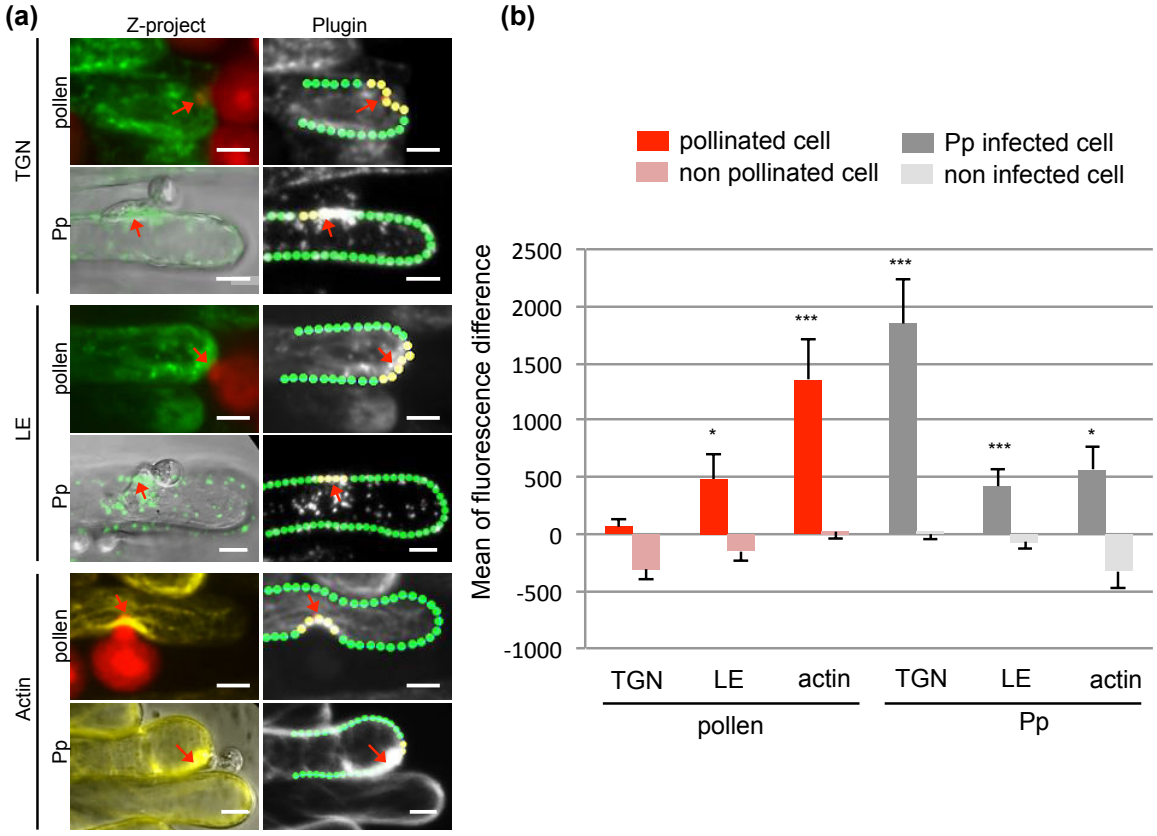

Fig. 22 / Cellular events triggered in stigmatic cells depend on the invader that attempts to penetrate.

(a) Stigmatic cells from 3 fluorescent marker lines (VHA-a1/TGN, 2xFyve/Late Endosome, LifeActin/Actin) were pollinated or infected with *P. parasitica*, for 10 minutes or 2 hours, respectively. The Z-project allows us to visualize the fluorescence in papillae (green or yellow channels) and the invader (red channel for the pollen or brightfield for *P. parasitica*). Fluorescence was quantified using a homemade ImageJ plugin. Briefly, it automatically depicts 2 zones: the contact zone (yellow circles) that encompasses the invader contact point (red arrow) and the surrounding zone (green circles). Fluorescence in each zone was quantified. Bar = 10 μm. (b) Mean of fluorescence differences (contact – surrounding) was represented on the graph. For each marker line and each interaction, 15 stigmatic cells were analysed. As control, fluorescence from

non-pollinated or non-infected papillae was quantified. In this case, to calculate the mean difference, we defined an arbitrary contact zone. For each type of controls,15 stigmatic cells were analysed. T-test, *pVal<0,05, ***pVal<0,01. Pp, *P. parasitica*; TGN, trans Golgi network; LE, late endosome.

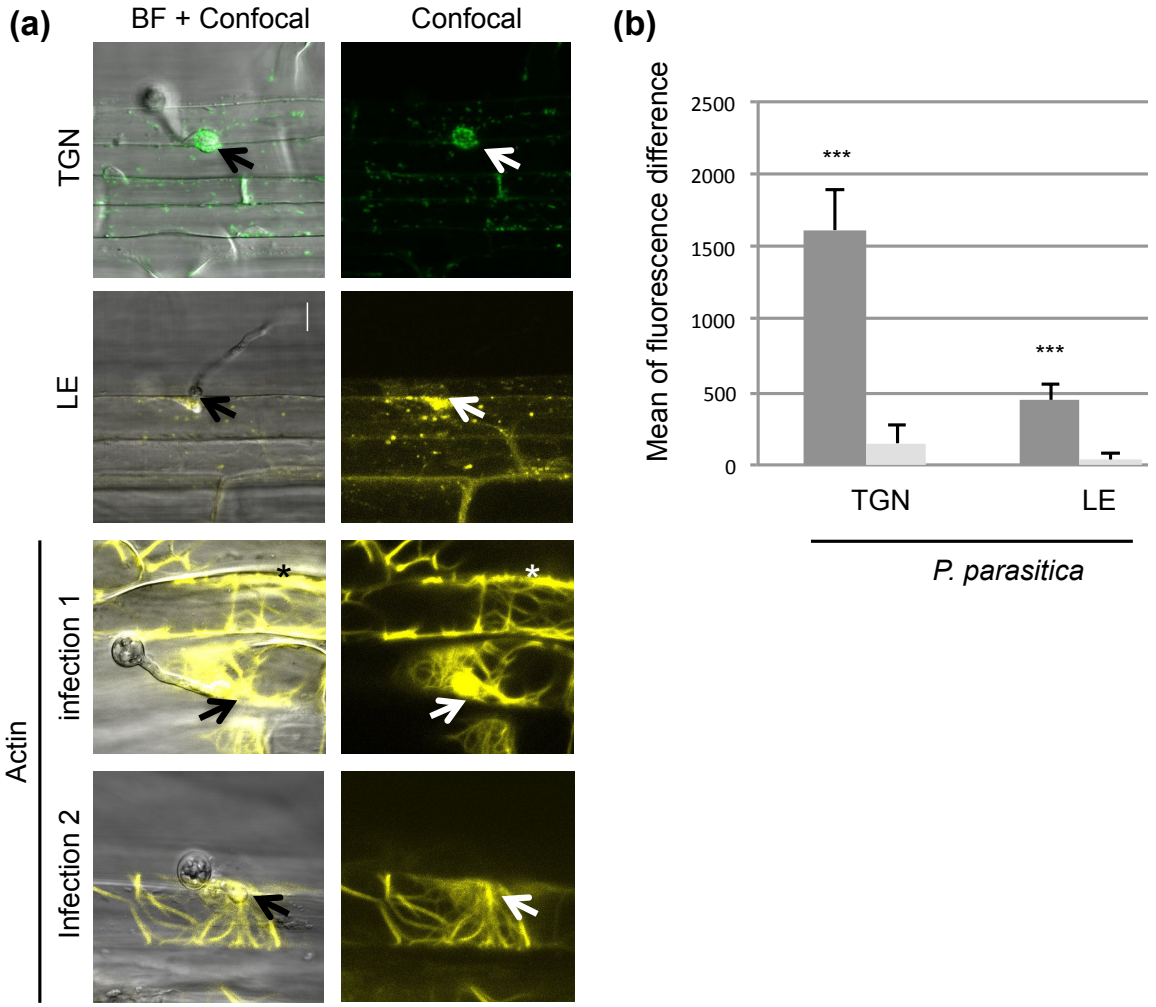

Fig. 23 / Cellular events triggered in root cells infected with by *P. parasitica*.
(a) Root cells from 3 fluorescent marker lines (VHA-a1/TGN, 2xFyve/Late Endosome, LifeActin/Actin) were infected with *P. parasitica* for 2,5 hours. Fluorescence was quantified using our ImageJ plugin, for vesicular marker lines (TGN and LE) as described in Fig. 22. For actin marker line, 2 out of 13 infected root cells are depicted. The asterisk (*) corresponds to a high surrounding fluorescence. The arrow points out the increase of fluorescence (TGN, LE, actin interaction 1) or the focalization of cables (actin interaction 2) at the hypha penetration site. (b) Mean of differences (contact – surrounding) was represented on the graph. For each marker line, 15 root cells were analysed. Fluorescence from non-infected root cells was quantified. In this case, to calculate the mean difference, we defined an arbitrary contact zone, 15 stigmatic cells for each type of control were analysed. T-test, ***pVal<0,01.

Common gene networks

We took advantage of transcriptomic analysis recently published by our groups to compare at the molecular level, pollen - stigma, *P. parasitica* - root and *H. arabidopisidis* - cotyledon interactions (Hok et al., 2011; Kodera et al., 2018; Le Berre et al., 2017). As we were interested in deciphering the early responses to invading cells, we restricted our comparison analysis to two interaction stages: (i) when invaders penetrate the epidermal surface, referred as early penetration stage (10 minutes post pollination, 2,5 hours after P. parasitica root infection or 8 hours after *H. arabidopsidis* cotyledon infection) and (ii) at later stage of interaction, when the growing pollen tube/hypha pass through the epidermis and reach the underlying tissue (60 map, 6-10 hours after *P. parasitica* root infection and 24 hours after *H. arabidopsidis* cotyledon infection). In the case of *H. arabidopsidis*, RNA extracted at 8 and 24 hai were mixed in equal quantity to produce an unique interaction sample (Hok et al., 2011); we thus, used this unique data set encompassing both interaction stages for our comparative analysis. We focused on up-regulated genes (Fold Change >=2) since more of those genes, compare to down-regulated genes, emerged from all transcriptomic analysis, and performed Venn diagram analysis (Fig. 24a,b). At early penetration stage, the percentage of shared up-regulated genes between pollination and *P. parasitica* infection is 3,5% whereas only 0,3% up-regulated genes were common between pollination and *H. arabidopsidis* infection (Fig. 24a). Similarly, at later stage of interaction, the common gene percentage reached 12% between the response to pollen and to *P. parasitica*, whereas only 1,1% were shared between pollination and *H. arabidopsidis* infection (Fig. 24b). These results suggest that the molecular stigmatic response to pollen is closer to the one triggered by *P. parasitica* in root cells, whereas transduction pathways triggered by the pollen or the *H. arabidopsidis* hypha should be quite divergent.

Interestingly, when we mapped the 43 and 255 common up-regulated genes between pollination and *P. parasitica* infection to KEGG pathways (Kanehisa et al., 2017), we found three plant-pathogen interaction pathways known as pattern-triggered immunity (PTI) induced by fungal PAMP or bacterial flg22 and EF-Tu. These PTI pathways has already been highlighted in others studies (Kodera et al., 2018; Zhang et al., 2017) but here we found that additionally to common induced pathways, the molecular players involved are identical, with 7 common up-regulated genes. These results suggest that not only at the cellular level, but also at the molecular level, plant responses to *P. parasitica* and to pollen are sharing common mechanisms.

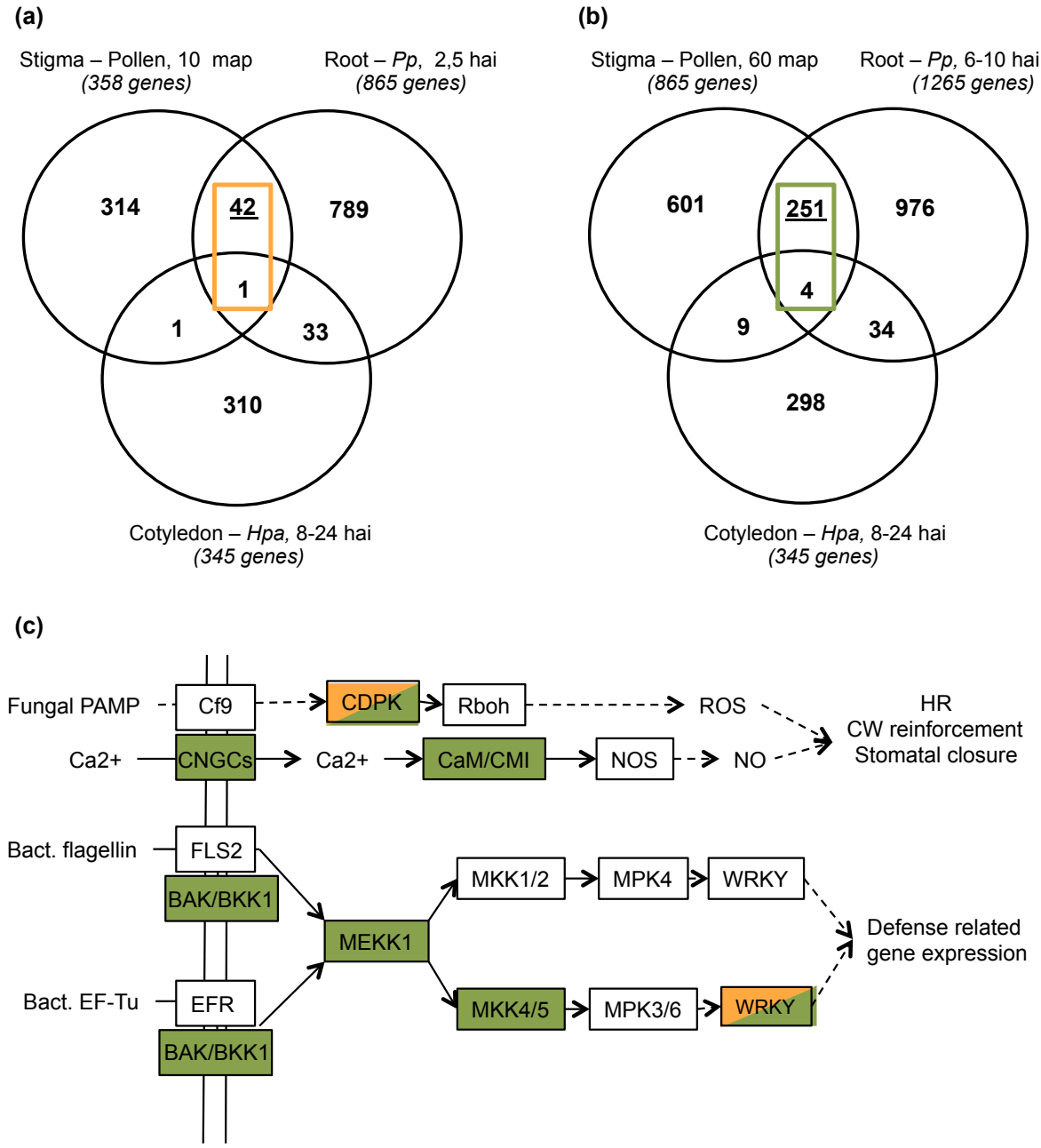

Fig. 24 / Common pathways induced in response to pollination and oomycete infection.
(a, b) Number of common genes induced (fold change >= 2) in response to pollen, *P. parasitica* (*Pp*) or *H. arabidopsidis* (*Hpa*) depicted by Venn diagrams (a) after early penetration or (b) after later interaction, during growth passing through the epidermis and reaching the underlying tissues. Only one gene list encompassing both stages in response to *H. arabidopsidis* is available. Number in parenthesis corresponds to the total number of genes included in each list. The intersection of Venn Diagrams indicates the number of common genes. (c) KEGG pathway mapping applied for genes commonly up regulated in response to pollen and to P. parasitica. Orange colored genes were induced during the penetration stage. Green colored genes were induced duringlater interaction stages.

Discussion

In this report, we aimed at deciphering the response of a single epidermal cell, the papilla, to the intrusion of three different types of invading growing cells: the pollen tube and hyphae of the two oomycetes, *P. parasitica* and *H. arabidopsidis.* These cell-cell interaction systems, i.e. stigma - pollen and stigma - oomycete, represent an attractive model since they allow to compare the behaviour of one single responding cell facing two types of intrusive organisms: a “positive” invader, the pollen tube that deliver the male gametes towards the ovules for fertilization and progeny production, and a “negative” invader, the oomycete hypha during plant - pathogen interaction.

Following inoculation, we found that *P. parasitica* zoospores accumulated massively at the top of the pistil (stigma) and to the root elongation zone, suggesting that both zones has common features that specifically allow zoospores attachment. The attraction by root exudates of zoospores from several *Phytophtora* species is not fully elucidated but a wide variety of components such as nutrients, amino acids, sugars, have already been identified as attractant cues (Deverall, 1977; Hosseini et al., 2014; Tyler, 2002; Yoneyama and Natsume, 2010). *A. thaliana* belongs to a plant family characterized by a dry stigma that do not secretes surface exudates, contrary to plant with wet stigmas that secretes sugar and others chemical components (Edlund et al., 2004; Elleman et al., 1992). Therefore, the specific accumulation of the *P. parasitica* zoospores at the stigma surface should not be linked to secretions. On the other hand, electrostatic forces have been suggested to function in both interactions systems. Swimming zoospores accumulation correlates with the natural electrostatic field generated by the root and may explain the asymmetric recruitment of spores. Additionally, a locally imposed electrical field leads to zoospores accumulation, and even overtake the chemical cues, suggesting electrical field as a major zoospores attracting factor (van West et al., 2002). Mathematic models predicted that the electric field is much greater at the extremity of the pistil compared to the rest of a flower and may participate to the electrodeposition of the pollen grains onto the stigma surface (Dai and Law, 1995; Vaknin et al., 2001). Although it remains still unknown how theses electrical signals are perceived and transduced into physiological responses, we may suggest that electrostatic forces could play a role in *P. parasitica* zoospores accumulation at the stigmatic surface.

Interestingly, although *H. arabidopsidis* oomycete invades aerial tissues as leaves or cotyledons, it was unable to penetrate the stigmatic epidermal cells contrary to *P. parasitica, a* root pathogen that attaches, penetrates the stigma and produces a hypha, which grows within the entire pistil. These differences in pathogenicity could be linked to their distinct infection strategies and lifestyle. Many biotrophic oomycetes, as *H.*

arabidopsidis, are strictly dependent on host tissues (obligate biotrophy) and have generally restricted host range; contrary to hemibiotrophic pathogens, such as *P. parasitica*, have the capacity to infect hundreds of different plant species (Fawke et al., 2015; Meng et al., 2014). Interestingly, *P. parasitica* zoospores produce an appressorium at the stigma surface while *H. arabidopsidis* conidiospores germinate, produce a germinative tube but never develop an appressorium. The appressorium that functions in penetration of the cell wall could be induced by topological features of the host surface (Latijnhouwers et al., 2003). Thus, stigma surface topography seems to be more favorable to *P. parasitica* infection that recognizes this epidermal cell as a potential host cell. In addition, our comparative transcriptomic analysis reveals that intrusion of a pollen tube or a hypha from *P. parasitica* triggers similar molecular mechanism in stigmatic cells or root cells respectively. It is tempting to speculate that this resemblance between both interaction types may also explain why *P. parasitica* zoospores penetrate stigmatic cell whereas H. parasitica conidiospores do not. Thus, mechanism by which invader recognize the cell surface as well as how the epidermal cell perceive the invader seems to be more similar between pollen and *P. parasitica* than between pollen and *H. parasitica*

Plants have the capacity to respond quickly to filamentous pathogens attempting to penetrate the epidermis (Hardham, 2007). In stigmatic cells, physiological and cellular changes in response to *P. parasitica* penetration and hyphal growth were observed, resembling to those triggered in root cells. Indeed, similarly as in roots, the hypha digests the stigma lipophilic layer and the cell wall to grow in close contact with the plasma membrane. During growth within the stigmatic tissue, the hypha is surrounded by a membrane layer labelled with the LTI6B protein that is normally localised at the stigmatic plasma membrane in non-infected cells. This layer isolates the hypha from the papilla cytoplasm. Such structure has already been described in rice leaf infected with the *Magnaporthe oryzae* fungus*;* beneath the appressorium, tubular primary hyphae invaginate the rice plasma membrane (Yi and Valent, 2013). Similarly, the arbuscular mycchorizal fungi triggers the invagination of the epidermal root cells plasma membrane which colocalise with the prepenetration apparatus, a cytoskeleton/ER-containing structure through which the fungal hypha cross the epidermis (Genre et al., 2005, 2009). Oomycetes develop specialized hyphae, named haustoria enveloped by a plant-derived membrane, the extrahaustorial membrane (EHM), which separates the pathogen from the host cell (Hardham, 2007). However, in natural pathosystem, the composition of this invaginated membrane is largely modified during the infection process. Several plant plasma membrane proteins are excluded for the EHM membrane, and conversely, some proteins detected within this modified membrane are absent from the rest of the plant plasma membrane (Bozkurt et al., 2015; Mackie et al., 1991). The composition of the

stigmatic derivated-membrane surrounding the growing hypha of *P. parasitica* remains to be determined.

Expansion of the host plasma membrane and modification of its protein composition during infection is coupled with an active vesicular trafficking (Bozkurt et al., 2015; Dörmann et al., 2014; Lu et al., 2012). Additionally, polarized secretion also has been shown to have an active role in plant defence and is generally associated with cell wall reinforcement and secretion of antimicrobial compounds (An et al., 2006; Takemoto et al., 2006). The actin network plays a central role in vesicular delivery at the plasma membrane. Takemoto and collaborators (2006) showed that in Arabidopsis epidermal cells, actin filaments reorganised in large bundles focusing around the oomycete penetration site. As previously described for other oomycete species, we showed that in root epidermal cells infected with *P. parasitica*, intracellular compartments (TGN and LE) accumulated around the penetrating hypha and actin cables focused at the penetration site. Vesicles originated from the TGN have been implicated in resistance mechanism against non adapted-powdery mildew fungi, *Blumeria graminis* and *Erysiphe pisi* and are involved in material deposition towards the cell wall apposition formed at the entry of the pathogen (reviewed in Dörmann et al., 2014). The LE, also known as Multivesicular Bodies (MVB), is an endocytic compartment transporting cargos to be degraded towards the vacuole. In *N. benthamiana* cells infected with the oomycete *Phytophthora infestans*, late endosome vesicles accumulate at the haustoria interface suggesting a rerouting of the LE pathway towards the EHM to provide the material for membrane expansion (Bozkurt et al., 2015). In barley epidermal cells infected with the biotrophic fungus *Blumeria graminis,* electron microscopy studies showed that MVB were present in the vicinity of the cell wall apposition (An et al., 2006). The authors proposed that MVB may release their internal vesicles into the extracellular space beneath fungal penetration attempt to participate to the cell wall apposition construction and secretion of antimicrobial compounds. In stigmatic cells infected with *P. parasitica*, we detected TGN and LE compartments accumulation in the vicinity of the hypha tip and mobilization of actin toward the penetration site. These cellular features are the signature of infected host cells suggesting that the pathogen triggers reprogramming of stigmatic cell machinery to respond to the intrusion. Whether this intense traffic associated with actin rearrangement are required to build the new plasma membrane around the hypha or to battle against the invading pathogen need to be elucidated.

When compared with the natural invading organism of the stigmatic cell, the pollen tube, similarities as well as divergences between both invading processes were highlighted. *P. parasitica* formed an appressorium-like structure at the stigmatic surface.

Appressoria are required to adhere to the plant surface and to secrete enzyme to digest the plant cell wall facilitating the hypha penetration (Ryder and Talbot, 2015). Similarly, a "foot" structure, composed of protein and lipids from the pollen surface extruded onto the papilla, is needed to loosen the stigmatic cell wall and prepare the pollen tube entry (Chapman and Goring, 2010). We can speculate that the appressorium-like structure, formed at the papilla surface, could be perceived by the stigmatic cell, as would be the "foot"; signalling that an organism attempts to penetrate the surface. Once passing thought the cuticle, the hypha and pollen tube act on the papilla cell wall to generate space for growing. Whereas the pollen tube softened the stigmatic cell wall to make its way in between the two layers, the hypha completely digests the cell wall to growth in close contact with the plasma membrane. In both cases, advancing pollen tube and hypha may exert a pressing force that should overcome the resistance provided by the invaded stigmatic cells. We estimated this mechanical pressure by measuring the papilla deformation and surprisingly, we found that the pollen tube, while growing engulfed within the cell wall, is applying more pressure towards the interior of the cell compared to the hypha. As diameters of the pollen tube and the hypha are similar, you may assume that this would be linked to differences in pushing forces exerted by these two growing organisms and/or variable resistance forces generated by the papilla (Sanati Nezhad and Geitmann, 2013).

One of the earliest host responses when attacked by an oomycete is the focalization of actin filaments at the site of attempted penetration (Hardham et al., 2008; Takemoto et al., 2003). Similarly, actin bundles focused at the site of pollen grain attachment and this actin reorganisation is essential for pollen germination (Iwano et al., 2007). Interestingly, Hardham and al. (2008) have shown that touching the surface of the *A. thaliana* cotyledon epidermis with a microneedle produced a rapid actin focalization at the contact point leading the authors to propose that actin reorganisation is triggered by detection of the mechanical pressure exerted by the invader. In stigmatic cells challenged by a hypha or a pollen tube, we detected a similar reorganisation of actin around the penetration site. This result suggests that, despite that both organism do not apply the same pressure, a threshold value for the physical forces required to stimulate actin reorganisation may have been reached in both cases. Such a mechanical threshold has been proposed to elicit subcellular reorganisation in epidermal cells infected with *H. arabidopsidis* (Branco et al., 2017; Hermanns et al., 2008). Alternatively, several experimental arguments demonstrated that physical signal alone could not account for the fully basal cellular response. A mutant strain of the rice filamentous fungus *Magnaporthe grisea* that fail to penetrate the plant cell wall and form a nonfunctional appressorium, is still able to trigger actin reorganisation and defence mechanism. A protein/lipid mixture

extracted from the pollen surface was sufficient to trigger accumulation of vesicles in Brassica stigmatic wall (Elleman and Dickinson, 1996) and elicits Ca^{2+} transport in Arabidopsis papillae (Iwano et al., 2014); two cellular events required for pollen germination and tube growth. These data support the idea that, in addition to mechanical perception, chemical molecules released by the pathogen or present at the surface of the pollen grain are necessary to trigger host cell cellular changes. Interestingly, our results showed that the VHA-a1 labeled-TGN mobilization in stigmatic cell occurs only in response to hyphal growth. Similarly, we never observed pollen tube enclosure by the stigmatic plasma membrane as observed for the hypha growing within an infected stigmatic or root epidermal cells. Taken together, these data suggests that the stigmatic cell is capable to recognize the invasive cell, triggering adapted response to an invader never meet throughout its life. Whether recognition depends on molecular or/and mechanical clues remains to be elucidated.

Materials and Methods

Plant, oomycete materials and culture conditions

Arabidopsis thaliana Col-0 and all transgenic plants were grown in growth chambers under a long-day conditions (16h light/8h dark at 21°C/19°C with a relative humidity around 60%). The pVHAa1-VHAa1:GFP line (Col-0) have been described previously (Dettmer et al., 2006). The pLAT52-EGFP line (Col-0) was obtained from A. Cheung and previously described (Rotman et al., 2003). *Phytophtora parasitica* Dastur isolated INRA-310 was maintained in the *Phytophthora* collection at INRA, Sophia Antipolis, France. The growth conditions and zoospores production were previously described (Galiana et al., 2005). The *P. parasitica* transformant expressing pCL380::GFP-GUS was previously described (Attard et al., 2014). The green florescence protein (GFP) or β-glucuronidase (GUS) expression signal increased 3 hours after inoculation, at the onset of penetration, and peaked six hours after inoculation. The *H. arabidopsidis* isolate Noco was transferred weekly onto the susceptible accession Col-0 as already described (Dangl et al., 1992).

Plasmid construction and generation of transgenic lines

Gateway® technology (Life Technologies, USA) and two set of Gateway®-compatible binary T-DNA destination vectors were used (Hellens et al., 2000; Karimi et al., 2002) for expression of transgenes in *A. thaliana*. The DNA fragment containing the *Brassica oleracea SLR1* promoter was inserted into a the pDONP4-P1R plasmid (Durand et al., 2014; Fobis-Loisy et al., 2007). The 165 bp-LTI6B fragment (Yamada et al., 2005) was introduced in the pDON207 plasmid. The *FYVE* domain (Simon et al., 2014) was

introduced into the plasmid pDONP2R-P3 in duplicate to generate a *2xFYVE* construct. CDS from GFP protein was introduced either in the pDON207 or in the pDONP2R-P3. The Gateway® entry clone containing the LifeActin peptide fused to *Venus* was provided by Takashi Ueda (Era et al., 2009). The *SLR1* promoter, the *LifeActin:Venus* and a *3'mock* sequence were inserted in the pB7m34GW . The *SLR1* promoter, the Lti6b fragment and the *GFP* CDS (+stop) were inserted in the pB7m34GW. The *SLR1* promoter, the *GFP* CDS (-stop) and the *2xFYVE* domain were inserted in the pB7m34GW. We generated a pACT11-*RFP* construct by amplifying the promoter of the *A. thaliana Actin 11* gene (Huang et al., 1997) and inserting it into the pGreenII gateway vector containing the *RFP* coding sequence. *Arabidopsis* Col-0 transgenic plants were generated using *Agrobacterium tumefaciens*-mediated transformation according to (Logemann et al., 2006).

Transcriptomic data production and analysis

Pollination RNAseq data were produced as described (Kodera et al., 2018). Briefly, *A. thaliana* Col-0 stigmas (stage 13-14 according to Smyth et al., 1990) were pollinated with mature *A. thaliana C24* pollen grains. Stigmas were harvested 10 minutes after pollination, when the pollen tube starts to penetrate the stigmatic cell or 60 minutes after pollination, when the pollen tube is reaching the underlying tissue). RNA were extracted and sequenced. mRNA from stigmas side (Col-0 background) were retrieved thanks to a SNP-based method. *P. parasitica* transcriptomic data were produced as previously described (Le Berre et al., 2017). Briefly, roots from *A. thaliana* Col-0 were inoculated with *P*. *parasitica*. Total RNA were recovered (i) 2.5 hours after inoculation when the pathogen is penetrating the root epidermis, and, (ii) 6 and 10 hours after inoculation during the early biotrophic colonization. Corresponding RNA were used for hybridizations (affymetrix microarrays). *H. arabidopsidis* transcriptomes were produced as previously described (Hok et al., 2011). Briefly, cotyledons from the ecotype Col0 were inoculated with *H. arabidopsidis.* Total RNA at 8 (penetration) and 24 h after inoculation (invasive growth) were extracted and mixed to produce the samples used for hybridizations (affymetrix microarrays). Pathway analysis was performed using and KEGG PATHWAY Database using KEGG Mapper system (http://www.kegg.jp/kegg/tool/map_pathway2.html) (Kanehisa et al., 2017).

Oomycetes pathogen assays and histochemical analysis.

Pathogen assays with the *P. parasitica* and *H. arabidopsidis* isolates were performed as previously described (respectively Le Berre et al., 2017 and Hok et al., 2014). The GUS

reporter activity staining in plant tissues was performed as previously described (Hok et al., 2011).

Pollination assay and aniline blue staining

Mature stigmas (stage 13 to 14 according to Smyth et al., 1990) were emasculated and pollinated with mature pollen. 24 hours after pollination, stigma were fixed in acetic acid 10%, ethanol 50% and stained with aniline blue for epifluorescence microscopy observation as previously described (Kitashiba et al., 2011).

Transmission Electron microscopy

Mature stigmas were pollinated with *A. thaliana* pollen grains or infected with *P. parasitica*. Roots were infected with *P. parasitica*. One hour after pollination or 1.5 hours post inoculation, samples were fixed in a solution containing 2.5% glutaraldehyde and 2.5% paraformaldehyde in 0.1 M phosphate buffer (pH 7.2) and after 4 rounds of 30 min vacuum, they were incubated in fixative for 12 hours at room temperature. Pistils and roots were then washed in phosphate buffer and further fixed in 1% osmium tetroxide in 0.1 M phosphate buffer (pH 7.2) for 1.5 hours at room temperature. After rinsing in phosphate buffer and distilled water, samples were dehydrated through an ethanol series, impregnated in increasing concentrations of SPURR resin over a period of 3 days before being polymerized at 70°C for 18 h, sectioned (65 nm sections) and imaged at 80 kV using an FEI TEM tecnaiSpirit with 4 k x 4 k eagle CCD.

Confocal microscopy

Pollinated stigmas were observed with a Zeiss microscope (Zeiss 800 or AxioObserver Z1 equipped with a spinning disk module) with a 40x objective. Oomycetes infected tissues (stigma, root and leaves) were observed with a Zeiss 880 confocal microscope with a 63x objective. GFP was exited at 488 nm and fluorescent detected between 500 and 550nm. RFP was exited at 561 nm and fluorescent detected between 550 and 600 nm. Pollinated stigmas were imaged every 0.4 µm encompassing the entire volume of the stigma, using the serial confocal method. Infected tissues were imaged each 0.4 µm encompassing the entire volume of the stigma and half of the root thickness, using the z-stack confocal protocol. Images were processed with ImageJ software.

Fluorescence quantification

From the serial confocal images obtained with VHA, 2xFYVE or LifAct fluorescence, we generated a Z project for visualizing the fluorescent stigmatic cell and the invader (pollen or *P. parasitica*). We manually choose one slide from the stack that corresponds to the

focus plan of the contact site with the pollen tube or hypha. On this selected slide, we manually draw the stigmatic cell periphery, define the contact site and fix the size of the circles in which the fluorescence will be quantified by the image J script (2.6 mm). Then, the plugin automatically depicts 2 zones; the contact zone that encompasses the invader contact point and the surrounding zone. Fluorescence in each zone is quantified. Mean of difference (contact – surrounding) is calculated by the script. Fluorescence from non-pollinated or non-infected stigmatic cells were quantified. In this case, we manually draw the periphery of the cell; fix the size of the circles (2.6 mm). To calculate the mean difference, we define an arbitrary contact zone between circle 6 and 10 for controls linked to pollen and between circle 6 and 11 for controls linked to *P. parasitica*.
The imageJ plugin is available on demand.

Acknowledgements

We thank all the SICE and the IPO members for fruitful discussions. We thank A. Chaboud for generating the pAct11-RFP line. We thank the Bordeaux Imaging Center for the TEM work and especially L. Brocard and B. Batailler. This work was supported by Grant ANR-14-CE11-0021.

Author contribution

L.R., S.H. designed and performed most of the experiments. L.R. performed all the experiments on pistil – pollen interaction, except the aniline blue performed by F.R. L.R. performed the experiments on LTI6B-GFP labeled stigmatic cells infected by *P. parasitica* (Fig. 19d-h) and all the deformation experiments (Fig. 21). S.H., J.Y.L.B. and N.K.M. performed the experiment on pistil – *P.parasitica* interaction except the ones mentioned above. A.A. and J.Y.L.B. performed the experiments on root infected by *P. parasitica*. V.A. performed experiments on *H. arabidopsidis.* The TEM experiments were subcontracted excepted the sample fixations, which were performed by S.H., A.A and L.R. V.B. set up the Image J script. L.R. and I.F.L. performed the images quantification for pollen – pistil interactions and A.A. and S.H. for root/stigma - *P. parasitica* interactions. The deformation measurements were performed in doubled blind by I.F.L. and L.R. C.K. A.A and H.K. analysed the transcriptomic data. L.R., S.H., A.A., M.G., H.K., T.G. and I.F.L. analysed the data. L.R., I.F.L., T.G. and A.A. wrote the manuscript.

References

An, Q., Huckelhoven, R., Kogel, K.-H., and van Bel, A.J.E. (2006). Multivesicular bodies participate in a cell wall-associated defence response in barley leaves attacked by the pathogenic powdery mildew fungus. Cellular Microbiology *8*, 1009–1019.

Attard, A., Gourgues, M., Galiana, E., Panabières, F., Ponchet, M., and Keller, H. (2007). Strategies of attack and defense in plant–oomycete interactions, accentuated for Phytophthora parasitica Dastur (syn. P. Nicotianae Breda de Haan). Journal of Plant Physiology *165*, 83–94.

Attard, A., Evangelisti, E., Kebdani-Minet, N., Panabières, F., Deleury, E., Maggio, C., Ponchet, M., and Gourgues, M. (2014). Transcriptome dynamics of Arabidopsis thaliana root penetration by the oomycete pathogen Phytophthora parasitica. BMC Genomics *15*, 1–20.

Bozkurt, T.O., Belhaj, K., Dagdas, Y.F., Chaparro-Garcia, A., Wu, C.-H., Cano, L.M., and Kamoun, S. (2015). Rerouting of Plant Late Endocytic Trafficking Toward a Pathogen Interface: Rerouting of Endocytic Pathway to Pathogen Interface. Traffic *16*, 204–226.

Branco, R., Pearsall, E.-J., Rundle, C.A., White, R.G., Bradby, J.E., and Hardham, A.R. (2017). Quantifying the plant actin cytoskeleton response to applied pressure using nanoindentation. Protoplasma *254*, 1127–1137.

Chapman, L.A., and Goring, D.R. (2010). Pollen-pistil interactions regulating successful fertilization in the Brassicaceae. Journal of Experimental Botany *61*, 1987–1999.

Dai, Y., and Law, S.E. (1995). Modeling the transient electric field produced by a charged pollen cloud entering a flower. In IAS ’95. Conference Record of the 1995 IEEE Industry Applications Conference Thirtieth IAS Annual Meeting, (Orlando, FL, USA: IEEE), pp. 1395–1402.

Dangl, J.L., Ritter, C., Gibbon, M.J., Mur, L.A., Wood, J.R., Goss, S., Mansfield, J., Taylor, J.D., and Vivian, A. (1992). Functional homologs of the Arabidopsis RPM1 disease resistance gene in bean and pea. Plant Cell *4*, 1359–1369.

Dettmer, J., Hong-Hermesdorf, A., Stierhof, Y.-D., and Schumacher, K. (2006). Vacuolar H+-ATPase activity is required for endocytic and secretory trafficking in Arabidopsis. Plant Cell *18*, 715–730.

Deverall, B.J. (1977). Defence Mechanisms of Plants (Cambridge University Press).

Dickinson, H. (1995). Dry stigmas, water and self-incompatibility in Brassica. Sexual Plant Reproduction *8*, 1–10.

Dörmann, P., Kim, H., Ott, T., Schulze-Lefert, P., Trujillo, M., Wewer, V., and Hückelhoven, R. (2014). Cell-autonomous defense, re-organization and trafficking of membranes in plant-microbe interactions. New Phytologist *204*, 815–822.

Dresselhaus, T., and Márton, M.L. (2009). Micropylar pollen tube guidance and burst: adapted from defense mechanisms? Current Opinion in Plant Biology *12*, 773–780.

Durand, E., Méheust, R., Soucaze, M., Goubet, P.M., Gallina, S., Poux, C., Fobis-Loisy, I., Guillon, E., Gaude, T., Sarazin, A., et al. (2014). Dominance hierarchy arising from the evolution of a complex small RNA regulatory network. Science *346*, 1200–1205.

Edlund, A.F., Swanson, R., and Preuss, D. (2004). Pollen and Stigma Structure and Function: The Role of Diversity in Pollination. The Plant Cell *16*, S84–S97.

Elleman, C.J., and Dickinson, H.G. (1996). Identification of pollen components regulating pollination-specific responses in the stigmatic papillae of Brassica oleracea. New Phytologist *133*, 197–205.

Elleman, C.J., Franklin-Tong, V., and Dickinson, H.G. (1992). Pollination in species with dry stigmas: the nature of the early stigmatic response and the pathway taken by pollen tubes. New Phytologist *121*, 413–424.

Era, A., Tominaga, M., Ebine, K., Awai, C., Saito, C., Ishizaki, K., Yamato, K.T., Kohchi, T., Nakano, A., and Ueda, T. (2009). Application of Lifeact reveals F-actin dynamics in Arabidopsis thaliana and the liverwort, Marchantia polymorpha. Plant Cell Physiol. *50*, 1041–1048.

Fawke, S., Doumane, M., and Schornack, S. (2015). Oomycete Interactions with Plants: Infection Strategies and Resistance Principles. Microbiology and Molecular Biology Reviews *79*, 263–280.

Fobis-Loisy, I., Chambrier, P., and Gaude, T. (2007). Genetic transformation of Arabidopsis lyrata: specific expression of the green fluorescent protein (GFP) in pistil tissues. Plant Cell Rep. *26*, 745–753.

Galiana, E., Rivière, M.-P., Pagnotta, S., Baudouin, E., Panabières, F., Gounon, P., and Boudier, L. (2005). Plant-induced cell death in the oomycete pathogen Phytophthora parasitica. Cellular Microbiology *7*, 1365–1378.

Genre, A., Chabaud, M., Timmers, T., Bonfante, P., and Barker, D.G. (2005). Arbuscular Mycorrhizal Fungi Elicit a Novel Intracellular Apparatus in Medicago truncatula Root Epidermal Cells before Infection. The Plant Cell *17*, 3489–3499.

Genre, A., Ortu, G., Bertoldo, C., Martino, E., and Bonfante, P. (2009). Biotic and Abiotic Stimulation of Root Epidermal Cells Reveals Common and Specific Responses to Arbuscular Mycorrhizal Fungi. Plant Physiol *149*, 1424–1434.

Hardham, A.R. (2007). Cell biology of plant - oomycete interactions. Cellular Microbiology *9*, 31–39.

Hardham, A.R., Takemoto, D., and White, R.G. (2008). Rapid and dynamic subcellular reorganization following mechanical stimulation of Arabidopsis epidermal cells mimics responses to fungal and oomycete attack. BMC Plant Biol *8*, 1–14.

Hellens, R.P., Edwards, E.A., Leyland, N.R., Bean, S., and Mullineaux, P.M. (2000). pGreen: a versatile and flexible binary Ti vector for Agrobacterium-mediated plant transformation. Plant Molecular Biology *42*, 819–832.

Hermanns, M., Slusarenko, A.J., and Schlaich, N.L. (2008). The early organelle migration response of Arabidopsis to Hyaloperonospora arabidopsidis is independent of RAR1, SGT1b, PAD4 and NPR1. Physiological and Molecular Plant Pathology *72*, 96–101.

Hok, S., Danchin, E.G.J., Allasia, V., Panabières, F., Attard, A., and Keller, H. (2011). An Arabidopsis (malectin-like) leucine-rich repeat receptor-like kinase contributes to downy mildew disease: An LRR-RLK involved in disease susceptibility. Plant, Cell & Environment *34*, 1944–1957.

Hok, S., Allasia, V., Andrio, E., Naessens, E., Ribes, E., Panabières, F., Attard, A., Ris, N., Clément, M., Barlet, X., et al. (2014). The receptor kinase IMPAIRED OOMYCETE SUSCEPTIBILITY1 attenuates abscisic acid responses in Arabidopsis. Plant Physiol. *166*, 1506–1518.

Hosseini, S., Heyman, F., Olsson, U., Broberg, A., Funck Jensen, D., and Karlsson, M. (2014). Zoospore chemotaxis of closely related legume-root infecting *Phytophthora* species towards host isoflavones. Plant Pathology *63*, 708–714.

Huang, S., An, Y.Q., McDowell, J.M., McKinney, E.C., and Meagher, R.B. (1997). The Arabidopsis ACT11 actin gene is strongly expressed in tissues of the emerging inflorescence, pollen, and developing ovules. Plant Mol. Biol. *33*, 125–139.

Iwano, M., Shiba, H., Matoba, K., Miwa, T., Funato, M., Entani, T., Nakayama, P., Shimosato, H., Takaoka, A., Isogai, A., et al. (2007). Actin Dynamics in Papilla Cells of Brassica rapa during Self- and Cross-Pollination. Plant Physiol *144*, 72–81.

Iwano, M., Igarashi, M., Tarutani, Y., Kaothien-Nakayama, P., Nakayama, H., Moriyama, H., Yakabe, R., Entani, T., Shimosato-Asano, H., Ueki, M., et al. (2014). A Pollen Coat–Inducible Autoinhibited Ca2+-ATPase Expressed in Stigmatic Papilla Cells Is Required for Compatible Pollination in the Brassicaceae. The Plant Cell *26*, 636–649.

Kandasamy, M.K., Nasrallah, J.B., and Nasrallah, M.E. (1994). Pollen-pistil interactions and developmental regulation of pollen tube growth in Arabidopsis. Development *120*, 3405–3418.

Kanehisa, M., Furumichi, M., Tanabe, M., Sato, Y., and Morishima, K. (2017). KEGG: new perspectives on genomes, pathways, diseases and drugs. Nucleic Acids Res. *45*, D353–D361.

Karimi, M., Inzé, D., and Depicker, A. (2002). GATEWAY^{TM} vectors for Agrobacterium-mediated plant transformation. Trends in Plant Science *7*, 193–195.

Kitashiba, H., Liu, P., Nishio, T., Nasrallah, J.B., and Nasrallah, M.E. (2011). Functional test of Brassica self-incompatibility modifiers in Arabidopsis thaliana. Proc Natl Acad Sci U S A *108*, 18173–18178.

Kodera, C., Just, J., Rocha, M.D., Larrieu, A., Riglet, L., Legrand, J., Rozier, F., Gaude, T., and Fobis-Loisy, I. (2018). The molecular signatures of compatible and incompatible pollination. BioRxiv 374843.

Latijnhouwers, M., de Wit, P.J.G.M., and Govers, F. (2003). Oomycetes and fungi: similar weaponry to attack plants. Trends in Microbiology *11*, 462–469.

Le Berre, J.-Y., Gourgues, M., Samans, B., Keller, H., Panabières, F., and Attard, A. (2017). Transcriptome dynamic of Arabidopsis roots infected with Phytophthora parasitica identifies VQ29, a gene induced during the penetration and involved in the restriction of infection. PLOS ONE *12*, e0190341.

Logemann, E., Birkenbihl, R.P., Ülker, B., and Somssich, I.E. (2006). An improved method for preparing Agrobacterium cells that simplifies the Arabidopsis transformation protocol. Plant Methods *2*, 16.

Lu, Y.-J., Schornack, S., Spallek, T., Geldner, N., Chory, J., Schellmann, S., Schumacher, K., Kamoun, S., and Robatzek, S. (2012). Patterns of plant subcellular responses to successful oomycete infections reveal differences in host cell reprogramming and endocytic trafficking: Oomycete host cell reprogramming. Cellular Microbiology *14*, 682–697.

Mackie, A.J., Roberts, A.M., Callow, J.A., and Green, J.R. (1991). Molecular differentiation in pea powdery-mildew haustoria. Planta *183*, 399–408.

Meng, Y., Zhang, Q., Ding, W., and Shan, W. (2014). Phytophthora parasitica: a model oomycete plant pathogen. Mycology *5*, 43–51.

Mondragón-Palomino, M., John-Arputharaj, A., Pallmann, M., and Dresselhaus, T. (2017). Similarities between Reproductive and Immune Pistil Transcriptomes of Arabidopsis Species. Plant Physiology *174*, 1559–1575.

Nasrallah, J.B. (2005). Recognition and rejection of self in plant self-incompatibility: comparisons to animal histocompatibility. Trends in Immunology *26*, 412–418.

Riglet, L., Rozier, F., Kodera, C., Fobis-Loisy, I., and Gaude, T. (2018). KATANIN-dependent mechanical properties of the stigmatic cell wall regulate pollen tube pathfinding. BioRxiv 384321.

Rotman, N., Rozier, F., Boavida, L., Dumas, C., Berger, F., and Faure, J.-E. (2003). Female Control of Male Gamete Delivery during Fertilization in Arabidopsis thaliana. Current Biology *13*, 432–436.

Ryder, L.S., and Talbot, N.J. (2015). Regulation of appressorium development in pathogenic fungi. Current Opinion in Plant Biology *26*, 8–13.

Safavian, D., and Goring, D.R. (2013). Secretory Activity Is Rapidly Induced in Stigmatic Papillae by Compatible Pollen, but Inhibited for Self-Incompatible Pollen in the Brassicaceae. PLoS One *8*, e84286.

Safavian, D., Zayed, Y., Indriolo, E., Chapman, L., Ahmed, A., and Goring, D.R. (2015). RNA Silencing of Exocyst Genes in the Stigma Impairs the Acceptance of Compatible Pollen in Arabidopsis. Plant Physiol *169*, 2526–2538.

Samuel, M.A., Chong, Y.T., Haasen, K.E., Aldea-Brydges, M.G., Stone, S.L., and Goring, D.R. (2009). Cellular Pathways Regulating Responses to Compatible and Self-Incompatible Pollen in Brassica and Arabidopsis Stigmas Intersect at Exo70A1, a Putative Component of the Exocyst Complex. Plant Cell *21*, 2655–2671.

Samuel, M.A., Tang, W., Jamshed, M., Northey, J., Patel, D., Smith, D., Siu, K.W.M., Muench, D.G., Wang, Z.-Y., and Goring, D.R. (2011). Proteomic Analysis of Brassica Stigmatic Proteins Following the Self-incompatibility Reaction Reveals a Role for Microtubule Dynamics During Pollen Responses. Mol Cell Proteomics *10*, M111.011338.

Sanabria, N., Goring, D., Nürnberger, T., and Dubery, I. (2008). Self/nonself perception and recognition mechanisms in plants: a comparison of self-incompatibility and innate immunity. New Phytologist *178*, 503–514.

Sanati Nezhad, A., and Geitmann, A. (2013). The cellular mechanics of an invasive lifestyle. Journal of Experimental Botany *64*, 4709–4728.

Schreiber, L. (2010). Transport barriers made of cutin, suberin and associated waxes. Trends in Plant Science *15*, 546–553.

Simon, M.L.A., Platre, M.P., Assil, S., van Wijk, R., Chen, W.Y., Chory, J., Dreux, M., Munnik, T., and Jaillais, Y. (2014). A multi-colour/multi-affinity marker set to visualize phosphoinositide dynamics in Arabidopsis. Plant J. *77*, 322–337.

Smyth, D.R., Bowman, J.L., and Meyerowitz, E.M. (1990). Early flower development in Arabidopsis. The Plant Cell *2*, 755–767.

Takemoto, D., Jones, D.A., and Hardham, A.R. (2003). GFP-tagging of cell components reveals the dynamics of subcellular re-organization in response to infection of *Arabidopsis* by oomycete pathogens. The Plant Journal *33*, 775–792.

Takemoto, D., Jones, D.A., and Hardham, A.R. (2006). Re-organization of the cytoskeleton and endoplasmic reticulum in the Arabidopsis pen1-1 mutant inoculated with the non-adapted powdery mildew pathogen, Blumeria graminis f. sp. hordei. Molecular Plant Pathology *7*, 553–563.

Tyler, B.M. (2002). Molecular basis of recognition between Phytophtora pathogens and their hosts. Annual Review of Phytopathology *40*, 137–167.

Vaknin, Y., Gan-mor, S., Bechar, A., Ronen, B., and Eisikowitch, D. (2001). Are flowers morphologically adapted to take advantage of electrostatic forces in pollination? New Phytologist *152*, 301–306.

van West, P., Morris, B.M., Reid, B., Appiah, A.A., Osborne, M.C., Campbell, T.A., Shepherd, S.J., and Gow, N.A.R. (2002). Oomycete Plant Pathogens Use Electric Fields to Target Roots. Molecular Plant-Microbe Interactions *15*, 790–798.

Yamada, K., Fuji, K., Shimada, T., Nishimura, M., and Hara-Nishimura, I. (2005). Endosomal proteases facilitate the fusion of endosomes with vacuoles at the final step of the endocytotic pathway. The Plant Journal *41*, 888–898.

Yi, M., and Valent, B. (2013). Communication Between Filamentous Pathogens and Plants at the Biotrophic Interface. Annual Review of Phytopathology *51*, 587–611.

Yoneyama, K., and Natsume, M. (2010). 4.13 Allelochemicals for Plant–Plant and Plant–Microbe Interactions. 539–561.

Zhang, T., Gao, C., Yue, Y., Liu, Z., Ma, C., Zhou, G., Yang, Y., Duan, Z., Li, B., Wen, J., et al. (2017). Time-Course Transcriptome Analysis of Compatible and Incompatible Pollen-Stigma Interactions in Brassica napus L. Front Plant Sci *8*, 1–15.

5

Conclusion and Perspectives

Cell-cell interactions between epidermal cells and invading organisms remain a central question in biology. Via two antagonistic systems, one that leads to fertilization and another one that leads to infection, we have shown that the stigmatic epidermal cell constitutes an invaluable model to investigate how the plant cell responds to biotic stress at the cellular as well as molecular level. However, during our experimental work, we had to face unanticipated problems linked to particular properties of the papilla cell surface and to specific requirements to monitor pollen tube growth *in vivo*.

The stigmatic epidermal cell, a very specific tissue and a technical challenge

Monitoring the dynamics of intracellular compartments and cytoskeleton markers in the stigma papilla following pollen deposition or oomycete infection revealed to be particularly challenging in several respects. First, most of the drugs classically used in cell biology were unable to penetrate the papilla cell wall and either could not be used in this study. Implementation of alternative protocols, such as the use of lanolin, had to be done to allow oryzalin delivery into the cytosol. The impermeability of the stigma cell surface to reagents likely results from the presence of wax covering the thick cuticle. Contrasting with this feature, upon pollination, the papilla rapidly delivers water for pollen grain hydration. These contrasting characteristics support the idea that pollen-stigma interaction induces essential changes in the permeability of the papilla surface, whose nature remains to be uncovered. Second, microscope observation of the pollen - stigma interaction necessitates working in the absence of an aqueous medium to prevent any artificial rehydration of pollen grains. When mounting was performed in the air, some marker lines appeared less fluorescent than in water and this limited our observations. Third, because most endomembrane compartment or cytoskeleton marker lines available have the fusion protein driven by the CaMV35S promoter, which is poorly active in papilla cells, it was necessary to generate new marker lines using the SLR1 promoter specifically active in stigmatic cells. Besides, several lines we produced, either with the SLR1 or the endogenous promoter of the protein of interest did not lead to sufficient fluorescence for proper compartment labelling. Fourth, the measurement of the cell wall stiffness by AFM revealed to be very tricky due to the papilla shape of stigmatic cells, which strongly complicated the placement of the indenter on the cell surface. A special mounting medium had to be set up for this purpose. Finally, because one aim of the study was to follow pollen tube growth through live cell imaging, I participated in setting up the most appropriate protocol for this time-lapse analysis.

Further investigations about the role of the mechanical properties of stigmatic cells in pollen tube trajectory

Our results suggest that mechanical properties of the stigmatic cells play a key role in early pollen tube guidance. This represents the first characterization of a mechanical cue involved in pollen tube guidance in natural growth conditions. Although we have demonstrated a function of KATANIN in these properties, how cell wall components and/or their organisation are involved in this process remains to be elucidated. Interestingly, we found that though cell walls of *xxt1 xxt2* papillae had similar reduced stiffness to those of *ktn1-5*, they did not trigger the pollen tube coiled phenotype observed in *ktn1-5*. This divergence in response is probably due to differences in the CMF organisation between the two mutants. Indeed, CMFs in *xxt1 xxt2* walls were found to be straighter, bundled and more longitudinal to the cell axis in hypocotyl cells than in Col-0 controls (Xiao et al., 2016), whereas CMFs often form bands and run in different directions in the KATANIN *fra2* mutant walls compared with WT cells (Burk and Ye, 2002). Despite our many efforts to determine CMF orientation in papilla cells to elucidate whether these differences in cellulose patterning are conserved in stigmatic cells, our preliminary results did not allow us to draw clear conclusion, mainly because of technical difficulties. Further attempts should be carried out, for instance by testing new cuticle degrading reagents that could permit a more efficient entry of the cellulose stain within papilla cells. Alternatively, Field-Emission Scanning Electron Microscopy (FESEM), which has a high-resolution imaging for determining cell wall cellulose microfibril orientation (Zheng et al., 2017) should be attempted. Furthermore, analysis of the cell wall components of both mutants, for example using Fourier-transform infrared spectroscopy (FTIR) technique, could also provide additional cues to explain why *ktn1-5* mutant stigmas cause the coiled phenotype. It is worth noting that a previous study of the Arabidopsis *mor1-1* temperature-sensitive microtubule mutant, which exhibits microtubule shortening and disorganisation (Whittington et al., 2001), reported faster pollen germination and pollen tube growth when stigmas of *mor1-1* were pollinated with WT pollen grains compared with WT stigmas (Samuel et al., 2011). This raises the question as to whether pollen tubes could present the coiled phenotype in *mor1-1* stigmas like in *ktn1-5*. Intriguingly, disruption of CMTs in *mor1-1* root epidermal cells was not accompanied by alteration of CMF orientation, which remained transverse (Sugimoto et al., 2003). Thus, if *mor1-1* stigmas behave like *ktn1-5*, we cannot exclude that a mechanism independent of CMF orientation might be involved in the coiled phenotype of pollen tubes observed in *ktn1-5*. This mechanism might involve MAPs or other proteins bound to CMTs that would not be properly delivered to the plasma membrane or interact with their target components due to the disorganised CMT network

related to the loss of KTN1 function. Importantly, KATANIN1 activity is regulated by ROP GTPase signalling and an effector of the ROP6 GTPase, RIC1, has been shown to physically interact with KTN1 (Lin et al., 2013). Whether this signalling pathway is important for pollen – stigma interactions remains to be elucidated and could be one of the future directions for this project.

Based on our data reported in the BIORXIV manuscript, we suggest that the anisotropy / mechanical properties of the stigmatic tissue participate in the early guidance of pollen tubes. Given our collaboration with two biophysics teams in Grenoble and at ENS Lyon, it could be interesting in designing an *in vitro* assay of pollen tube growth with the aim of reproducing the coiled phenotype on artificial substrates. For example, we could test synthetic substrates with adjustable stiffness and shapes, mimicking the stigma, and examine the direction taken by a pollen tube growing in a culture medium of variable density. Additionally, the data obtained in this *in vitro* system may give additional information for the modelling approach.

Speculating on the functional role of CMT dynamics and mechanical modifications within papillae during its development

Studying mechanical properties have led us to highlight that the coiled phenotype was not only observed in *ktn1-5* stigmatic cells but also in stage-15 papillae. At this late stage of stigma development, we found that cell wall stiffness and CMT array of Col-0 papilla cells were close to those of *ktn1-5* papillae, which probably explain the increased coiled phenotype observed for pollen tubes. This is likely to be related to isotropic orientation of CMTs and CMFs known to occur at the end of the cell elongation process . Whether the coiled phenotype on late Col-0 stigmas is also associated with a decrease in KTN1 abundance, which can be hypothesised based on our *ktn1-5* analysis, remains to be elucidated. Our finding raises new questions about the biological interest of these stigmatic changes during development. Indeed, for aged stigmas, modifications of CMT arrays and mechanical properties of the cell wall, accompanied by an acceleration of the pollen tube growth, could be seen as beneficial for the plant by favouring ultimate fertilization and seed set on old flowers, and hence supporting dissemination of the species. Actually, the pistil length increases with aging and similarly the journey the pollen tube has to travel to reach the ovules. Whether the tubes are able to reach the ovules quicker on old pistils remains yet to be determined. Preliminary experiments (data not shown) I carried out show that the seed set is similar when pistils are pollinated at stages 12 to 15, which may reflect a faster pollen tube growth on old pistils. This is in accordance with recent evidence reported by Gao and collaborators (2018), showing that stigma

senescence, associated with a loss of seed production is only initiated 72h after anthesis, corresponding to the stage 16-17 (Gao et al., 2018).

Stigma epidermal cell responses to Oomycete infection and pollen tube growth

The second part of my experimental work dealt with the study of the epidermal cell responses to two types of invading growing cells, the pollen tube, and the oomycete hyphae. To this end, we set up a live cell imaging system that allowed us to monitor the dynamics of intracellular components such as actin filaments, *trans*-golgi network and late endosomes. Taking the stigmatic cell as responding cell, we highlighted that the papilla is able to mediate its response depending on the invader identity. Among others, our results showed that an actin focalization is triggered during both types of interaction. Further analysis would then be needed to examine the feedback from actin to the growth of these invading cells, i.e., for instance, in which manner papilla actin destabilization may modify these interactions. To this end, during my PhD, and related to the pollen-stigma interaction, I tested a series of actin loss-of-function mutants (data not shown), such as mutants impaired in *ACTIN 1*, *ACTIN 7*, and *ACTIN 11*, or in the actin depolymerizing factors *ADF3* and *ADF4*, all these genes being expressed in WT stigmas. The mutant pistils were pollinated with WT pollen. However, no defect in pollen germination or tube growth was observed. This result might be explained by a possible redundancy between members of the actin family. To circumvent this problem, drugs altering the actin cytoskeleton could be used, such as latrunculin B, employing the protocol I set up for treating the stigma with oryzalin. Interestingly, the actin depolymerizing drug cytochalasin D was previously used in pollination assay in *Brassica rapa* and led to a reduced rate of pollen germination, underlining a role for actin in pollination (Iwano et al., 2007). Similarly, the role of vesicular trafficking could also be studied by functional analysis. I thus pollinated several loss-of-function mutants impaired in trafficking functions (for instance *ECHIDNA* and the SNAREs *VTI12* and *VTI11*) and observed the WT pollen tube path by SEM, but here again no pollen tube phenotype was detected. The use of drugs affecting trafficking pathways could also be considered in further experiments. In the stigma-oomycete interaction, if actin focalisation participates in the reinforcement of the cell wall papilla at the infection site and/or in targeting secretory vesicles to bring defence components, affecting these pathways could enhance the susceptibility of the stigmatic cell to the pathogen. Altogether, these experiments could help us to decipher the functional role of stigmatic actin and vesicular trafficking during interaction with invading cells.

Mechanoperception of the stigmatic cell to physical forces produced by the growing pollen tube or Oomycete hypha

Because mechanical stress exerted on a plant cell provokes the reorganisation of CMTs (Hamant et al., 2008; Hardham et al., 2008), CMTs can be used as a proxy to monitor cell response to pressure, for instance that produced by the growing pollen tube or oomycete hypha. To this end, we generated several CMT marker lines that unfortunately gave too low fluorescence labelling to monitor CMT movement during invading growth. As previously mentioned, this is partly due to the fact that stigmas have to be mounted in the air, and therefore a high fluorescence of fusion markers is needed for proper imaging. In the future, new marker lines will have to be produced, for instance by tagging the protein of interest with two or three fluorescent proteins. These new constructs should allow us to determine whether and how CMT arrays reorganise during pollen tube and hyphal growth in papilla cells.

In line with this cell imaging analysis, exploring how the stigmatic cell perceives the physical stress mediated by the pollen tube and oomycete hypha upstream of the CMT response is a major concern. Indeed, even though mechanotransduction pathways have not been clearly identified in plants, cell wall sensors have been reported (Ringli, 2010; Wolf et al., 2012). Interestingly, a genetic screen for mutants that do not respond to external mechanostimuli identified the receptor-like kinase FERONIA. In this latter work, FERONIA was shown to regulate the Ca^{2+}-dependent transduction of mechanical stimuli in roots (Shih et al., 2014). Interestingly, Ca^{2+} is known to play a role in both pollen-stigma and plant-pathogen interactions (Chen et al., 2015). How these genes may affect the invading growth within stigmatic cells appears one of the very exciting directions to follow for the future of this project. In that scenario, we could analyse mutants or transgenic lines impaired in FERONIA, or FERONIA-like family members, and monitor how this affects the invading growth behaviour and papilla response.

6

References

Agudelo, C.G., Sanati, A., Ghanbari, M., Packirisamy, M., and Geitmann, A. (2012). A microfluidic platform for the investigation of elongation growth in pollen tubes. J. Micromechanics Microengineering *22*, 115009.

Agudelo, C.G., Sanati Nezhad, A., Ghanbari, M., Naghavi, M., Packirisamy, M., and Geitmann, A. (2013). TipChip: a modular, MEMS-based platform for experimentation and phenotyping of tip-growing cells. Plant J. *73*, 1057–1068.

Albenne, C., Canut, H., and Jamet, E. (2013). Plant cell wall proteomics: the leadership of Arabidopsis thaliana. Front. Plant Sci. *4*.

Albenne, C., Canut, H., Hoffmann, L., and Jamet, E. (2014). Plant Cell Wall Proteins: A Large Body of Data, but What about Runaways? Proteomes *2*, 224–242.

Albersheim, P., Darvill, A., Roberts, K., Sederoff, R., and Staehelin, A. (2010). Plant Cell Walls (Garland Science).

Alexopoulos, C.J., Blackwell, M., and Mims, C.W. (1996). Introductory mycology (New York : Wiley).

Arioli, T., Peng, L., Betzner, A.S., Burn, J., Wittke, W., Herth, W., Camilleri, C., Höfte, H., Plazinski, J., Birch, R., et al. (1998). Molecular Analysis of Cellulose Biosynthesis in Arabidopsis. Science *279*, 717–720.

Atmodjo, M.A., Hao, Z., and Mohnen, D. (2013). Evolving Views of Pectin Biosynthesis. Annu. Rev. Plant Biol. *64*, 747–779.

Baskin, T.I., and Jensen, O.E. (2013). On the role of stress anisotropy in the growth of stems. J. Exp. Bot. *64*, 4697–4707.

Baskin, T.I., Beemster, G.T.S., Judy-March, J.E., and Marga, F. (2004). Disorganization of Cortical Microtubules Stimulates Tangential Expansion and Reduces the Uniformity of Cellulose Microfibril Alignment among Cells in the Root of Arabidopsis. Plant Physiol. *135*, 2279–2290.

Beauzamy, L., Louveaux, M., Hamant, O., and Boudaoud, A. (2015). Mechanically, the Shoot Apical Meristem of Arabidopsis Behaves like a Shell Inflated by a Pressure of About 1 MPa. Front. Plant Sci. *6*.

Bichet, A., Desnos, T., Turner, S., Grandjean, O., and Höfte, H. (2001). BOTERO1 is required for normal orientation of cortical microtubules and anisotropic cell expansion in Arabidopsis. Plant J. *25*, 137–148.

Boisson-Dernier, A., Roy, S., Kritsas, K., Grobei, M.A., Jaciubek, M., Schroeder, J.I., and Grossniklaus, U. (2009). Disruption of the pollen-expressed FERONIA homologs ANXUR1 and ANXUR2 triggers pollen tube discharge. Dev. Camb. Engl. *136*, 3279–3288.

Bosch, M., Cheung, A.Y., and Hepler, P.K. (2005). Pectin methylesterase, a regulator of pollen tube growth. Plant Physiol. *138*, 1334–1346.

Bouquin, T., Mattsson, O., Næsted, H., Foster, R., and Mundy, J. (2003). The Arabidopsis lue1 mutant defines a katanin p60 ortholog involved in hormonal control of microtubule orientation during cell growth. J. Cell Sci. *116*, 791–801.

Bringmann, M., Landrein, B., Schudoma, C., Hamant, O., Hauser, M.-T., and Persson, S. (2012a). Cracking the elusive alignment hypothesis: the microtubule–cellulose synthase nexus unraveled. Trends Plant Sci. *17*, 666–674.

Bringmann, M., Li, E., Sampathkumar, A., Kocabek, T., Hauser, M.-T., and Persson, S. (2012b). POM-POM2/CELLULOSE SYNTHASE INTERACTING1 Is Essential for the Functional Association of Cellulose Synthase and Microtubules in Arabidopsis. Plant Cell *24*, 163–177.

Burk, D.H., and Ye, Z.-H. (2002). Alteration of Oriented Deposition of Cellulose Microfibrils by Mutation of a Katanin-Like Microtubule-Severing Protein. Plant Cell *14*, 2145–2160.

Burk, D.H., Liu, B., Zhong, R., Morrison, W.H., and Ye, Z.-H. (2001). A Katanin-like Protein Regulates Normal Cell Wall Biosynthesis and Cell Elongation. Plant Cell *13*, 807–828.

Burri, J.T., Vogler, H., Läubli, N.F., Hu, C., Grossniklaus, U., and Nelson, B.J. (2018). Feeling the force: how pollen tubes deal with obstacles. New Phytol.

Buschmann, H., Fabri, C.O., Hauptmann, M., Hutzler, P., Laux, T., Lloyd, C.W., and Schäffner, A.R. (2004). Helical Growth of the Arabidopsis Mutant tortifolia1 Reveals a Plant-Specific Microtubule-Associated Protein. Curr. Biol. *14*, 1515–1521.

Cameron, C., and Geitmann, A. (2018). Cell mechanics of pollen tube growth. Curr. Opin. Genet. Dev. *51*, 11–17.

Cavalier, D.M., Lerouxel, O., Neumetzler, L., Yamauchi, K., Reinecke, A., Freshour, G., Zabotina, O.A., Hahn, M.G., Burgert, I., Pauly, M., et al. (2008). Disrupting Two Arabidopsis thaliana Xylosyltransferase Genes Results in Plants Deficient in Xyloglucan, a Major Primary Cell Wall Component. Plant Cell *20*, 1519–1537.

Chae, K., Kieslich, C.A., Morikis, D., Kim, S.-C., and Lord, E.M. (2009). A Gain-of-Function Mutation of Arabidopsis Lipid Transfer Protein 5 Disturbs Pollen Tube Tip Growth and Fertilization. Plant Cell *21*, 3902–3914.

Chapman, L.A., and Goring, D.R. (2010). Pollen-pistil interactions regulating successful fertilization in the Brassicaceae. J. Exp. Bot. *61*, 1987–1999.

Chebli, Y., and Geitmann, A. (2017). Cellular growth in plants requires regulation of cell wall biochemistry. Curr. Opin. Cell Biol. *44*, 28–35.

Chen, J., Gutjahr, C., Bleckmann, A., and Dresselhaus, T. (2015). Calcium Signaling during Reproduction and Biotrophic Fungal Interactions in Plants. Mol. Plant *8*, 595–611.

Coen, E., and Rebocho, A.B. (2016). Resolving Conflicts: Modeling Genetic Control of Plant Morphogenesis. Dev. Cell *38*, 579–583.

Corson, F., Hamant, O., Bohn, S., Traas, J., Boudaoud, A., and Couder, Y. (2009). Turning a plant tissue into a living cell froth through isotropic growth. Proc. Natl. Acad. Sci. *106*, 8453–8458.

Cosgrove, D.J. (2000). Expansive growth of plant cell walls. Plant Physiol. Biochem. PPB *38*, 109–124.

Cosgrove, D.J. (2001). Wall Structure and Wall Loosening. A Look Backwards and Forwards. Plant Physiol. *125*, 131–134.

Cosgrove, D.J. (2014). Re-constructing our models of cellulose and primary cell wall assembly. Curr. Opin. Plant Biol. *22*, 122–131.

Cosgrove, D.J. (2016). Catalysts of plant cell wall loosening. F1000Research.

Cosgrove, D.J. (2018). Diffuse Growth of Plant Cell Walls. Plant Physiol. *176*, 16–27.

Crowell, E.F., Timpano, H., Desprez, T., Franssen-Verheijen, T., Emons, A.-M., Höfte, H., and Vernhettes, S. (2011). Differential Regulation of Cellulose Orientation at the Inner and Outer Face of Epidermal Cells in the Arabidopsis Hypocotyl. Plant Cell *23*, 2592–2605.

Daher, F.B., and Geitmann, A. (2011). Actin is Involved in Pollen Tube Tropism Through Redefining the Spatial Targeting of Secretory Vesicles. Traffic *12*, 1537–1551.

Damineli, D.S.C., Portes, M.T., and Feijó, J.A. (2017). One Thousand and One Oscillators at the Pollen Tube Tip: The Quest for a Central Pacemaker Revisited. In Pollen Tip Growth: From Biophysical Aspects to Systems Biology, G. Obermeyer, and J. Feijó, eds. (Cham: Springer International Publishing), pp. 391–413.

Dearnaley, J.D.W., Clark, K.M., Heath, I.B., Lew, R.R., and Goring, D.R. (1999). Neither compatible nor self-incompatible pollinations of Brassica napus involve reorganization of the papillar cytoskeleton. New Phytol. *141*, 199–207.

Delph, L.F., Weinig, C., and Sullivan, K. (1998). Why Fast-Growing Pollen Tubes Give Rise to Vigorous Progeny: The Test of a New Mechanism. Proc. Biol. Sci. *265*, 935–939.

Desai, A., and Mitchison, T.J. (1997). MICROTUBULE POLYMERIZATION DYNAMICS. Annu. Rev. Cell Dev. Biol. *13*, 83–117.

Desprez, T., Juraniec, M., Crowell, E.F., Jouy, H., Pochylova, Z., Parcy, F., Höfte, H., Gonneau, M., and Vernhettes, S. (2007). Organization of cellulose synthase complexes involved in primary cell wall synthesis in Arabidopsis thaliana. Proc. Natl. Acad. Sci. U. S. A. *104*, 15572–15577.

Dickinson, H. (1995). Dry stigmas, water and self-incompatibility in Brassica. Sex. Plant Reprod. *8*, 1–10.

Dick-Pérez, M., Zhang, Y., Hayes, J., Salazar, A., Zabotina, O.A., and Hong, M. (2011). Structure and Interactions of Plant Cell-Wall Polysaccharides by Two- and Three-Dimensional Magic-Angle-Spinning Solid-State NMR. Biochemistry *50*, 989–1000.

Dong, J., Kim, S.T., and Lord, E.M. (2005). Plantacyanin Plays a Role in Reproduction in Arabidopsis. Plant Physiol. *138*, 778–789.

Doughty, J. (2000). Cysteine-rich Pollen Coat Proteins (PCPs) and their Interactions with StigmaticS (Incompatibility) and S -Related Proteins in Brassica: Putative Roles in SI and Pollination. Ann. Bot. *85*, 161–169.

Durand-Smet, P., Chastrette, N., Guiroy, A., Richert, A., Berne-Dedieu, A., Szecsi, J., Boudaoud, A., Frachisse, J.-M., Bendhamane, M., Hamant, O., et al. (2014). A Comparative Mechanical Analysis of Plant and Animal Cells Reveals Convergence across Kingdoms. Biophys. J. *107*, 2237–2244.

Duruflé, H., Clemente, H.S., Balliau, T., Zivy, M., Dunand, C., and Jamet, E. (2017). Cell wall proteome analysis of Arabidopsis thaliana mature stems. Proteomics *17*, 1600449.

Elleman, C.J., and Dickinson, H.G. (1990). The role of the exine coating in pollen-stigma interactions in Brassica oleracea L. New Phytol. *114*, 511–518.

Elleman, C.J., and Dickinson, H.G. (1994). Pollen—stigma interaction during sporophytic self-incompatibility in Brassica oleracea. In Genetic Control of Self-Incompatibility and Reproductive Development in Flowering Plants, E.G. Williams, A.E. Clarke, and R.B. Knox, eds. (Dordrecht: Springer Netherlands), pp. 67–87.

Elleman, C.J., and Dickinson, H.G. (1996). Identification of pollen components regulating pollination-specific responses in the stigmatic papillae of Brassica oleracea. New Phytol. *133*, 197–205.

Elleman, C.J., Franklin-Tong, V., and Dickinson, H.G. (1992). Pollination in species with dry stigmas: the nature of the early stigmatic response and the pathway taken by pollen tubes. New Phytol. *121*, 413–424.

Elliott, A., and Shaw, S.L. (2018). Update: Plant Cortical Microtubule Arrays. Plant Physiol. *176*, 94–105.

Endler, A., Kesten, C., Schneider, R., Zhang, Y., Ivakov, A., Froehlich, A., Funke, N., and Persson, S. (2015). A Mechanism for Sustained Cellulose Synthesis during Salt Stress. Cell *162*, 1353–1364.

Escobar-Restrepo, J.-M., Huck, N., Kessler, S., Gagliardini, V., Gheyselinck, J., Yang, W.-C., and Grossniklaus, U. (2007). The FERONIA Receptor-like Kinase Mediates Male-Female Interactions During Pollen Tube Reception. Science *317*, 656–660.

Fan, Y., Burkart, G.M., and Dixit, R. (2018). The Arabidopsis SPIRAL2 Protein Targets and Stabilizes Microtubule Minus Ends. Curr. Biol. *28*, 987-994.e3.

Fawke, S., Doumane, M., and Schornack, S. (2015). Oomycete Interactions with Plants: Infection Strategies and Resistance Principles. Microbiol. Mol. Biol. Rev. *79*, 263–280.

Feijó, J.A., Sainhas, J., Holdaway-Clarke, T., Cordeiro, M.S., Kunkel, J.G., and Hepler, P.K. (2001). Cellular oscillations and the regulation of growth: the pollen tube paradigm. BioEssays *23*, 86–94.

Fiebig, A., Mayfield, J.A., Miley, N.L., Chau, S., Fischer, R.L., and Preuss, D. (2000). Alterations in CER6, a Gene Identical to CUT1, Differentially Affect Long-Chain Lipid Content on the Surface of Pollen and Stems. Plant Cell *12*, 2001–2008.

Fisher, D.D., and Cyr, R.J. (1998). Extending the Microtubule/Microfibril Paradigm: Cellulose Synthesis Is Required for Normal Cortical Microtubule Alignment in Elongating Cells. Plant Physiol. *116*, 1043–1051.

Fobis-Loisy, I., Chambrier, P., and Gaude, T. (2007). Genetic transformation of Arabidopsis lyrata: specific expression of the green fluorescent protein (GFP) in pistil tissues. Plant Cell Rep. *26*, 745–753.

Frank, M.J., and Smith, L.G. (2002). A Small, Novel Protein Highly Conserved in Plants and Animals Promotes the Polarized Growth and Division of Maize Leaf Epidermal Cells. Curr. Biol. *12*, 849–853.

Fu, Y., Li, H., and Yang, Z. (2002). The ROP2 GTPase Controls the Formation of Cortical Fine F-Actin and the Early Phase of Directional Cell Expansion during Arabidopsis Organogenesis. Plant Cell *14*, 777–794.

Fu, Y., Gu, Y., Zheng, Z., Wasteneys, G., and Yang, Z. (2005). Arabidopsis Interdigitating Cell Growth Requires Two Antagonistic Pathways with Opposing Action on Cell Morphogenesis. Cell *120*, 687–700.

Furutani, I., Watanabe, Y., Prieto, R., Masukawa, M., Suzuki, K., Naoi, K., Thitamadee, S., Shikanai, T., and Hashimoto, T. (2000). The SPIRAL genes are required for directional control of cell elongation in Aarabidopsis thaliana. Development *127*, 4443–4453.

Gao, Z., Daneva, A., Salanenka, Y., Van Durme, M., Huysmans, M., Lin, Z., De Winter, F., Vanneste, S., Karimi, M., Van de Velde, J., et al. (2018). KIRA1 and ORESARA1 terminate flower receptivity by promoting cell death in the stigma of Arabidopsis. Nat. Plants.

Gaude, T., and Dumas, C. (1986). Organization of stigma surface components in Brassica: a cytochemical study. J. Cell Sci. *82*, 203–216.

Ghanbari, M., Nezhad, A.S., Agudelo, C.G., Packirisamy, M., and Geitmann, A. (2014). Microfluidic positioning of pollen grains in lab-on-a-chip for single cell analysis. J. Biosci. Bioeng. *117*, 504–511.

Goddard, R.H., Wick, S.M., Silflow, C.D., and Snustad, D.P. (1994). Microtubule Components of the Plant Cell Cytoskeleton. Plant Physiol. *104*, 1–6.

Goring, D.R. (2018). Exocyst, exosomes, and autophagy in the regulation of Brassicaceae pollen-stigma interactions. J. Exp. Bot. *69*, 69–78.

Gossot, O., and Geitmann, A. (2007). Pollen tube growth: coping with mechanical obstacles involves the cytoskeleton. Planta *226*, 405–416.

Govers, F. (2001). Misclassification of pest as “fungus” puts vital research on wrong track.

Hamada, T. (2007). Microtubule-associated proteins in higher plants. J. Plant Res. *120*, 79–98.

Hamada, T. (2014). Chapter One - Microtubule Organization and Microtubule-Associated Proteins in Plant Cells. In International Review of Cell and Molecular Biology, K.W. Jeon, ed. (Academic Press), pp. 1–52.

Hamant, O., Heisler, M.G., Jönsson, H., Krupinski, P., Uyttewaal, M., Bokov, P., Corson, F., Sahlin, P., Boudaoud, A., Meyerowitz, E.M., et al. (2008). Developmental Patterning by Mechanical Signals in Arabidopsis. Science *322*, 1650–1655.

Hammami, H., Aliverdi, A., and Parsa, M. (2014). Effectiveness of Clodinafop-Propargyl, Haloxyfop-p-methyl and Difenzoquat-methyl-sulfate Plus Adigor® and Propel™ Adjuvants in Controlling Avena ludoviciana Durieu. J. Agric. Sci. Technol. *16*, 291–299.

Hardham, A.R., Takemoto, D., and White, R.G. (2008). Rapid and dynamic subcellular reorganization following mechanical stimulation of Arabidopsis epidermal cells mimics responses to fungal and oomycete attack. BMC Plant Biol. *8*, 1–14.

Harholt, J., Suttangkakul, A., and Scheller, H.V. (2010). Biosynthesis of Pectin. Plant Physiol. *153*, 384–395.

Hartman, J.J., and Vale, R.D. (1999). Microtubule Disassembly by ATP-Dependent Oligomerization of the AAA Enzyme Katanin. Science *286*, 782–785.

He, B., Xi, F., Zhang, X., Zhang, J., and Guo, W. (2007). Exo70 interacts with phospholipids and mediates the targeting of the exocyst to the plasma membrane. EMBO J. *26*, 4053–4065.

Heilmann, I., and Ischebeck, T. (2016). Male functions and malfunctions: the impact of phosphoinositides on pollen development and pollen tube growth. Plant Reprod. *29*, 3–20.

Hématy, K., Sado, P.-E., Van Tuinen, A., Rochange, S., Desnos, T., Balzergue, S., Pelletier, S., Renou, J.-P., and Höfte, H. (2007). A Receptor-like Kinase Mediates the Response of Arabidopsis Cells to the Inhibition of Cellulose Synthesis. Curr. Biol. *17*, 922–931.

Herth, W. (1983). Arrays of plasma-membrane “rosettes” involved in cellulose microfibril formation of Spirogyra. Planta *159*, 347–356.

Hervieux, N., Dumond, M., Sapala, A., Routier-Kierzkowska, A.-L., Kierzkowski, D., Roeder, A.H.K., Smith, R.S., Boudaoud, A., and Hamant, O. (2016). A Mechanical Feedback Restricts Sepal Growth and Shape in Arabidopsis. Curr. Biol. *26*, 1019–1028.

Heslop-Harrison, Y., and Shivanna, K.R. (1977). The Receptive Surface of the Angiosperm Stigma. Ann. Bot. *41*, 1233–1258.

Higashiyama, T., Kuroiwa, H., Kawano, S., and Kuroiwa, T. (1998). Guidance in Vitro of the Pollen Tube to the Naked Embryo Sac of Torenia fournieri. Plant Cell *10*, 2019–2031.

Himmelspach, R., Williamson, R.E., and Wasteneys, G.O. (2003). Cellulose microfibril alignment recovers from DCB-induced disruption despite microtubule disorganization. Plant J. *36*, 565–575.

His, I., and Driouich, A. (2001). Altered pectin composition in primary cell walls of korrigan, a dwarf mutant of Arabidopsis defcient in a membrane-bound endo-1,4-b-glucanase. 11.

Höfte, H. (2015). The Yin and Yang of Cell Wall Integrity Control: Brassinosteroid and FERONIA Signaling. Plant Cell Physiol. *56*, 224–231.

Höfte, H., and Voxeur, A. (2017). Plant cell walls. Curr. Biol. *27*, R865–R870.

Huck, N., Moore, J.M., Federer, M., and Grossniklaus, U. (2003). The Arabidopsis mutant feronia disrupts the female gametophytic control of pollen tube reception. Development *130*, 2149–2159.

Hulskamp, M., Schneitz, K., and Pruitt, R.E. (1995). Genetic Evidence for a Long-Range Activity That Directs Pollen Tube Guidance in Arabidopsis. Plant Cell *7*, 57–64.

Indriolo, E., Safavian, D., and Goring, D.R. (2014). The ARC1 E3 Ligase Promotes Two Different Self-Pollen Avoidance Traits in Arabidopsis. Plant Cell *26*, 1525–1543.

Iwano, M., Shiba, H., Miwa, T., Che, F.-S., Takayama, S., Nagai, T., Miyawaki, A., and Isogai, A. (2004). Ca2+ Dynamics in a Pollen Grain and Papilla Cell during Pollination of Arabidopsis. Plant Physiol. *136*, 3562–3571.

Iwano, M., Shiba, H., Matoba, K., Miwa, T., Funato, M., Entani, T., Nakayama, P., Shimosato, H., Takaoka, A., Isogai, A., et al. (2007). Actin Dynamics in Papilla Cells of Brassica rapa during Self- and Cross-Pollination. Plant Physiol. *144*, 72–81.

Iwano, M., Igarashi, M., Tarutani, Y., Kaothien-Nakayama, P., Nakayama, H., Moriyama, H., Yakabe, R., Entani, T., Shimosato-Asano, H., Ueki, M., et al. (2014). A Pollen Coat–Inducible Autoinhibited Ca2+-ATPase Expressed in Stigmatic Papilla Cells Is Required for Compatible Pollination in the Brassicaceae. Plant Cell *26*, 636–649.

Janson, J., Reinders, M.C., Tuyl, J.M.V., and Keijzer, C.J. (1993). Pollen tube growth in Lilium longiflorum following different pollination techniques and flower manipulations. Acta Bot. Neerlandica *42*, 461–472.

Johnson, K.L., Gidley, M.J., Bacic, A., and Doblin, M.S. (2018). Cell wall biomechanics: a tractable challenge in manipulating plant cell walls 'fit for purpose'! Curr. Opin. Biotechnol. *49*, 163–171.

Judelson, H.S. (2017). Metabolic Diversity and Novelties in the Oomycetes. Annu. Rev. Microbiol. *71*, 21–39.

Kandasamy, M.K., Nasrallah, J.B., and Nasrallah, M.E. (1994). Pollen-pistil interactions and developmental regulation of pollen tube growth in Arabidopsis. Development *120*, 3405–3418.

Ketelaar, T. (2013). The actin cytoskeleton in root hairs: all is fine at the tip. Curr. Opin. Plant Biol. *16*, 749–756.

Ketelaar, T., Meijer, H.J.G., Spiekerman, M., Weide, R., and Govers, F. (2012). Effects of latrunculin B on the actin cytoskeleton and hyphal growth in Phytophthora infestans. Fungal Genet. Biol. *49*, 1014–1022.

Kim, S., Mollet, J.-C., Dong, J., Zhang, K., Park, S.-Y., and Lord, E.M. (2003). Chemocyanin, a small basic protein from the lily stigma, induces pollen tube chemotropism. Proc. Natl. Acad. Sci. *100*, 16125–16130.

Knoblauch, M., Vendrell, M., de Leau, E., Paterlini, A., Knox, K., Ross-Elliot, T., Reinders, A., Brockman, S.A., Ward, J., and Oparka, K. (2015). Multispectral Phloem-Mobile Probes: Properties and Applications1. Plant Physiol. *167*, 1211–1220.

Kroeger, J.H., Daher, F.B., Grant, M., and Geitmann, A. (2009). Microfilament Orientation Constrains Vesicle Flow and Spatial Distribution in Growing Pollen Tubes. Biophys. J. *97*, 1822–1831.

Kurdyukov, S., Faust, A., Nawrath, C., Bär, S., Voisin, D., Efremova, N., Franke, R., Schreiber, L., Saedler, H., Métraux, J.-P., et al. (2006). The Epidermis-Specific Extracellular BODYGUARD Controls Cuticle Development and Morphogenesis in Arabidopsis. Plant Cell *18*, 321–339.

Lalonde, B.A., Nasrallah, M.E., Dwyer, K.G., Chen, C.H., Barlow, B., and Nasrallah, J.B. (1989). A highly conserved Brassica gene with homology to the S-locus-specific glycoprotein structural gene. Plant Cell *1*, 249–258.

Lampugnani, E.R., Khan, G.A., Somssich, M., and Persson, S. (2018). Building a plant cell wall at a glance. J Cell Sci *131*, jcs207373.

Landrein, B., and Hamant, O. (2013). How mechanical stress controls microtubule behavior and morphogenesis in plants: history, experiments and revisited theories. Plant J. *75*, 324–338.

Landrein, B., Lathe, R., Bringmann, M., Vouillot, C., Ivakov, A., Boudaoud, A., Persson, S., and Hamant, O. (2013). Impaired Cellulose Synthase Guidance Leads to Stem Torsion and Twists Phyllotactic Patterns in Arabidopsis. Curr. Biol. *23*, 895–900.

Latijnhouwers, M., de Wit, P.J.G.M., and Govers, F. (2003). Oomycetes and fungi: similar weaponry to attack plants. Trends Microbiol. *11*, 462–469.

Lazzaro, M.D., Donohue, J.M., and Soodavar, F.M. (2003). Disruption of cellulose synthesis by isoxaben causes tip swelling and disorganizes cortical microtubules in elongating conifer pollen tubes. Protoplasma *220*, 201–207.

Ledbetter, M.C., and Porter, K.R. (1963). A “Microtubule” in Plant Cell Fine Structure. J. Cell Biol. *19*, 239–250.

Lennon, K.A., Roy, S., Hepler, P.K., and Lord, E.M. (1998). The structure of the transmitting tissue of Arabidopsis thaliana (L.) and the path of pollen tube growth. Sex. Plant Reprod. *11*, 49–59.

Li, H., Shen, J.-J., Zheng, Z.-L., Lin, Y., and Yang, Z. (2001). The Rop GTPase Switch Controls Multiple Developmental Processes in Arabidopsis. Plant Physiol. *126*, 670–684.

Li, S., Lei, L., Somerville, C.R., and Gu, Y. (2012). Cellulose synthase interactive protein 1 (CSI1) links microtubules and cellulose synthase complexes. Proc. Natl. Acad. Sci. U. S. A. *109*, 185–190.

Lin, D., Cao, L., Zhou, Z., Zhu, L., Ehrhardt, D., Yang, Z., and Fu, Y. (2013). Rho GTPase Signaling Activates Microtubule Severing to Promote Microtubule Ordering in Arabidopsis. Curr. Biol. *23*, 290–297.

Lindeboom, J.J., Nakamura, M., Hibbel, A., Shundyak, K., Gutierrez, R., Ketelaar, T., Emons, A.M.C., Mulder, B.M., Kirik, V., and Ehrhardt, D.W. (2013). A Mechanism for Reorientation of Cortical Microtubule Arrays Driven by Microtubule Severing. Science *342*, 1245533.

Lolle, S.J., and Cheung, A.Y. (1993). Promiscuous Germination and Growth of Wildtype Pollen from Arabidopsis and Related Species on the Shoot of the Arabidopsis Mutant, fiddlehead. Dev. Biol. *155*, 250–258.

Lolle, S.J., Cheung, A.Y., and Sussex, I.M. (1992). Fiddlehead: an Arabidopsis mutant constitutively expressing an organ fusion program that involves interactions between epidermal cells. Dev. Biol. *152*, 383–392.

Lolle, S.J., Berlyn, G.P., Engstrom, E.M., Krolikowski, K.A., Reiter, W.D., and Pruitt, R.E. (1997). Developmental regulation of cell interactions in the Arabidopsis fiddlehead-1 mutant: a role for the epidermal cell wall and cuticle. Dev. Biol. *189*, 311–321.

Louveaux, M., Rochette, S., Beauzamy, L., Boudaoud, A., and Hamant, O. (2016). The impact of mechanical compression on cortical microtubules in Arabidopsis: a quantitative pipeline. Plant J. *88*, 328–342.

Luptovčiak, I., Samakovli, D., Komis, G., and Šamaj, J. (2017). KATANIN 1 Is Essential for Embryogenesis and Seed Formation in Arabidopsis. Front. Plant Sci. *8*.

Ma, J.F., Liu, Z.H., Chu, C.P., Hu, Z.Y., Wang, X.L., and Zhang, X.S. (2012). Different regulatory processes control pollen hydration and germination in Arabidopsis. Sex. Plant Reprod. *25*, 77–82.

Maas, S.L.N., Breakefield, X.O., and Weaver, A.M. (2017). Extracellular vesicles: unique intercellular delivery vehicles. Trends Cell Biol. *27*, 172–188.

Majda, M., Grones, P., Sintorn, I.-M., Vain, T., Milani, P., Krupinski, P., Zagórska-Marek, B., Viotti, C., Jönsson, H., Mellerowicz, E.J., et al. (2017). Mechanochemical Polarization of Contiguous Cell Walls Shapes Plant Pavement Cells. Dev. Cell *43*, 290-304.e4.

Mao, G., Buschmann, H., Doonan, J.H., and Lloyd, C.W. (2006). The role of MAP65-1 in microtubule bundling during Zinnia tracheary element formation. J. Cell Sci. *119*, 753–758.

Mascarenhas, J. (1993). Molecular Mechanisms of Pollen Tube Growth and Differentiation. Plant Cell *5*, 1303–1314.

Mayfield, J.A., and Preuss, D. (2000). Rapid initiation of Arabidopsis pollination requires the oleosin-domain protein GRP17. Nat. Cell Biol. *2*, 128.

McClinton, R.S., Chandler, J.S., and Callis, J. (2001). cDNA isolation, characterization, and protein intracellular localization of a katanin-like p60 subunit from Arabidopsis thaliana. Protoplasma *216*, 181–190.

McNally, F.J., and Vale, R.D. (1993). Identification of katanin, an ATPase that severs and disassembles stable microtubules. Cell *75*, 419–429.

Mei, Y., Gao, H.-B., Yuan, M., and Xue, H.-W. (2012). The Arabidopsis ARCP Protein, CSI1, Which Is Required for Microtubule Stability, Is Necessary for Root and Anther Development. Plant Cell *24*, 1066–1080.

Meng, Y., Zhang, Q., Ding, W., and Shan, W. (2014). Phytophthora parasitica: a model oomycete plant pathogen. Mycology *5*, 43–51.

Michard, E., Simon, A.A., Tavares, B., Wudick, M.M., and Feijó, J.A. (2017). Signaling with Ions: The Keystone for Apical Cell Growth and Morphogenesis in Pollen Tubes. Plant Physiol. *173*, 91–111.

Micheli, F. (2001). Pectin methylesterases: cell wall enzymes with important roles in plant physiology. Trends Plant Sci. *6*, 414–419.

Mirabet, V., Das, P., Boudaoud, A., and Hamant, O. (2011). The Role of Mechanical Forces in Plant Morphogenesis. Annu. Rev. Plant Biol. *62*, 365–385.

Mitchison, T., and Kirschner, M. (1984). Dynamic instability of microtubule growth. Nature *312*, 237–242.

Miyazaki, S., Murata, T., Sakurai-Ozato, N., Kubo, M., Demura, T., Fukuda, H., and Hasebe, M. (2009). ANXUR1 and 2, Sister Genes to FERONIA/SIRENE, Are Male Factors for Coordinated Fertilization. Curr. Biol. *19*, 1327–1331.

Mizukami, A.G., Inatsugi, R., Jiao, J., Kotake, T., Kuwata, K., Ootani, K., Okuda, S., Sankaranarayanan, S., Sato, Y., Maruyama, D., et al. (2016). The AMOR Arabinogalactan Sugar Chain Induces Pollen-Tube Competency to Respond to Ovular Guidance. Curr. Biol. *26*, 1091–1097.

Mizuta, Y., and Higashiyama, T. (2018). Chemical signaling for pollen tube guidance at a glance. J. Cell Sci. *131*, jcs208447.

Mollet, J.-C., Park, S.-Y., Nothnagel, E.A., and Lord, E.M. (2000). A Lily Stylar Pectin Is Necessary for Pollen Tube Adhesion to an in Vitro Stylar Matrix. Plant Cell *12*, 1737–1749.

Munson, M., and Novick, P. (2006). The exocyst defrocked, a framework of rods revealed. Nat. Struct. Mol. Biol. *13*, 577–581.

Nakamura, M., Lindeboom, J.J., Saltini, M., Mulder, B.M., and Ehrhardt, D.W. (2018). SPR2 protects minus ends to promote severing and reorientation of plant cortical microtubule arrays. J. Cell Biol. *217*, 915–927.

Nakayama, N., Smith, R.S., Mandel, T., Robinson, S., Kimura, S., Boudaoud, A., and Kuhlemeier, C. (2012). Mechanical Regulation of Auxin-Mediated Growth. Curr. Biol. *22*, 1468–1476.

Nixon, B.T., Mansouri, K., Singh, A., Du, J., Davis, J.K., Lee, J.-G., Slabaugh, E., Vandavasi, V.G., O'Neill, H., Roberts, E.M., et al. (2016). Comparative Structural and Computational Analysis Supports Eighteen Cellulose Synthases in the Plant Cellulose Synthesis Complex. Sci. Rep. *6*, 28696.

Obermeyer, G., and Feijó, J. (2017). Pollen Tip Growth: From Biophysical Aspects to Systems Biology (Springer).

Okuda, S., Tsutsui, H., Shiina, K., Sprunck, S., Takeuchi, H., Yui, R., Kasahara, R.D., Hamamura, Y., Mizukami, A., Susaki, D., et al. (2009). Defensin-like polypeptide LUREs are pollen tube attractants secreted from synergid cells. Nature *458*, 357–361.

Onelli, E., Idilli, A.I., and Moscatelli, A. (2015). Emerging roles for microtubules in angiosperm pollen tube growth highlight new research cues. Front. Plant Sci. *6*.

Palanivelu, R., and Preuss, D. (2006). Distinct short-range ovule signals attract or repel Arabidopsis thaliana pollen tubes in vitro. BMC Plant Biol. *6*, 7.

Panteris, E., and Adamakis, I.-D.S. (2012). Aberrant microtubule organization in dividing root cells of p60-katanin mutants. Plant Signal. Behav. *7*, 16–18.

Panteris, E., Adamakis, I.D.S., Voulgari, G., and Papadopoulou, G. (2011). A role for katanin in plant cell division: Microtubule organization in dividing root cells of fra2 and lue1 Arabidopsis thaliana mutants. Cytoskeleton *68*, 401–413.

Paredez, A.R., Somerville, C.R., and Ehrhardt, D.W. (2006). Visualization of Cellulose Synthase Demonstrates Functional Association with Microtubules. Science *312*, 1491–1495.

Park, Y.B., and Cosgrove, D.J. (2012). A Revised Architecture of Primary Cell Walls Based on Biomechanical Changes Induced by Substrate-Specific Endoglucanases1. Plant Physiol. *158*, 1933–1943.

Park, Y.B., and Cosgrove, D.J. (2015). Xyloglucan and its Interactions with Other Components of the Growing Cell Wall. Plant Cell Physiol. *56*, 180–194.

Park, S.-Y., Jauh, G.-Y., Mollet, J.-C., Eckard, K.J., Nothnagel, E.A., Walling, L.L., and Lord, E.M. (2000). A Lipid Transfer–like Protein Is Necessary for Lily Pollen Tube Adhesion to an in Vitro Stylar Matrix. Plant Cell *12*, 151–163.

Parre, E., and Geitmann, A. (2005). More Than a Leak Sealant. The Mechanical Properties of Callose in Pollen Tubes. Plant Physiol. *137*, 274–286.

Peaucelle, A., Louvet, R., Johansen, J.N., Höfte, H., Laufs, P., Pelloux, J., and Mouille, G. (2008). Arabidopsis Phyllotaxis Is Controlled by the Methyl-Esterification Status of Cell-Wall Pectins. Curr. Biol. *18*, 1943–1948.

Peaucelle, A., Braybrook, S.A., Le Guillou, L., Bron, E., Kuhlemeier, C., and Höfte, H. (2011). Pectin-Induced Changes in Cell Wall Mechanics Underlie Organ Initiation in Arabidopsis. Curr. Biol. *21*, 1720–1726.

Pelloux, J., Rustérucci, C., and Mellerowicz, E.J. (2007). New insights into pectin methylesterase structure and function. Trends Plant Sci. *12*, 267–277.

Persson, S., Paredez, A., Carroll, A., Palsdottir, H., Doblin, M., Poindexter, P., Khitrov, N., Auer, M., and Somerville, C.R. (2007). Genetic evidence for three unique components in primary cell-wall cellulose synthase complexes in Arabidopsis. Proc. Natl. Acad. Sci. *104*, 15566–15571.

Pleskot, R., Cwiklik, L., Jungwirth, P., Žárský, V., and Potocký, M. (2015). Membrane targeting of the yeast exocyst complex. Biochim. Biophys. Acta *1848*, 1481–1489.

Preuss, D., Lemieux, B., Yen, G., and Davis, R.W. (1993). A conditional sterile mutation eliminates surface components from Arabidopsis pollen and disrupts cell signaling during fertilization. Genes Dev. *7*, 974–985.

Ray, S.M., Park, S.S., and Ray, A. (1997). Pollen tube guidance by the female gametophyte. Dev. Camb. Engl. *124*, 2489–2498.

Richmond, T.A., and Somerville, C.R. (2000). The Cellulose Synthase Superfamily. Plant Physiol. *124*, 495–498.

Ringli, C. (2010). Monitoring the Outside: Cell Wall-Sensing Mechanisms. PLANT Physiol. *153*, 1445–1452.

Ristaino, J.B. (2002). Tracking historic migrations of the Irish potato famine pathogen, Phytophthora infestans. Microbes Infect. *4*, 1369–1377.

Roelofsen, P.A., and Houwink, A.L. (1953). Architecture and growth of the primary cell wall in some plant hairs and in the Phycomyces sporangiophore. Acta Bot. Neerlandica *2*, 218–225.

Rojas, E.R., Hotton, S., and Dumais, J. (2011). Chemically Mediated Mechanical Expansion of the Pollen Tube Cell Wall. Biophys. J. *101*, 1844–1853.

Rotman, N., Rozier, F., Boavida, L., Dumas, C., Berger, F., and Faure, J.-E. (2003). Female Control of Male Gamete Delivery during Fertilization in Arabidopsis thaliana. Curr. Biol. *13*, 432–436.

Safavian, D., and Goring, D.R. (2013). Secretory Activity Is Rapidly Induced in Stigmatic Papillae by Compatible Pollen, but Inhibited for Self-Incompatible Pollen in the Brassicaceae. PLoS ONE *8*, e84286.

Safavian, D., Zayed, Y., Indriolo, E., Chapman, L., Ahmed, A., and Goring, D.R. (2015). RNA Silencing of Exocyst Genes in the Stigma Impairs the Acceptance of Compatible Pollen in Arabidopsis. Plant Physiol. *169*, 2526–2538.

Sampathkumar, A., Krupinski, P., Wightman, R., Milani, P., Berquand, A., Boudaoud, A., Hamant, O., Jönsson, H., and Meyerowitz, E.M. (2014). Subcellular and supracellular mechanical stress prescribes cytoskeleton behavior in Arabidopsis cotyledon pavement cells. ELife *3*, e01967.

Samuel, M.A., Chong, Y.T., Haasen, K.E., Aldea-Brydges, M.G., Stone, S.L., and Goring, D.R. (2009). Cellular Pathways Regulating Responses to Compatible and Self-Incompatible Pollen in Brassica and Arabidopsis Stigmas Intersect at Exo70A1, a Putative Component of the Exocyst Complex. Plant Cell *21*, 2655–2671.

Samuel, M.A., Tang, W., Jamshed, M., Northey, J., Patel, D., Smith, D., Siu, K.W.M., Muench, D.G., Wang, Z.-Y., and Goring, D.R. (2011). Proteomic Analysis of Brassica Stigmatic Proteins Following the Self-incompatibility Reaction Reveals a Role for Microtubule Dynamics During Pollen Responses. Mol. Cell. Proteomics MCP *10*, M111.011338.

Sanati Nezhad, A., and Geitmann, A. (2013). The cellular mechanics of an invasive lifestyle. J. Exp. Bot. *64*, 4709–4728.

Sanati Nezhad, A., Naghavi, M., Packirisamy, M., Bhat, R., and Geitmann, A. (2013). Quantification of cellular penetrative forces using lab-on-a-chip technology and finite element modeling. Proc. Natl. Acad. Sci. *110*, 8093–8098.

Sassi, M., Ali, O., Boudon, F., Cloarec, G., Abad, U., Cellier, C., Chen, X., Gilles, B., Milani, P., Friml, J., et al. (2014). An Auxin-Mediated Shift toward Growth Isotropy Promotes Organ Formation at the Shoot Meristem in Arabidopsis. Curr. Biol. *24*, 2335–2342.

Scheller, H.V., and Ulvskov, P. (2010). Hemicelluloses. Annu. Rev. Plant Biol. *61*, 263–289.

Schmittgen, T.D., and Livak, K.J. (2008). Analyzing real-time PCR data by the comparative C(T) method. Nat. Protoc. *3*, 1101–1108.

Schneider, R., Hanak, T., Persson, S., and Voigt, C.A. (2016). Cellulose and callose synthesis and organization in focus, what's new? Curr. Opin. Plant Biol. *34*, 9–16.

Shih, H.-W., Miller, N.D., Dai, C., Spalding, E.P., and Monshausen, G.B. (2014). The Receptor-like Kinase FERONIA Is Required for Mechanical Signal Transduction in Arabidopsis Seedlings. Curr. Biol. *24*, 1887–1892.

Shoji, T., Narita, N.N., Hayashi, K., Asada, J., Hamada, T., Sonobe, S., Nakajima, K., and Hashimoto, T. (2004). Plant-Specific Microtubule-Associated Protein SPIRAL2 Is Required for Anisotropic Growth in Arabidopsis. Plant Physiol. *136*, 3933–3944.

Smyth, D.R., Bowman, J.L., and Meyerowitz, E.M. (1990). Early flower development in Arabidopsis. Plant Cell *2*, 755–767.

Sogo, A., and Tobe, H. (2005). Intermittent pollen-tube growth in pistils of alders (Alnus). Proc. Natl. Acad. Sci. *102*, 8770–8775.

Stoppin-Mellet, V., Gaillard, J., and Vantard, M. (2002). Functional evidence for in vitro microtubule severing by the plant katanin homologue. Biochem. J. *365*, 337–342.

Sugimoto, K., Himmelspach, R., Williamson, R.E., and Wasteneys, G.O. (2003). Mutation or drug-dependent microtubule disruption causes radial swelling without altering parallel cellulose microfibril deposition in Arabidopsis root cells. Plant Cell *15*, 1414–1429.

Suslov, D., and Verbelen, J.-P. (2006). Cellulose orientation determines mechanical anisotropy in onion epidermis cell walls. J. Exp. Bot. *57*, 2183–2192.

Szyjanowicz, P.M.J., McKinnon, I., Taylor, N.G., Gardiner, J., Jarvis, M.C., and Turner, S.R. (2004). The irregular xylem 2 mutant is an allele of korrigan that affects the secondary cell wall of Arabidopsis thaliana. Plant J. *37*, 730–740.

Takemoto, D., Jones, D.A., and Hardham, A.R. (2003). GFP-tagging of cell components reveals the dynamics of subcellular re-organization in response to infection of *Arabidopsis* by oomycete pathogens. Plant J. *33*, 775–792.

Takeuchi, H., and Higashiyama, T. (2012). A Species-Specific Cluster of Defensin-Like Genes Encodes Diffusible Pollen Tube Attractants in Arabidopsis. PLOS Biol. *10*, e1001449.

Tan, L., Eberhard, S., Pattathil, S., Warder, C., Glushka, J., Yuan, C., Hao, Z., Zhu, X., Avci, U., Miller, J.S., et al. (2013). An Arabidopsis Cell Wall Proteoglycan Consists of Pectin and Arabinoxylan Covalently Linked to an Arabinogalactan Protein. Plant Cell *25*, 270–287.

Taylor, N.G. (2008). Cellulose biosynthesis and deposition in higher plants. New Phytol. *178*, 239–252.

Thomas, C. (2012). Bundling actin filaments from membranes: some novel players. Front. Plant Sci. *3*.

Thomas, L.H., Forsyth, V.T., Šturcová, A., Kennedy, C.J., May, R.P., Altaner, C.M., Apperley, D.C., Wess, T.J., and Jarvis, M.C. (2013). Structure of Cellulose Microfibrils in Primary Cell Walls from Collenchyma. Plant Physiol. *161*, 465–476.

Turner, S., and Kumar, M. (2018). Cellulose synthase complex organization and cellulose microfibril structure. Philos. Transact. A Math. Phys. Eng. Sci. *376*.

Uyttewaal, M., Burian, A., Alim, K., Landrein, B., Borowska-Wykręt, D., Dedieu, A., Peaucelle, A., Ludynia, M., Traas, J., Boudaoud, A., et al. (2012). Mechanical Stress Acts via Katanin to Amplify Differences in Growth Rate between Adjacent Cells in Arabidopsis. Cell *149*, 439–451.

Vain, T., Crowell, E.F., Timpano, H., Biot, E., Desprez, T., Mansoori, N., Trindade, L.M., Pagant, S., Robert, S., Höfte, H., et al. (2014). The Cellulase KORRIGAN Is Part of the Cellulose Synthase Complex1. Plant Physiol. *165*, 1521–1532.

Wang, L., Clarke, L.A., Eason, R.J., Parker, C.C., Qi, B., Scott, R.J., and Doughty, J. (2016). PCP-B class pollen coat proteins are key regulators of the hydration checkpoint in *Arabidopsis thaliana* pollen-stigma interactions. New Phytol.

Wang, Q., Kong, L., Hao, H., Wang, X., Lin, J., Šamaj, J., and Baluška, F. (2005). Effects of Brefeldin A on Pollen Germination and Tube Growth. Antagonistic Effects on Endocytosis and Secretion. Plant Physiol. *139*, 1692–1703.

Wang, T., Park, Y.B., Cosgrove, D.J., and Hong, M. (2015). Cellulose-Pectin Spatial Contacts Are Inherent to Never-Dried Arabidopsis Primary Cell Walls: Evidence from Solid-State Nuclear Magnetic Resonance. Plant Physiol. *168*, 871–884.

Wasteneys, G.O., and Ambrose, J.C. (2009). Spatial organization of plant cortical microtubules: close encounters of the 2D kind. Trends Cell Biol. *19*, 62–71.

Wasteneys, G.O., and Galway, M.E. (2003). Remodeling the cytoskeleton for growth and form: an overview with some new views. Annu. Rev. Plant Biol. *54*, 691–722.

Whittington, A.T., Vugrek, O., Wei, K.J., Hasenbein, N.G., Sugimoto, K., Rashbrooke, M.C., and Wasteneys, G.O. (2001). MOR1 is essential for organizing cortical microtubules in plants. Nature *411*, 610–613.

Wightman, R., and Turner, S.R. (2007). Severing at sites of microtubule crossover contributes to microtubule alignment in cortical arrays: Microtubule dynamics. Plant J. *52*, 742–751.

Wightman, R., Chomicki, G., Kumar, M., Carr, P., and Turner, S.R. (2013). SPIRAL2 Determines Plant Microtubule Organization by Modulating Microtubule Severing. Curr. Biol. *23*, 1902–1907.

Wolf, S., and Greiner, S. (2012). Growth control by cell wall pectins. Protoplasma *249*, 169–175.

Wolf, S., Hématy, K., and Höfte, H. (2012). Growth Control and Cell Wall Signaling in Plants. Annu. Rev. Plant Biol. *63*, 381–407.

Xiao, C., Zhang, T., Zheng, Y., Cosgrove, D.J., and Anderson, C.T. (2016). Xyloglucan Deficiency Disrupts Microtubule Stability and Cellulose Biosynthesis in Arabidopsis, Altering Cell Growth and Morphogenesis. Plant Physiol. *170*, 234–249.

Yanagisawa, N., Sugimoto, N., Arata, H., Higashiyama, T., and Sato, Y. (2017). Capability of tip-growing plant cells to penetrate into extremely narrow gaps. Sci. Rep. *7*, 1403.

Yephremov, A., Wisman, E., Huijser, P., Huijser, C., Wellesen, K., and Saedler, H. (1999). Characterization of the FIDDLEHEAD gene of Arabidopsis reveals a link between adhesion response and cell differentiation in the epidermis. Plant Cell *11*, 2187–2201.

Žárský, V., Kulich, I., Fendrych, M., and Pečenková, T. (2013). Exocyst complexes multiple functions in plant cells secretory pathways. Curr. Opin. Plant Biol. *16*, 726–733.

Zerzour, R., Kroeger, J., and Geitmann, A. (2009). Polar growth in pollen tubes is associated with spatially confined dynamic changes in cell mechanical properties. Dev. Biol. *334*, 437–446.

Zhang, Q., Fishel, E., Bertroche, T., and Dixit, R. (2013). Microtubule Severing at Crossover Sites by Katanin Generates Ordered Cortical Microtubule Arrays in Arabidopsis. Curr. Biol. *23*, 2191–2195.

Zhang, T., Mahgsoudy-Louyeh, S., Tittmann, B., and Cosgrove, D.J. (2014). Visualization of the nanoscale pattern of recently-deposited cellulose microfibrils and matrix materials in never-dried primary walls of the onion epidermis. Cellulose *21*, 853–862.

Zhang, T., Vavylonis, D., Durachko, D.M., and Cosgrove, D.J. (2017). Nanoscale movements of cellulose microfibrils in primary cell walls. Nat. Plants *3*, 17056.

Zhang, Y., Liu, C.-M., Emons, A.-M.C., and Ketelaar, T. (2010). The Plant Exocyst. J. Integr. Plant Biol. *52*, 138–146.

Zheng, Y., Cosgrove, D.J., and Ning, G. (2017). High-Resolution Field Emission Scanning Electron Microscopy (FESEM) Imaging of Cellulose Microfibril Organization in Plant Primary Cell Walls. Microsc. Microanal. *23*, 1048–1054.

Zinkl, G.M., Zwiebel, B.I., Grier, D.G., and Preuss, D. (1999). Pollen-stigma adhesion in Arabidopsis: a species-specific interaction mediated by lipophilic molecules in the pollen exine. Development *126*, 5431–5440.

7

Appendix

The molecular signatures of compatible and incompatible pollination

Chie Kodera[1*], Jérémy Just[1], Martine Da Rocha[2], Antoine Larrieu[1,3], Lucie Riglet[1], Jonathan Legrand[1,4], Frédérique Rozier[1], Thierry Gaude[1], Isabelle Fobis-Loisy[1*]

[1] Laboratoire Reproduction et Développement des Plantes, Univ Lyon, ENS de Lyon, UCB Lyon, CNRS, INRA, Lyon, France

[2] INRA, Université Côte d'Azur, INRA, CNRS, ISA 400 route des Chappes BP 167, 06903 Sophia Antipolis Cedex, France

[3] Centre for Plant Sciences, Faculty of Biological Sciences, University of Leeds, Leeds, UK

[4] Laboratoire Reproduction et Développement des Plantes, Univ Lyon, ENS de Lyon, UCB Lyon, CNRS, INRA, Inria, F-69342, Lyon, France

[*] chie.kodera@ens-lyon.fr , isabelle.fobis-loisy@ens-lyon.fr

Abstract

Fertilization in flowering plants depends on the early contact and acceptance of pollen grains by the receptive papilla cells of the stigma. To identify the associated molecular pathways, we developed a transcriptomic analysis based on single nucleotide polymorphisms (SNPs) present in two Arabidopsis thaliana accessions, one used as female and the other as male. We succeeded in distinguishing 80 % of transcripts according to their parental origins and drew up a catalog of genes whose expression is modified after pollen-stigma interaction. Global analysis of our data reveals pattern-triggered immunity (PTI). From this analysis, we predicted the activation of the Mitogen-activated Protein Kinase 3 on the female side after compatible pollination, which we confirmed through expression and mutant analysis. Altogether this works provides the molecular signatures of compatible and incompatible pollination, highlights the active status of incompatible stigmas, and unravels a new MPK3-dependent cell wall feature associated with stigma-pollen interaction.

This article has been deposited on Biorxiv (doi: https://doi.org/10.1101/374843), and submitted to Nature Plants in July 2018.

Author Contribution

CK, JJ, MDR developed the data analysis pipeline and performed the bioinformatics analyses. AL, JL supported the bioinformatics analyses. AL helped with interpretation of

the transcriptomic data. CK is responsible for all experiments and analysis performed in the study except described below. FR produced and characterized Col-0/SRK14 and C24/SCR14 lines. CK and LR performed the image acquisition by scanning electron microscope. CK, LR, FR, IFL harvested plant materials and extracted RNA. CK, TG, IFL designed the study and CK, JJ, TG, IFL wrote the manuscript. All the authors contributed to the discussion.

Role of the female partner in pollen – stigma interactions

L. Riglet, T. Gaude, I. Loisy
UMR 5667, Reproduction et Développement des Plantes - ENS Lyon, France. Email: lucie.riglet@ens-lyon.fr

Question : What controls the first steps of plant reproduction ?

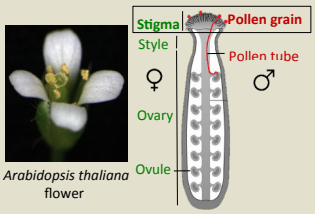

Arabidopsis thaliana flower

In plants, the female reproductive organ is covered with flask-shaped epidermal cells, the stigmatic papilla, capable of trapping the male partner (pollen grain). The pollen hydrates on the stigma and germinates a pollen tube that grows to transport the male gametes towards the ovules.

- What controls this early interaction between both partners ?
- What is the female role?

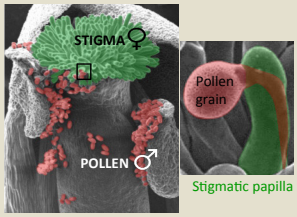

Aim : Towards an integrative model of pollen – stigma interaction using live imaging and genetic approaches

1. A working model: How pollen can be sense at the stigma surface?

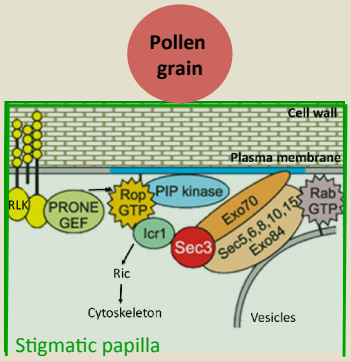

Adapted from Zarsky et al., 2009, New Phytol.

2. TGN vesicles move to and accumulate around the pollen tube during its growth

✓ Live imaging : dynamics of late, early and recycling endosomes and Golgi apparatus

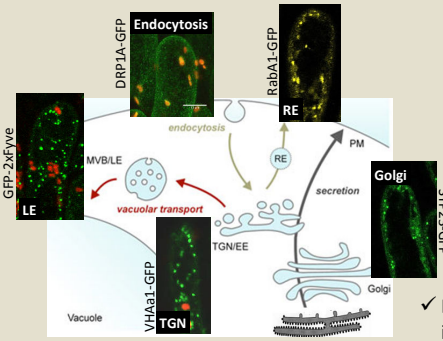

✓ Dynamics of *trans*-Golgi Network

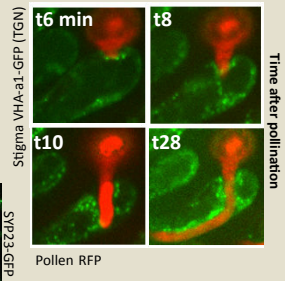

✓ Behavior of trafficking mutants in response to pollination

3. Proper organization of stigmatic cytoskeleton is necessary for pollen tube guidance towards the ovules

WT pollen tubes twist around the stigma papilla before finding their way to the ovary on microtubule mutants

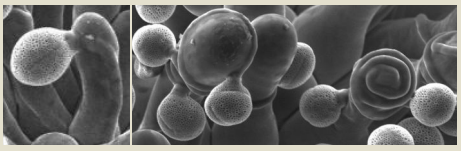
WT x WT MTs mutant (stigma) x WT pollen

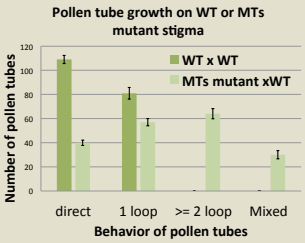

Actin polymerization along the pollen tube path

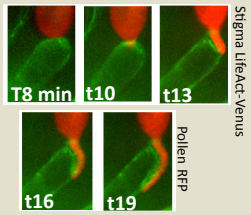

4. Role of ROP (Rho of plant) in pollination

✓ RT-PCR on stigma RNA

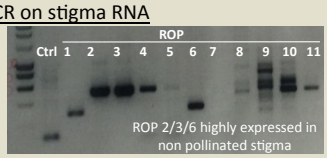

✓ Behavior of pollen grains on stigmas altered in ROP functions ?

Conclusion: Studying the cytoskeleton, vesicular trafficking and ROPs will allow us to construct an integrative model for pollen - stigma communication

This poster, presented at the 19th annual meeting of the Club Exocytose-Endocytose, Carry-Le-Rouet, France, May 26-28th 2016, received the best poster award.